APPENDICES CONCERNING THE EXPERIMENTAL AND ANALYTICAL RESEARCH PROGRAM

Volume IV of IV

Interim Report on Contract: PH-43-67-1136

Appendices C-H

TENSION, TENSION-COMPRESSION, AND HYSTERESIS TESTS

Appendix C

OBJECTIVES AND METHODOLOGY OVERVIEW

There were multiple objectives in the development of this series of experiments. The first was the design of a tension test which could be conducted statically or dynamically. The results were to be static and dynamic elastic moduli or functional stress-strain relationships (constitutive equations) and failure stresses. It was necessary that this test could be carried out on the bones of the skull and the component inner and outer tables as well as the diplöe. The second objective was development of a specimen and gripping system which would allow compressive as well as tensile forces to be applied to the specimen for the purpose of finding any transition modulus as a loading passes from tension to compression. An experimental design of this type would allow cyclic testing and the measurement of hysteresis or energy absorbed by the bone as the loads are applied and released. The third objective of this program is the determination of the relation of the physical properties to the skull anatomy and, further, the relationship of the measured properties to the skull microscopic structure through a series of histological studies .

The test procedures and specimen design have been developed and the test program is in its early stages at present. To meet these objectives it was necessary that the test specimen be very small due to the geometric limitations such as curvature and multilayered structure of the skull. The specimen size which has been chosen is shown in Figure 1. It is roughly one-half inch long and the cross-sectional area of the test section is about 2×10^{-3} in^2. The solution to the problem of gripping a specimen for tension,

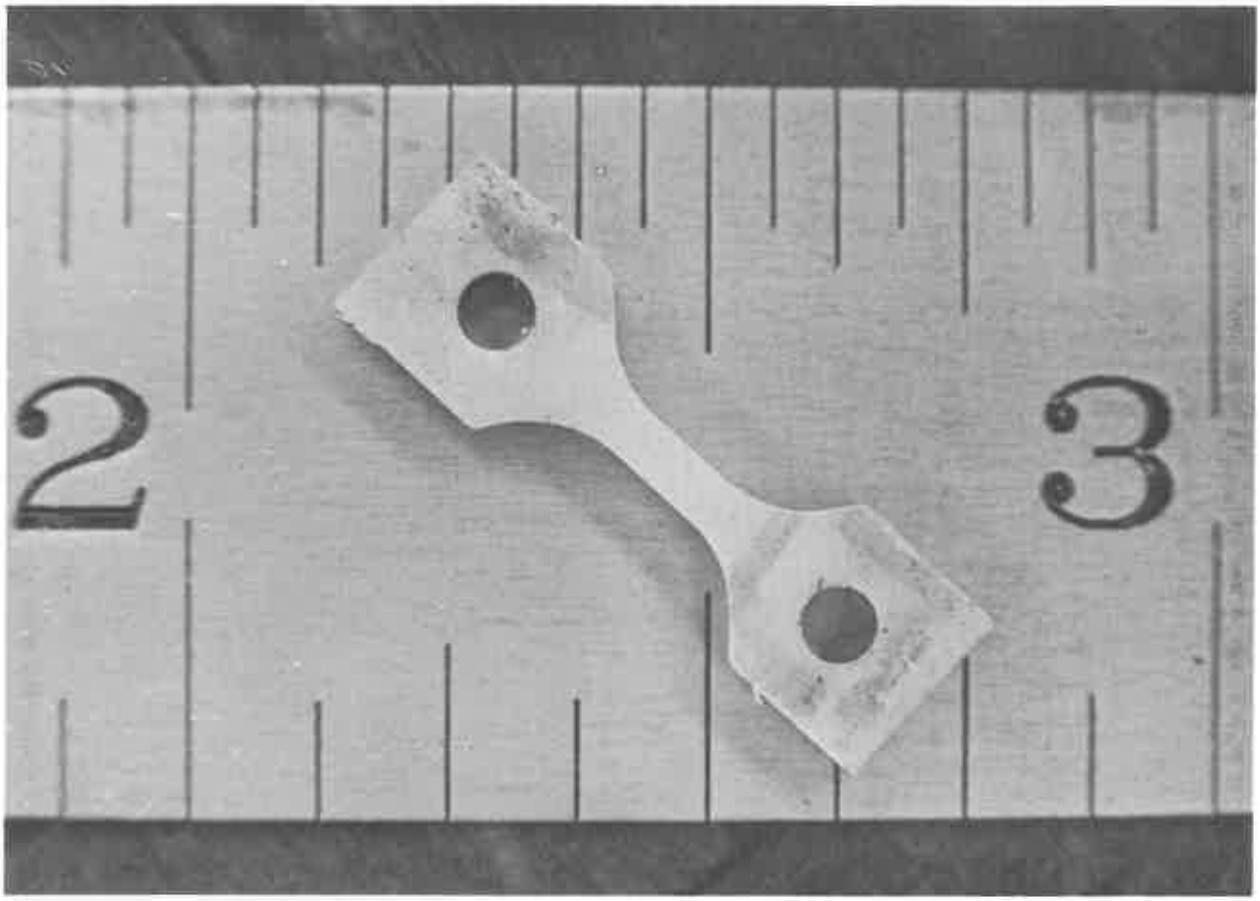

FIGURE 1. TENSION SPECIMEN

compression, cyclic, and dynamic loadings which was adopted involved applying a positive pressure to the specimen tabs as well as pinning the tab ends to prevent slipping, bending, and specimen breaking in the grips. The gripping system is shown in Figure 2.

In order to measure the strain it was decided that strain gages offered the greatest potential although it was found that the mounting of gages on these small specimens was extremely difficult and time consuming. An extensometer has been developed but this method has not been pursued in that it is felt that inertial effects and relatively low sensitivity limit the usefulness of this type of a device especially in the dynamic portion of this test program where the bulk of the experimentation is to be carried out.

The final objectives are being met by careful identification of the test specimens in relation to the anatomy of the skull from which they were removed. By the techniques described in the test procedure section of this appendix, the precise location and orientation in the skull is well known for any test specimen. With this information available meaningful histological studies of osteon orientation, etc. will be carried out. The particular histological techniques which will be used are currently being developed.

SPECIMEN PREPARATION

After a bone plug is acquired from an autopsy it is frozen at -10°C. The steps followed in specimen preparation are shown in Figures 3 and 4. As the specimen is removed from the refrigerator it possesses orientation marks. An appropriate layout of specimen blanks is then made on the specimen surface as shown in Figure 3b. Blocks are then cut from the bone plug as shown in

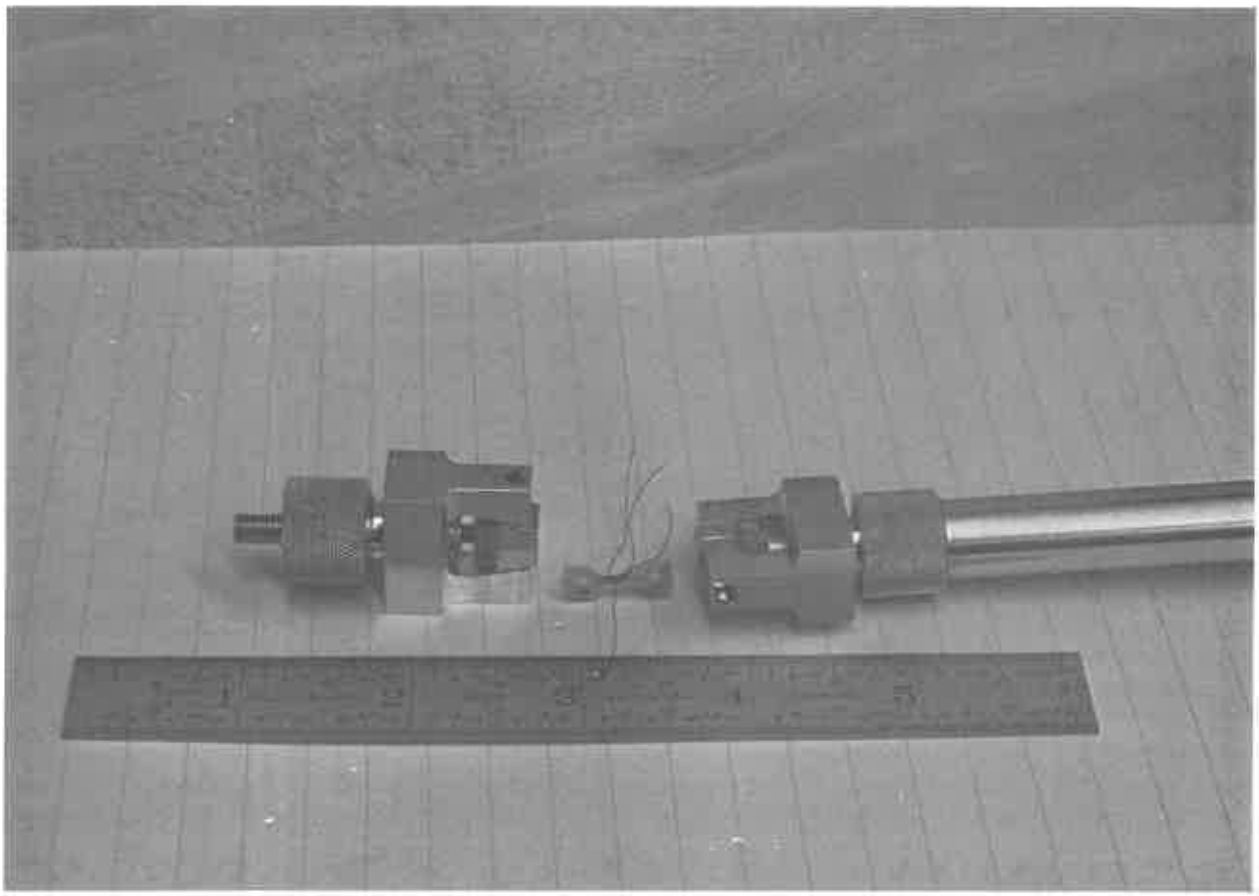

FIGURE 2. CLOSEUP OF GRIPPING

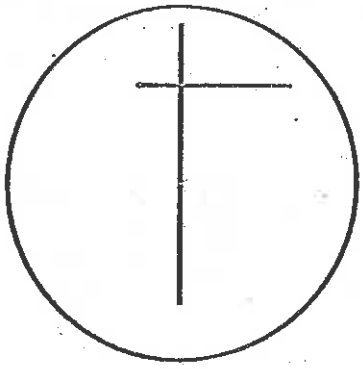

a. Orientation Marks upon Acquisition of Bone Plug

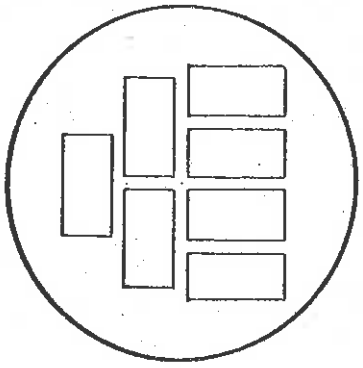

b. Layout Marks on Specimen Prior to Machining

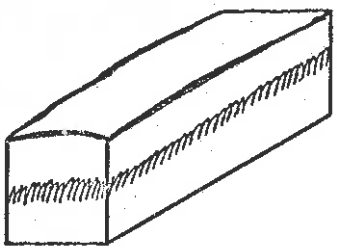

c. Block Cut from Bone Plug

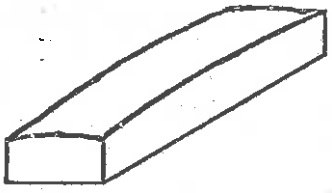

d. Slice from Outer Table, Diploe or Inner Table

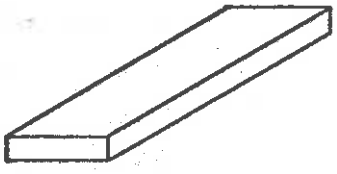

e. Milled Specimen Blank

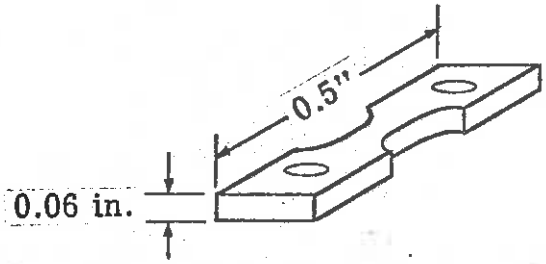

f. Finished Specimen

FIGURE 3. SPECIMEN FABRICATION

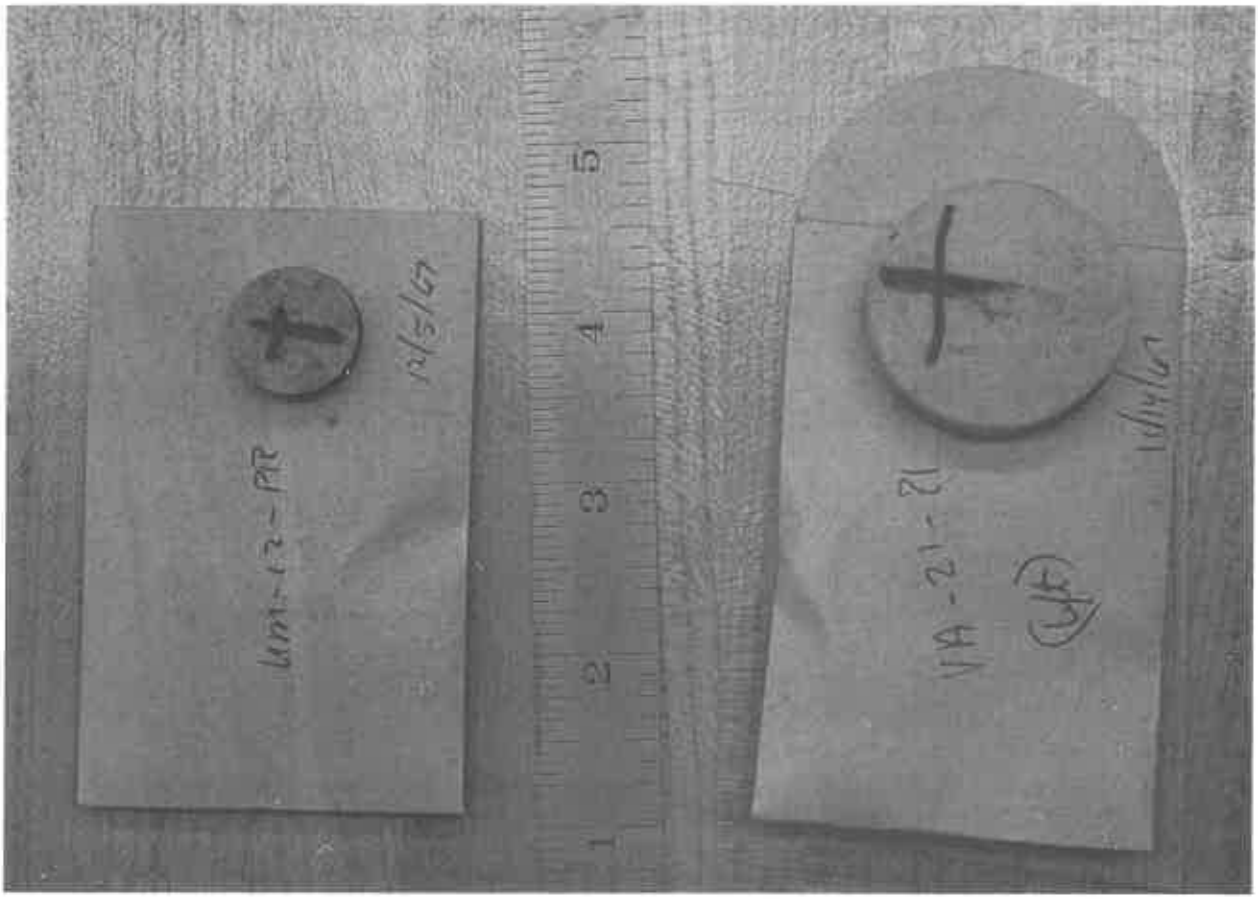

FIGURE 4. UNCUT BONE PLUGS

Figure 3c. The top, middle, and bottom may then be sliced into the rough specimen blank shown in Figure 3d. The blank is then milled true and finally a finished specimen is produced by mounting the blank in a template and using the mill as a routing table. The steps shown in Figures 3e and 3f are carried out on two Unimat lathe-mills with the aid of specially designed jigs, templates, and clamps. This setup is shown in the Figure 4. The time between steps a and f involves less than 30 minutes exposure to room temperature for a particular specimen. Heat production in cutting and milling is low.

The strain gaging procedure is time-consuming and difficult. Epoxy-backed foil gages with grid sizes ranging from 0.015 in. to 0.04 in. have been used. They are preleaded and then mounted on the specimen using Eastman 910 cement. The minimum time for the mounting of two strain gages on a specimen is one hour. If the actual test is included a specimen is exposed to room temperature for about two hours after removal from storage. About one-half of the tests proceed without mishap from the beginning of strain-gaging to the conclusion of a successful test. The success ratio is increasing rapidly as experience is gained and it is estimated that several hundred tests will be included in the final report for this project.

TEST PROCEDURES AND INSTRUMENTATION

The actual test procedure consists of the following steps: 1. alignment of grips; 2. mount specimen in grips; 3. solder strain gage leads into recorder circuitry; 4. calibrate strain gage bridge; 5. check circuit stability; 6. measure bending strains induced in specimen; 7. measure hysteresis, tension, and compression load-strain curves by performing several tension-compression cycles to a moderate load; 8. perform a tension test to failure.

The testing machine is a 10,000 pound capacity Instron floor model testing machine with reversible loading design. The load cell is a 1000 pound capacity tension-compression cell. Load versus strain curves are obtained by running the load and strain signals through Honeywell bridge-excitation-balance units into an x-y recorder. Dynamic tests will be recorded on a Honeywell visicorder, tape recorder, or on a storage oscilloscope using similar apparatus. The strain gage bridge circuitry is designed so that either tension or bending strains can be measured. An overview of the experimental setup is shown in Figure 5. The head travel rate for the tests carried out thus far is 0.02 in/min. indicating that this is essentially a static test.

RESULTS

A drawing of a typical x-y plot of a test is shown in Figure 6. A series of three tests is actually performed on each specimen yielding considerable information not all of which has been evaluated for the initial series of tests. The bending test which is carried out first shows whether the specimen is properly lined up in the gripping system. If alignment is perfect no strain should appear.

The next series of tests involves performing a series of cycles from tension to compression for the purpose of finding energy absorption properties of bone, tension elastic modulus, compression modulus, and the modulus which exists as loading proceeds from tension to compression and back. It has been found that the hysteresis properties of bone seem to be large, i.e. a relatively large amount of energy is absorbed during cyclic loading from tension to compression. Quantification of this property is in process and comparisons will be made with other materials.

FIGURE 5. TENSION TEST INSTRUMENTATION

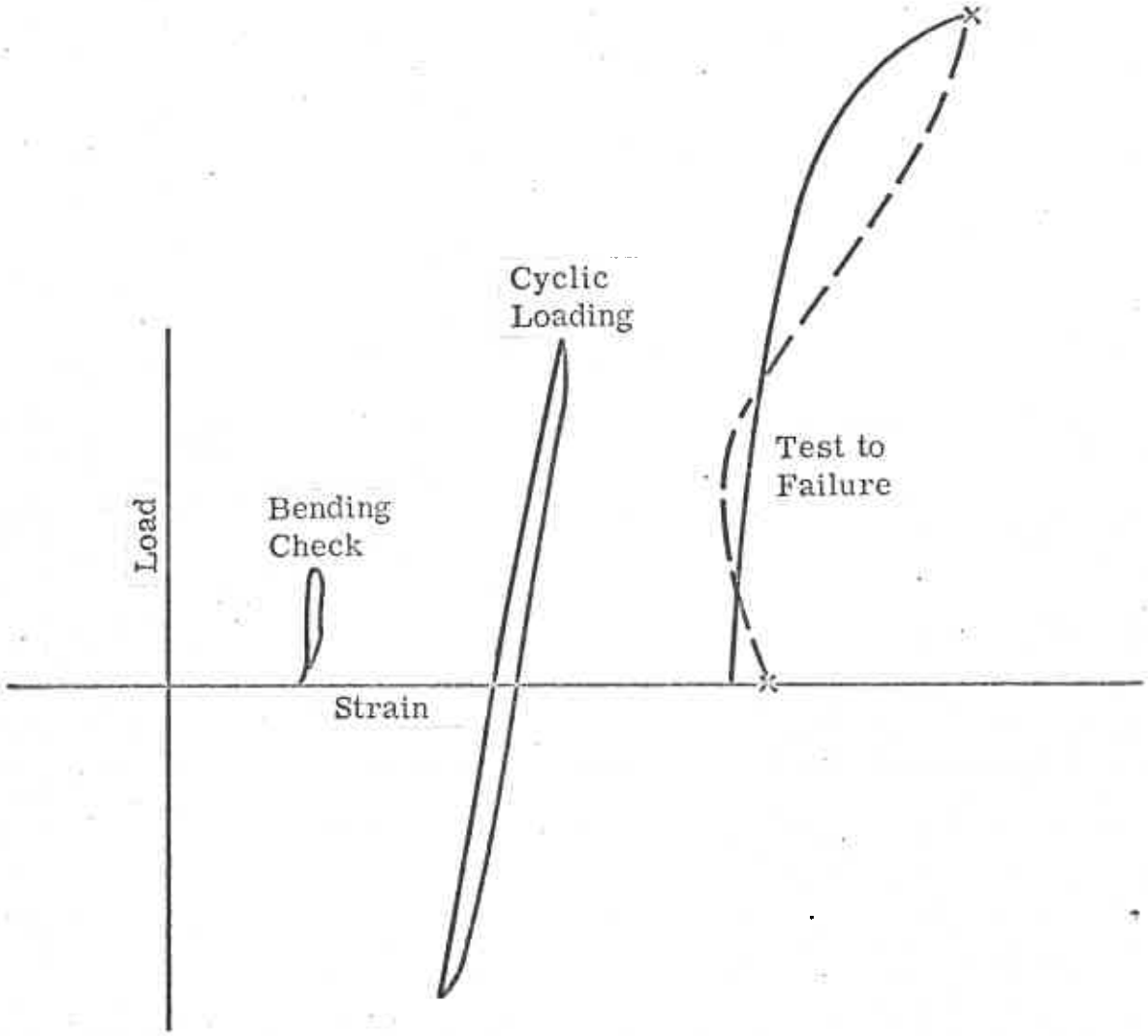

FIGURE 6. TENSION TEST

The final curve in Figure 6 is a standard load-strain curve. The specimen is loaded to failure. Several interesting and relevant properties have been observed and will receive quantification as further tests are performed. First, the curves seem nearly linear for about two-thirds of the load range indicating that a Young's modulus defining a linear material is a good approximation in the case of skull bone. Also it has been noted that bone is a brittle material as there is little yielding or permanent deformation induced before failure. A final property, which is observed when the specimen does not fracture through a strain gage destroying the electrical circuit, is the relaxation which takes place in the material when the load is released. The amount of strain induced is large indicating that bone is highly viscoelastic. Observations have shown that the bone assumes its initial strain level in about 15 minutes after the test has concluded. The viscoelastic properties will be quantified as the dynamic tests are carried out during the next several months.

A summary of the valid test results thus far obtained is shown in Table 1. The variation in breaking stress seems related to the homogeneity of the bone. Low breaking stresses seem to occur when there is some spongy bone, blood vessels, etc. present to initiate failure. These same features probably have something to do with the variation in values obtained for the tension modulus. The histological studies which are now in the early stages should yield some of the reasons for the variability. The average $E=2.11 \times 10^6$ psi and $\sigma_f = 9500$ psi are in line with other published figures for static bone tests.

TABLE I. TENSION TEST RESULTS

Specimen	Breaking stress (psi)		Tension Modulus (psi x 10^6)
VA1-2	2,750	(spongy)	-
VA1-4	5,220	(Spongy)	-
VA3-2	8,100		-
VA3-5	8,530		1.88
VA5-PL2	10,000		1.35
VA5-PL4	10,800		1.63
VA5-PL5	8,600		1.53
VA5-PL6	-		1.61
VA5-PL8	10,150		2.68
VA7-T1	12,500		2.86
VA7-T2	8,700		1.80
VA7-T5	11,630		2.79
VA8-PL4	13,750		1.66
VA9-PL2	10,800		2.70
Va9-PL3	11,100		2.38
VA9-PL5	9,500		2.58
VA9-PL6	6,100		-
VA9-PL7	7,700		-
VA12-PL2	4,980		-
VA12-PL3	10.800		1.94
VA12-PL4	9,250		1.96
VA12-PL5	10,300		2.07
VA12-PL6	7,100		

TABLE I. Continued

Specimen	Breaking stress (psi)	Tension Modulus (psi x 10^6)
VA13-PL1	4,760	1.8
VA13-PL2	4,830	2.25
VA13-PL4	9,400	2.0
VA13-PL5	9,300	1.95
VA14-PL2	9,660	-
VA14-PL3	10,300	2.32
VA14-PL5	13,200	-
VA14-PL6	11,000	2.02
VA16-PL2	10,500	1.98
VA16-PL3	9,500	-
VA16-PL4	10,820	2.42
VA16-PL5	11,700	2.96
VA16-PL7	9,950	1.85
VA32-PR3	13,300	1.79
VA32-PR5	13,200	1.68

STRUCTURAL COMPRESSION TESTS

Appendix D

INTRODUCTION

The objective of this test series was the determination of the crush failure characteristics of the diploë layer of the skull and the measurement of an average structural compression modulus of elasticity for rectangular blocks of skull bone. The compressive load was applied to the block in a direction perpendicular to the surface of the skull. A schematic of the test setup is shown in Figure 1. A series of seventy tests have been carried out to date on bone removed at autopsy and frozen until the test date.

INTRUMENTATION AND TESTING PROCEDURE

The testing of the specimens was done on a 10,000 lb. capacity Instron floor model testing machine. The specimens in the form of very small machined blocks were placed between a compression load cell and the traveling crosshead and then the rate of loading adjusted to the desired level. In the experiment, the rate of loading was 0.02 inches/min. The load was automatically recorded on a variable speed strip recorder.

The most typical curves obtained are shown in Figure 6. The curve shown at the top was the most frequently obtained. The loading of the specimen was stopped after the specimen was judged to have failed. There were several criteria for failure. One of these was that whenever the curve looked like the portion ABC in Figure 6 it was inevitable that the specimen had failed cataclysmically. All these failures were in the diploë. Another way of establishing failure was by visual inspection of the specimen and of

the load recording while the test was in progress. When no cataclysmic failure was observed, then either the failure was indicated by a sharp rise in the loading curve or by a constant horizontal loading curve as shown in the bottom two graphs in Figure 6. As mentioned above, failure in all cases was observed in the diploë. Also in most cases oil oozed out as the specimen was loaded. The amount of oil squeezed out varied widely.

MAKING OF TEST SPECIMENS

At autopsy, 3/4 inch diameter circular plugs were removed from the left and right parietal bones at various locations using a Stryker oscillating bone saw and plug cutter. Data was recorded on location and orientation of specimen, time of death, cause of death, age, sex, race, storage, etc. The specimen coding in Tables 1 and 2 provides a key to the data sheets.

The test specimens were made by first machining the circular discs flat on a milling machine using a jig for clamping the specimen. This piece was then sawed into smaller pieces and finished by machining it on a small drilling jig using an end mill as a cutter. The finished specimens were in the shape of very small blocks with all planes mutually perpendicular to each other. The specimens were loaded such that the load was applied perpendicular to the outer and inner table of the skull bone. The widths of the specimens varied from 0.20" to sizes considerably smaller; however, specimens were not very much larger than 0.20 inches. The height of most specimens varied between 0.160 inches and 0.230 inches.

METHOD OF DATA REDUCTION

Whenever the curves were as shown in Figure 6, the load as shown at A was taken as the failure load.

The modulus of elasticity E for compression was estimated from the portion DG in Figure 6. Quite often DG turned out to be nearly linear, in which case it was used in estimating E. When the portion DG was nonlinear, a straight line was fitted through it and this was used for estimating E.

The equation used for estimating the modulus of elasticity E for compression was as follows:

$$E = \frac{\Delta L}{\Delta \text{ Chart}} \times \frac{\ell_0}{A_0} \times \frac{\text{Chart Speed (in/min)}}{\text{Crosshead Speed (in/min)}}$$

where, E = Modulus of elasticity for compression, psi

ΔL = Load increment, lbf

Δ Chart = Distance on chart in inches corresponding to ΔL.

ℓ_0 = Original thickness of the specimen, inches

A_0 = Original cross-sectional area of the specimen, $(\text{inches})^2$

The breaking stress $\sigma_f = \frac{\text{Breaking Load lbf}}{A_0}$

RESULTS

A summary of the results obtained is shown below.

Values of the modulus of elasticity for compression, E, for the samples tested follow:

High E = 5.3×10^5 psi

Low E = 0.1035×10^5 psi

Median E = 1.70×10^5 psi

Arithmatic Mean E = 2.025×10^5 psi

Values of the breaking stress σ_f in compression for the samples tested are as follows:

High σ_f = 15.7 ksi

Low σ_f = 0.768 ksi

Median σ_f = 4.79 ksi

Arithmetic Mean σ_f = 5.3 ksi

The results are shown in Table I. The locations of the various specimens with respect to their coding are shown in Table II. Some average values of modulus are shown plotted in Figure 2 with respect to position on the skull. Each black spot in Figure 2 represents a circular area of approximately 3/4 inch diameter centered around the black spot. Since more than one block was tested from the same location from specimens obtained from different skulls, this chart shows more than one value at some points.

Figure 3 shows a plot of the modulus of elasticity E in compression vs. the breaking stress σ_f. There seems to be a substantial scatter in the data. However, this scatter seems to lie between a lower and an upper bound, the lower bound being the straight line whose equations is $\sigma_f = 0.675\ E + 550$, and the upper bound $\sigma_f = 2.45\ E$.

The distribution for the modulus of elasticity tends to approximate a normal distribution as shown in Figure 4 with a population mean of 2.1×10^5 psi and a standard deviation σ of 1.1×10^5 psi. Assuming a normal distribution it can be estimated that 70% of the skulls will have a value of modulus between 0.9×10^5 psi and 3.2×10^5 psi. The distribution of breaking stresses shown in Figure 5 does not plot as a straight line.

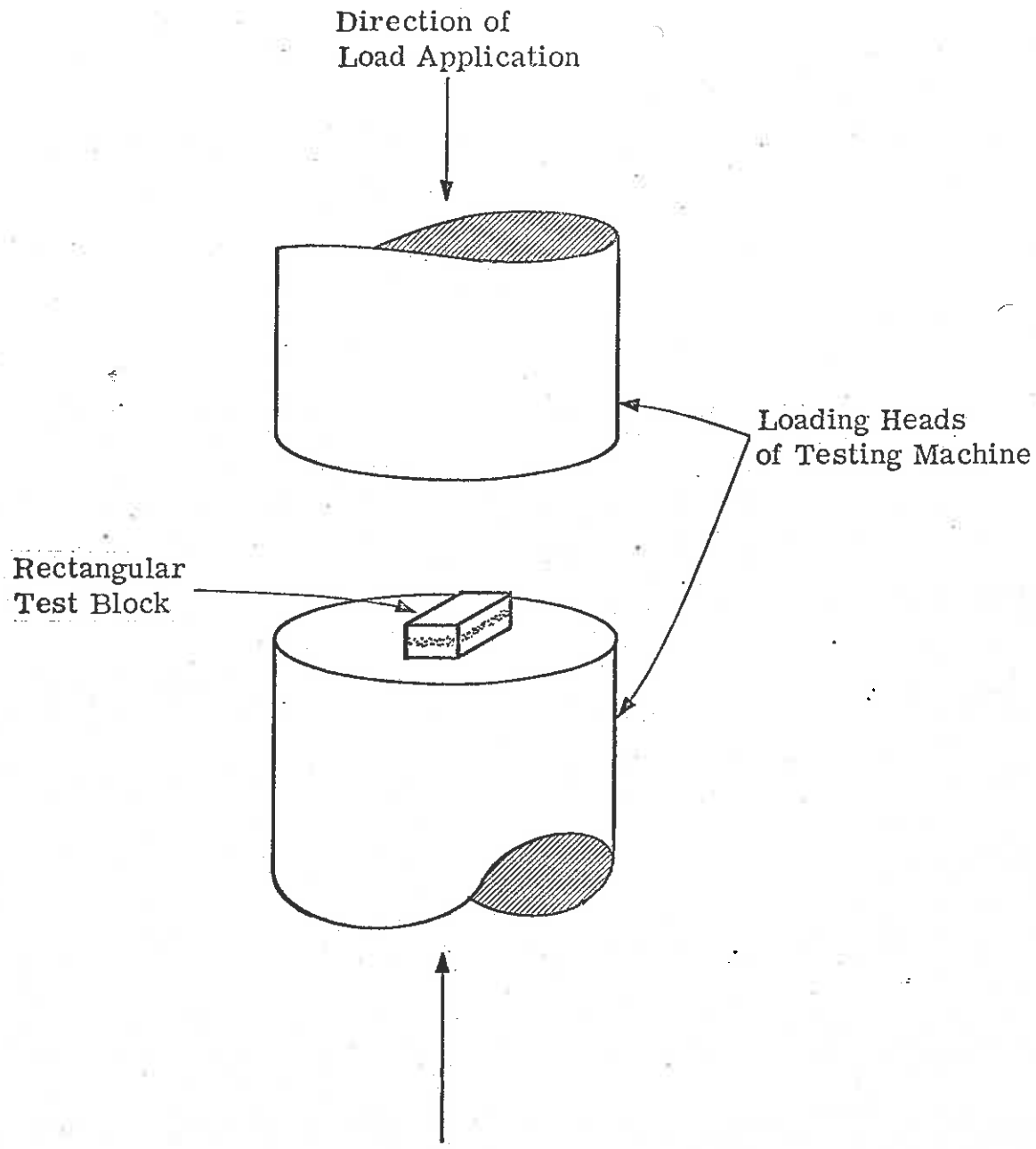

FIGURE 1. SCHEMATIC OF COMPRESSION TEST

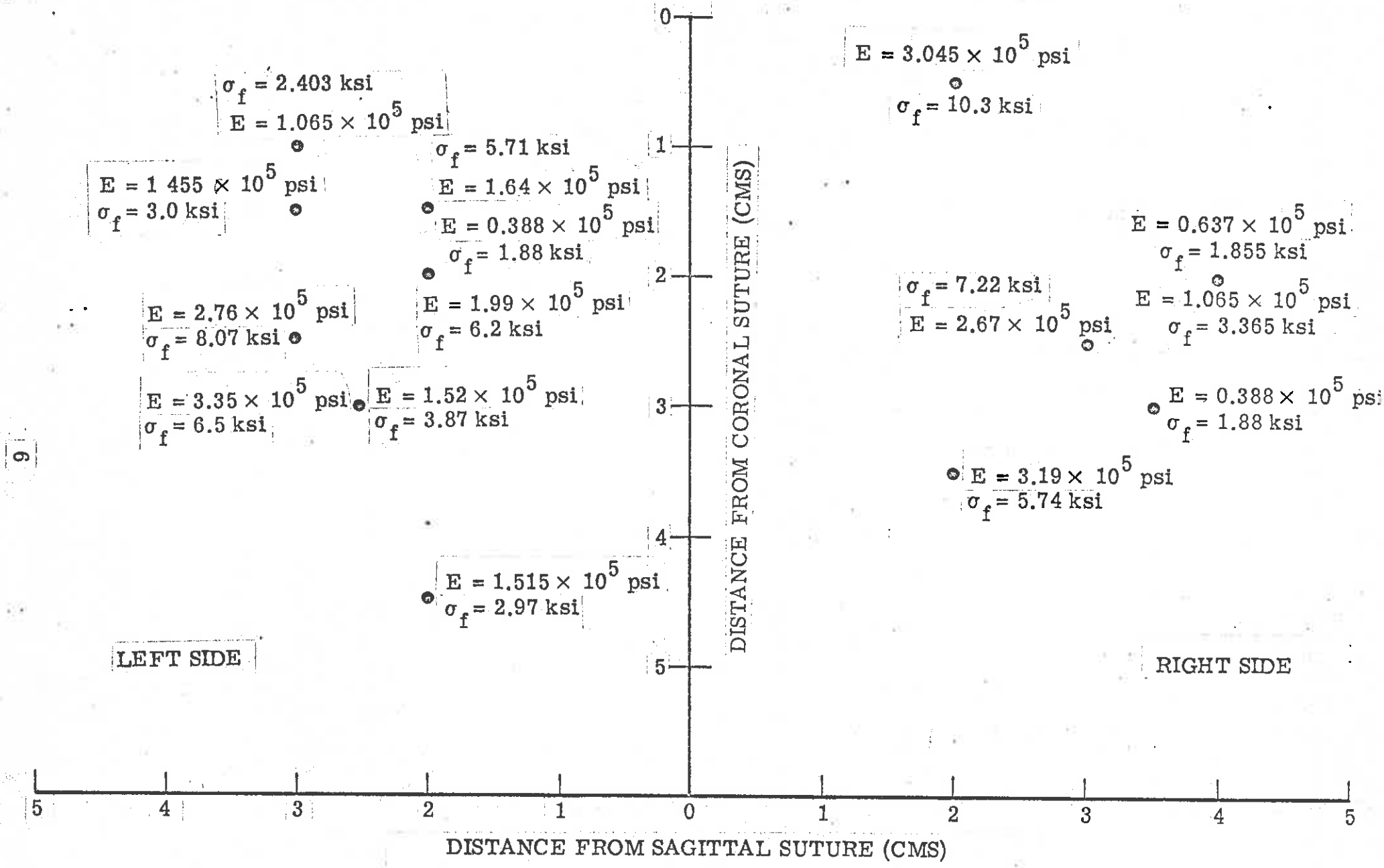

FIGURE 2. SPECIMEN LOCATION

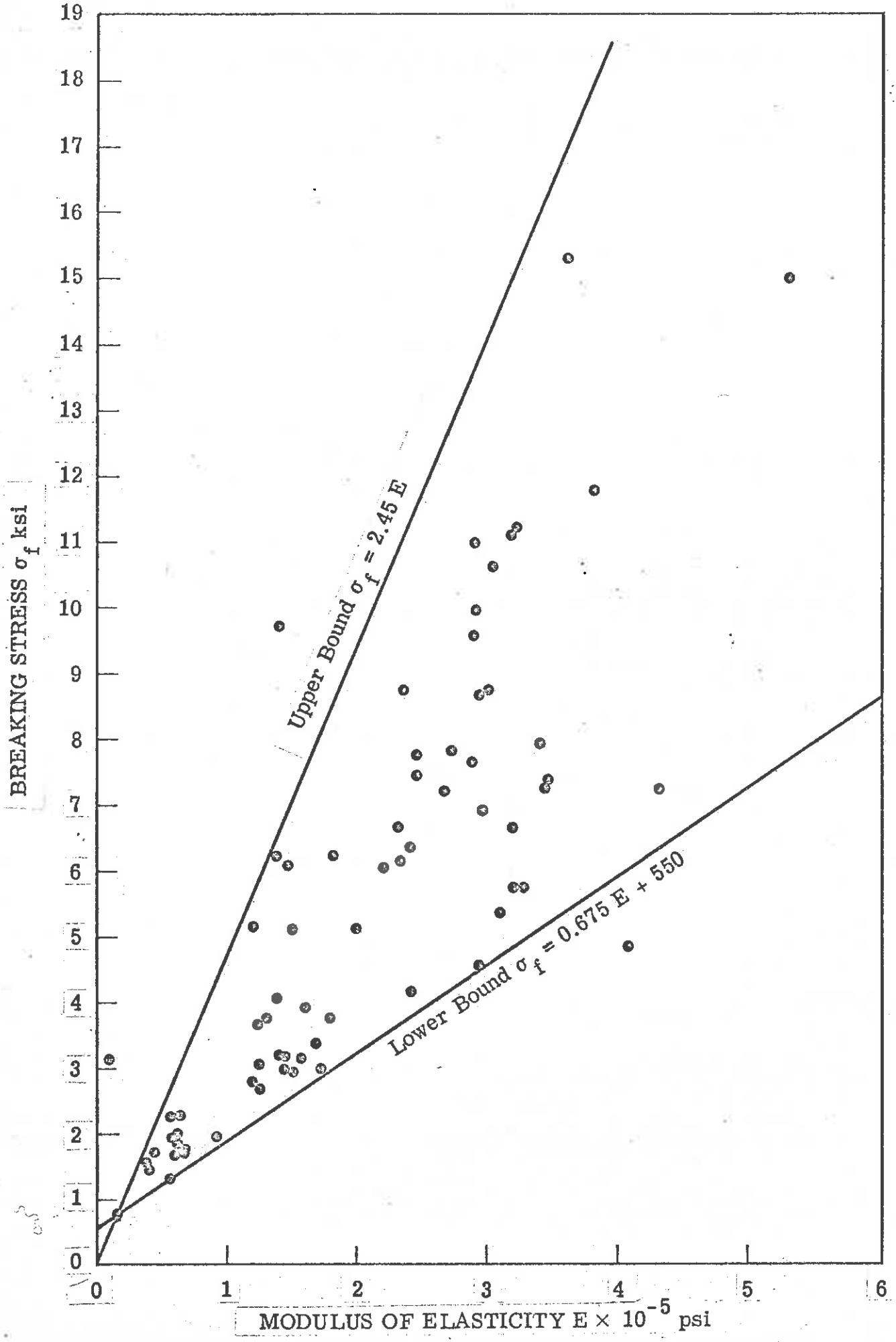

FIGURE 3. MODULUS OF ELASTICITY E psi VERSUS BREAKING STRESS σ_f ksi

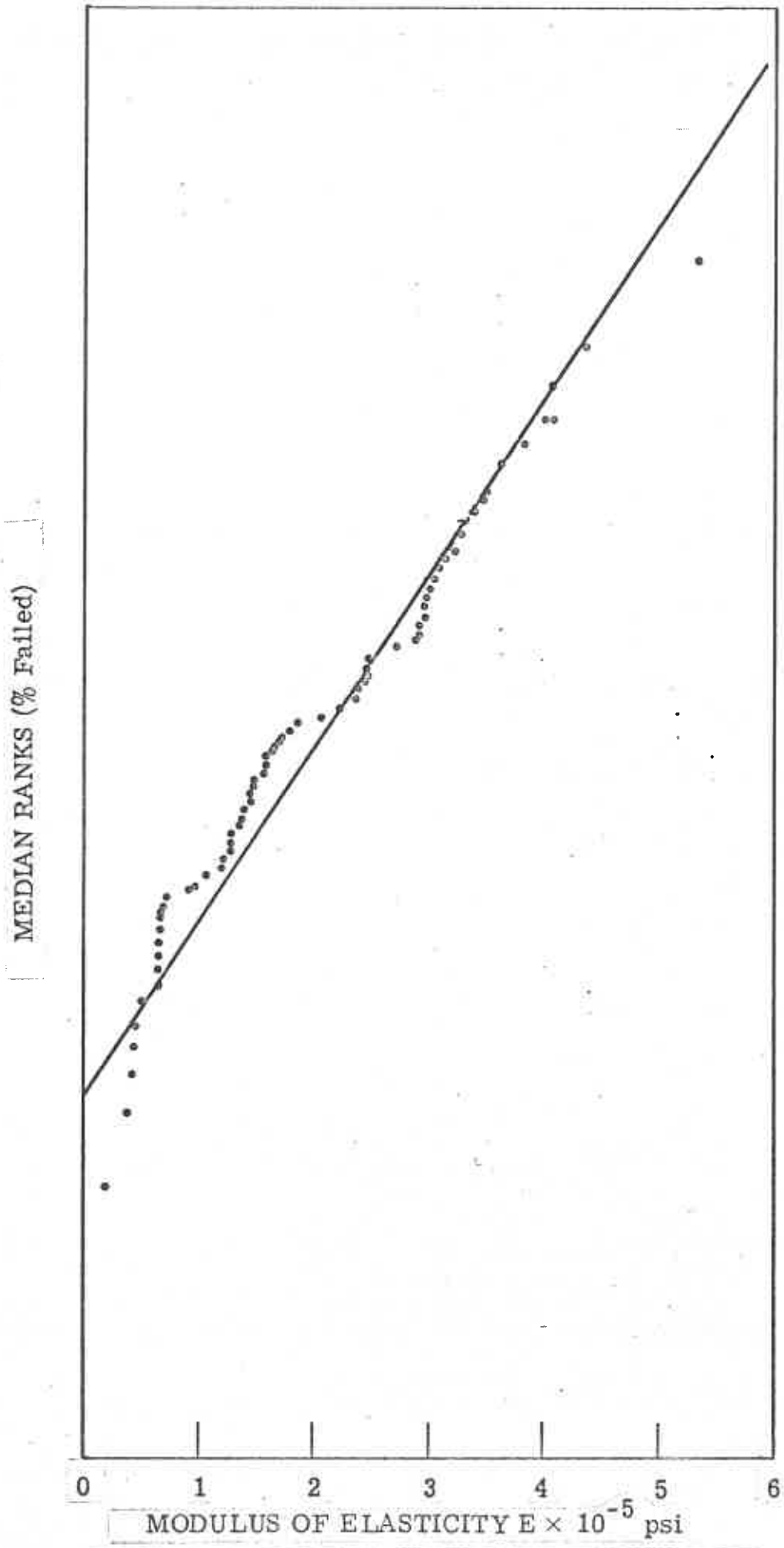

FIGURE 4. DISTRIBUTION OF ELASTIC MODULI

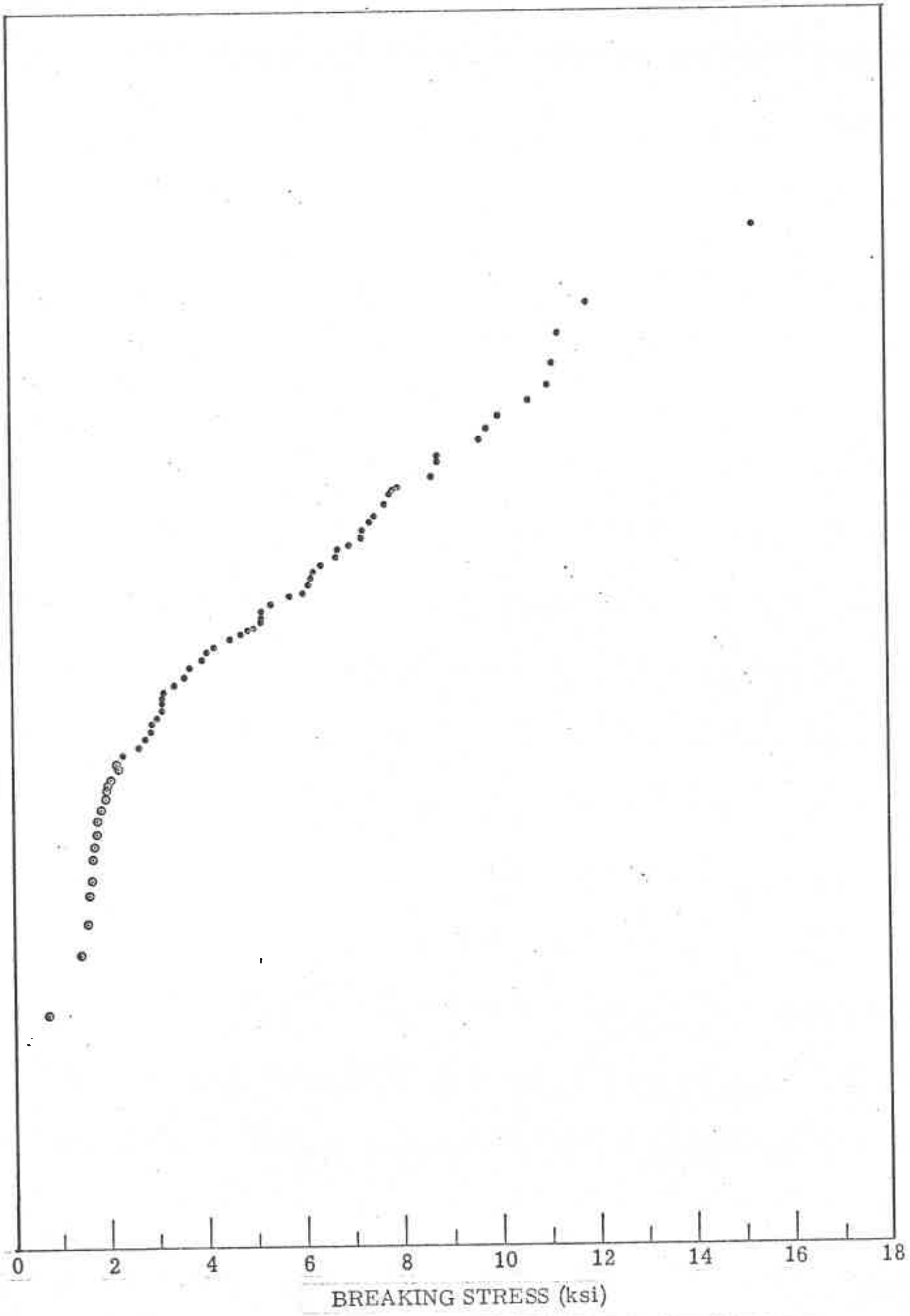

FIGURE 5. DISTRIBUTION OF BREAKING STRESSES

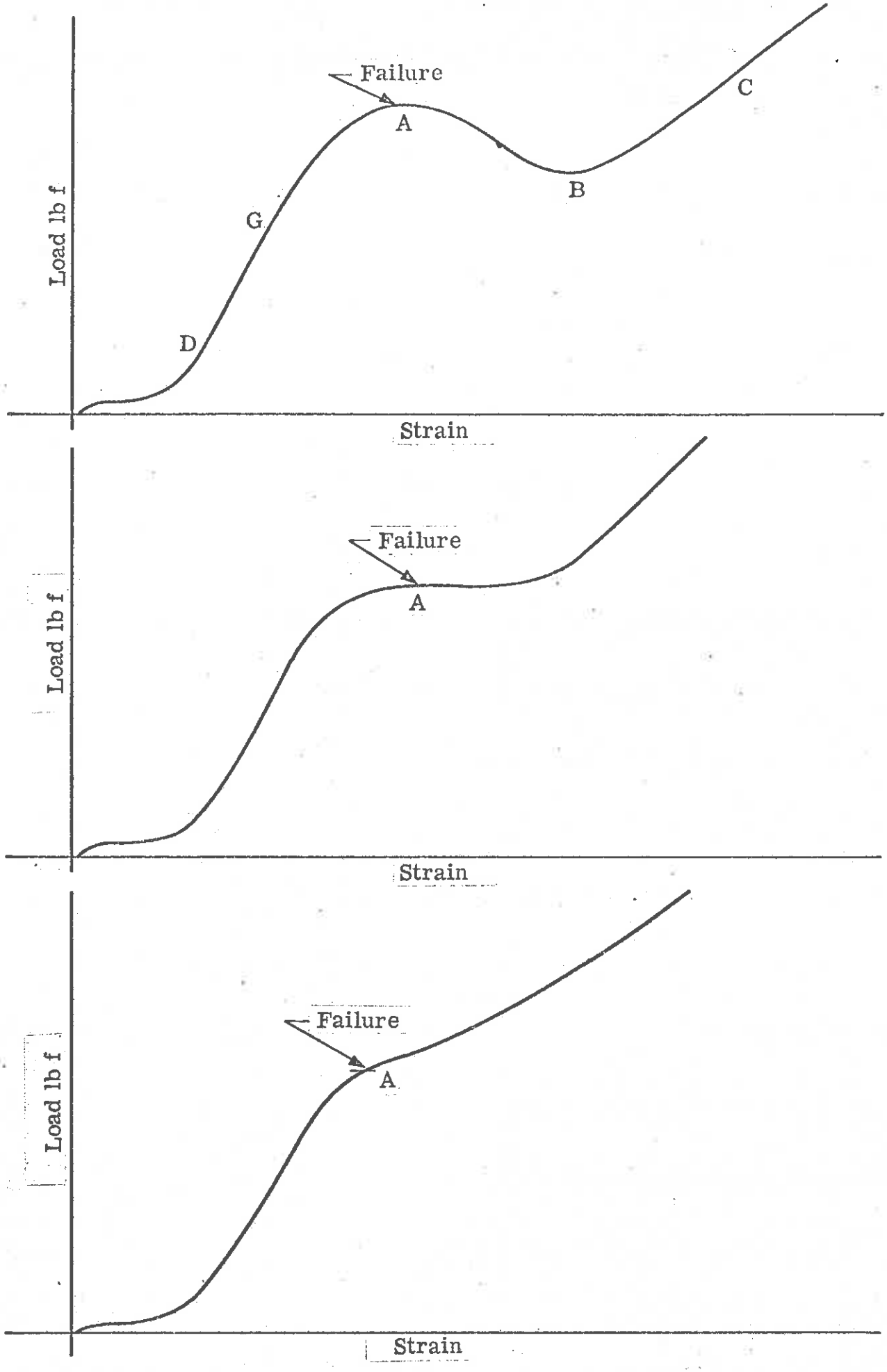

FIGURE 6. TYPICAL LOAD-STRAIN CURVES

TABLE I

Specimen Number	Average Compression Modulus of Elasticity E psi	Average Compression Breaking Stress ksi	Number of Compression Test Blocks From Specimen
UM-16-PL	1.52×10^5	3.87	4
UM-15-PL	3.35×10^5	6.5	6
UM-15-PR	3.19×10^5	5.74	4
UM-11-PL	1.64×10^5	5.71	5
UM-11-PR	2.67×10^5	7.22	4
UM-9-PL	1.065×10^5	2.403	3
UM-9-PR	0.637×10^5	1.855	3
UM-2-PL	2.76×10^5	8.07	6
UM-2-PR	3.04×10^5	10.3	6
UM-10-PL	0.677	1.795	3
UM-4-PL	1.455×10^5	3.00	6
UM-7-PR	0.388×10^5	1.88	5
UM-13-PL	0.446	1.84	3
UM-14-PL	1.515×10^5	2.97	1
UM-5-PL	1.99×10^5	6.2	5
UM-8-PR	1.065×10^5	3.365	3
UM-3P	4.24×10^5	14.26	3

TABLE II

Specimen Number	Location of Specimen		
	Posterior to Coronal Suture(cms)	Left of Sagital Suture(cms)	Right of Sagital Suture(cms)
UM-11-PL	1.5	2.0	
UM-11-PR	2.5		3.0
UM-15-PL	3.0	2.5	
UM-15-PR	3.5		2.0
UM-16-PL	3.0	2.5	
UM-9-PL	1.0	3.0	
UM-9-PR	2.0		4.0
UM-2-PL	3.0	2.5	
UM-2-PR	0.5		2.0
UM-10-PL	1.5	2.0	
UM-4-PL	3.0	1.5	
UM-7-PR	3.0		3.5
UM-14-PL	4.5	2.0	
UM-5-PL	2.0	2.0	
UM-8-PR	2.0		4.0
UM-13-PL			
UM-3P			

SHEAR TEST

Appendix E

The purpose of the shear test is to measure the shear strength of the diploë in human skull, when subjected to a single shear force as defined:

$$\tau_{max} = \frac{T \text{ (shear force)}}{A \text{ (area)}}$$

For this aspect of the study embalmed human calvariums are being used. These calvariums are from cadavers dissected by students at the University of Michigan Dental School. The age, sex, race, data and cause of death was recorded for each calvarium used. It will be noted (Table 1) that the test specimens came from different individuals, all of which are male and caucasian. The age, date and cause of death are similar for the three individuals.

After a significant number of tests have been completed using the fixed material from embalmed cadavers,a similar series of tests will be conducted using fresh unembalmed material. The fresh specimens will be removed at autopsy from cadavers at the University Hospital and Veterans Administration Hospital in Ann Arbor, Michigan. It will take considerably longer for this part of the shear study, as it will not be possible to remove as many plugs from each fresh cadaver. The disadvantage to this will be the difference in sex, age and cause of death of each individual.

For each of the three calvariums used so far in this study, circular plugs (Figure 1) are cut from the calvarium using a 3/8" I.D. Stryker Bone Plug Cutter with a Stryker Autopsy Saw. Water is generously applied to the blade of the cutter during the procedure to act as a lubricant and to prevent burning of the plug.

A reference system was designed to identify the location of bone plugs removed from the calvarium. This system is an adapation of the system used by Dr. James H. McElhaney of the Biomechanics Laboratories at West Virginia University.

The system is based on the two promient suture lines of the skull cap; coronal and sagittal. The procedure is as follows:

1. Locate the bregma as the intersection of the coronal and sagittal lines.
2. Locate the lambda as the intersection of the lamboidal and sagittal suture lines.
3. A straight line is drawn between these two points along the sagittal suture, and extended forward to the cut edge of the skull.
4. A straight line is drawn from the bregma, along the coronal suture, to the cut edge of the skull on both the left and right sides.
5. Using a compass, 1/2" arcs are drawn across the sagittal suture line using the bregma as the starting point. (Step 3) There will be 8 or 9 such arcs depending on the size of the skull. The 1/2" arcs are also drawn across, anterior to the cut edge of the skull (Figure 2).
6. The same procedure is used in drawing 1/2" arcs along the coronal suture line. Approximately 6 or 7 arcs can be drawn depending on the size of the skull.
7. With the use of a compass, lines are drawn parallel to the sagittal suture line (step 3) on both the left and right halves of the skull cap.
8. Lines are drawn parallel to the coronal suture lines (step 4) on both the left and the right halves of the skull. These lines are posterior to the lamboidal suture, and anterior to the cut edge.

The spaces between the lines parallel to the sagittal suture on the left half of the skull are lettered A,B,C,etc. On the right side of the skull the corresponding spaces are lettered AA, BB, CC, etc. (Figure 3). The spaces between the lines parallel and posterior to the coronal suture are numbered 1, 2, 3, etc. (Figure 3). The spaces anterior to the coronal suture are numbered 21, 22, 23, etc. The plugs are removed from the squares formed by the intersection of the lines, and are given both a letter and number to correspond to the space from which they were removed; A-4, B-6, CC-6, etc. The calvarium will have a sieve-like appearance when all plugs have been removed (Figure 4).

After the specimen has been removed from the calvarium, the diameter is measured, and then it is placed in specially designed grips, (Figure 5). The load is applied by a 10,000 lb. capacity floor model Instron testing machine. It is important that the specimen be placed in the middle of the grip (Figure 6) so that the shear will occur through the diplöe. When the specimen is positioned the shear force is applied. This force is recorded on the Instron chart and the failure load is determined.

The shear stress is formulated using the following calculation.

$$\text{Area} = \frac{\pi d^2}{4}$$

$$\text{Shear stress} = \frac{\text{failure load}}{\text{area}}$$

It would be premature to make any definite conclusion concerning the shear data obtained at this point. There does appear to be a pattern developing from the shear tests performed on the three embalmed calvariums which have been completed. The pattern observed so far is that plugs

taken from the same locations, but from different skulls, appear to have a shear stress which at times is similar. Plugs C-6 (Table-2) from the three skulls have a failure shearing stress which is within 60 psi. Many of the plugs taken from the three skulls at the same location have a shear stress which is within 100-200 psi.

With considerably more testing on both embalmed and unembalmed material, any pattern which may be developing at this point will be further proven out.

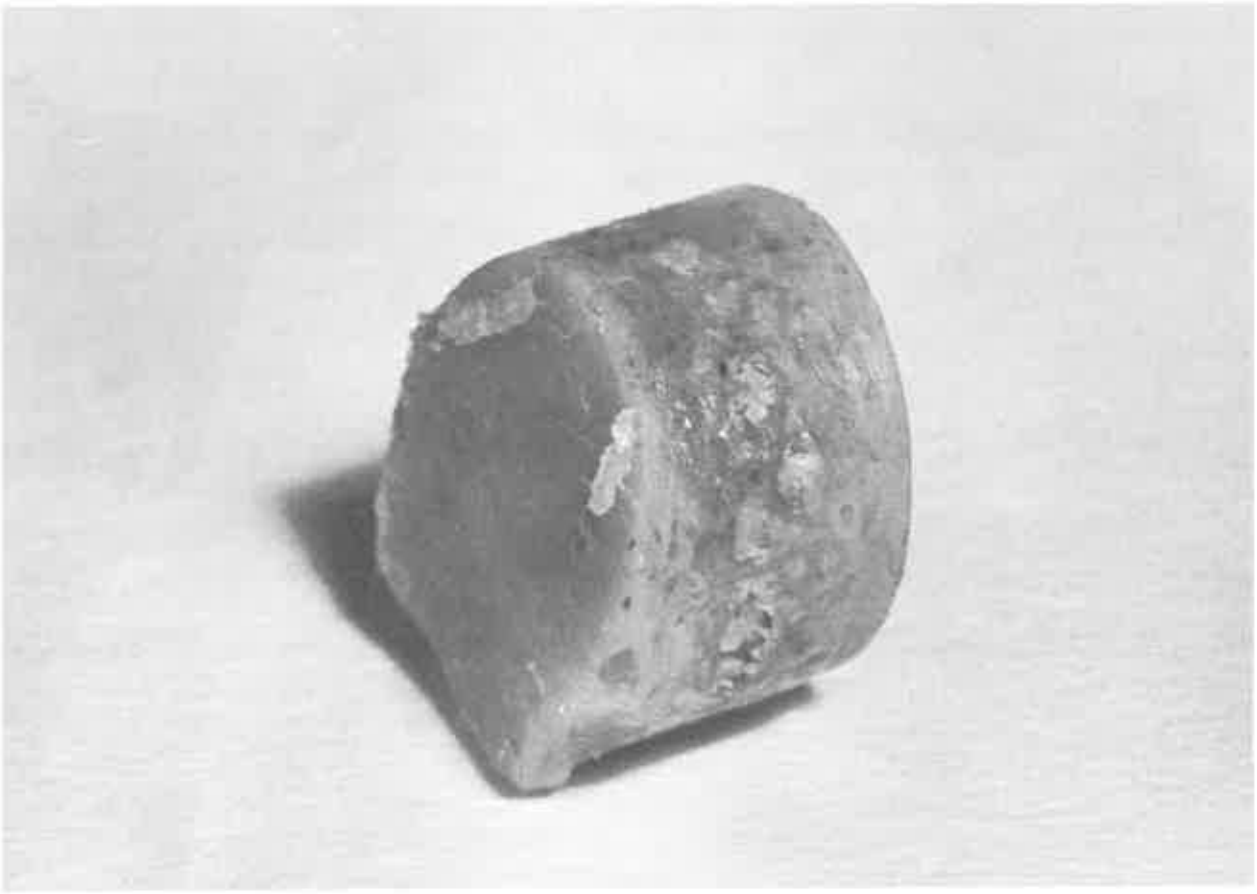

FIGURE 1. 3/8-IN BONE PLUG

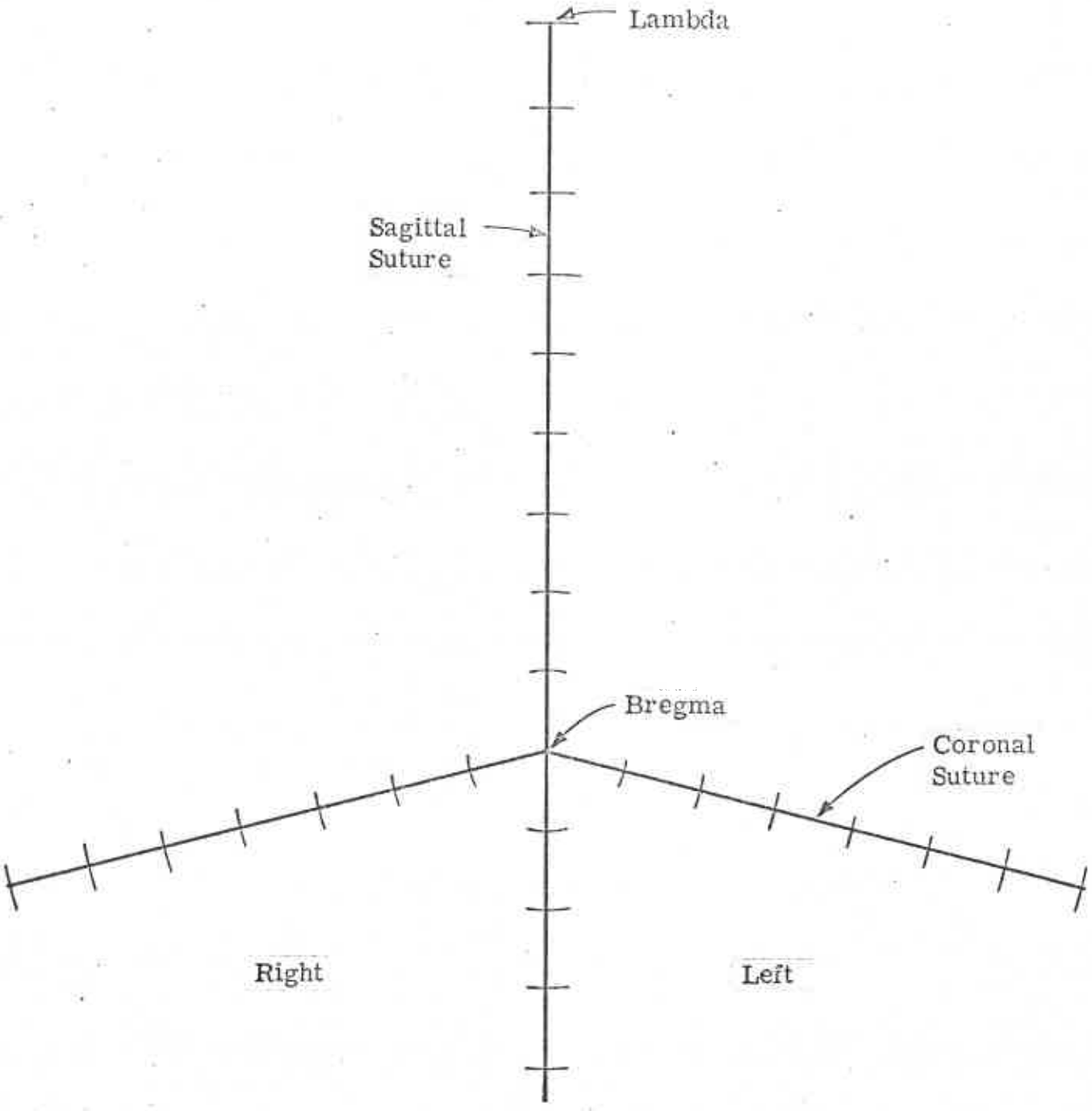

FIGURE 2. DIAGRAM OF SUTURE LINES WITH 1/2" ARCS

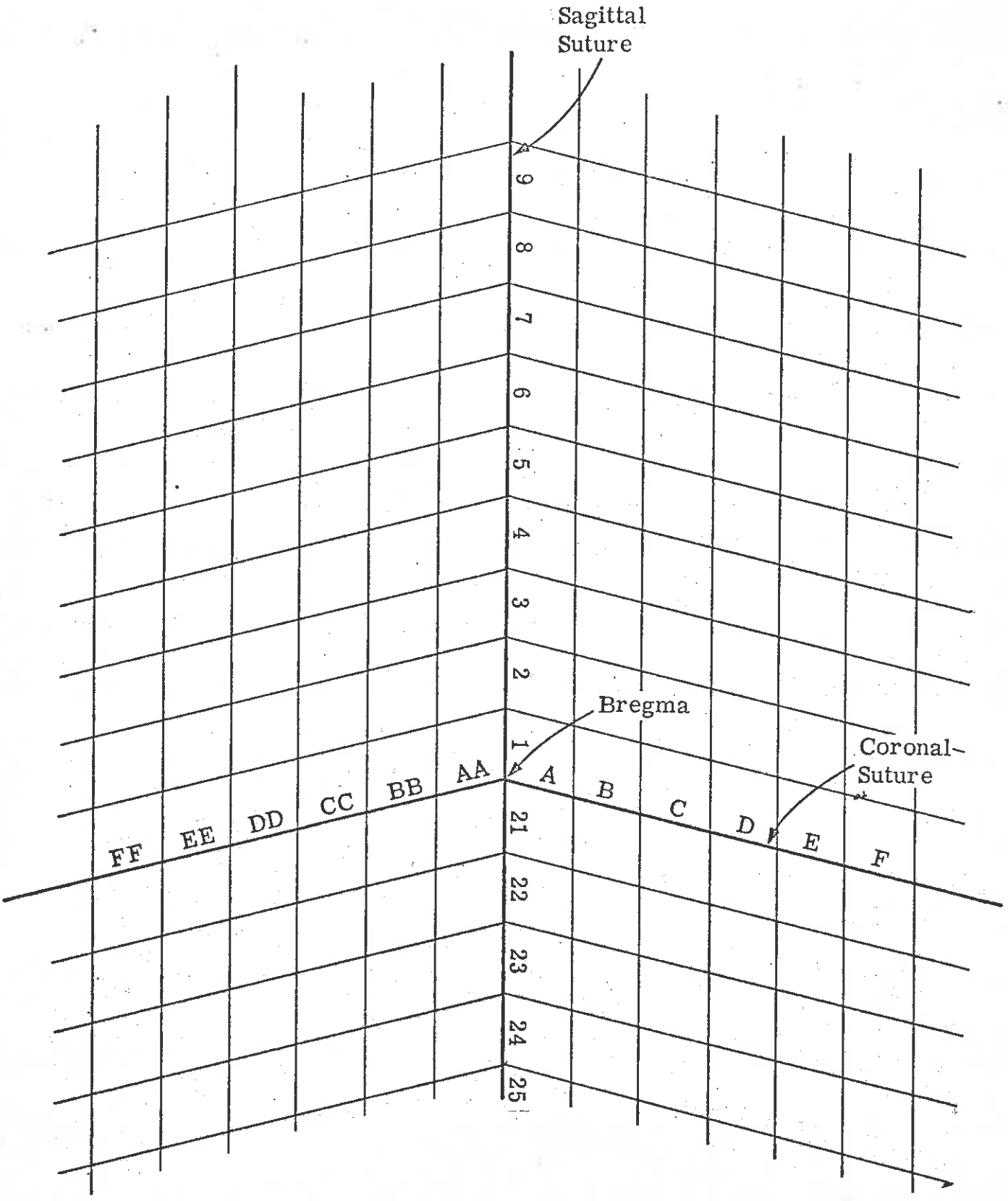

FIGURE 3. REFERENCE SYSTEM FOR CALVARIUM

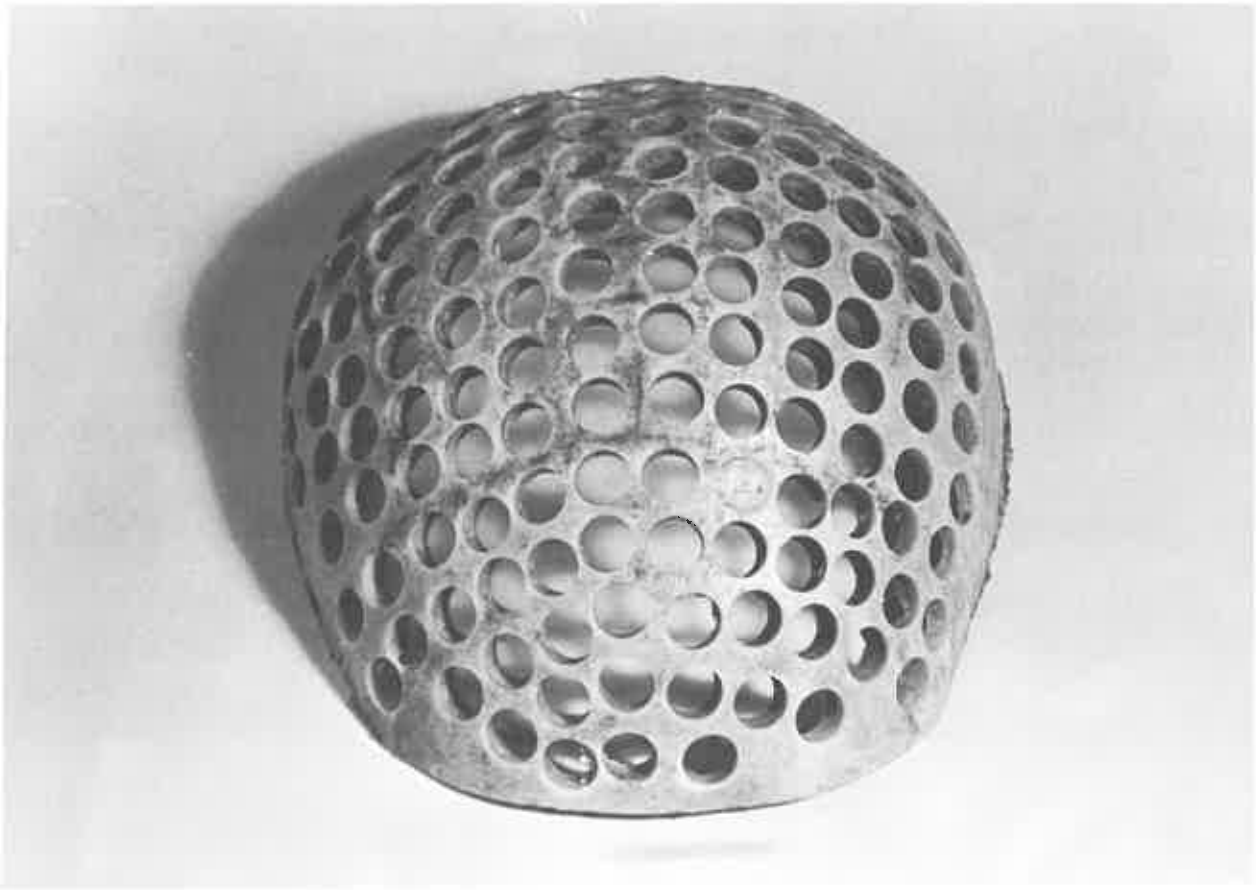

FIGURE 4. CUT CALVARIUM

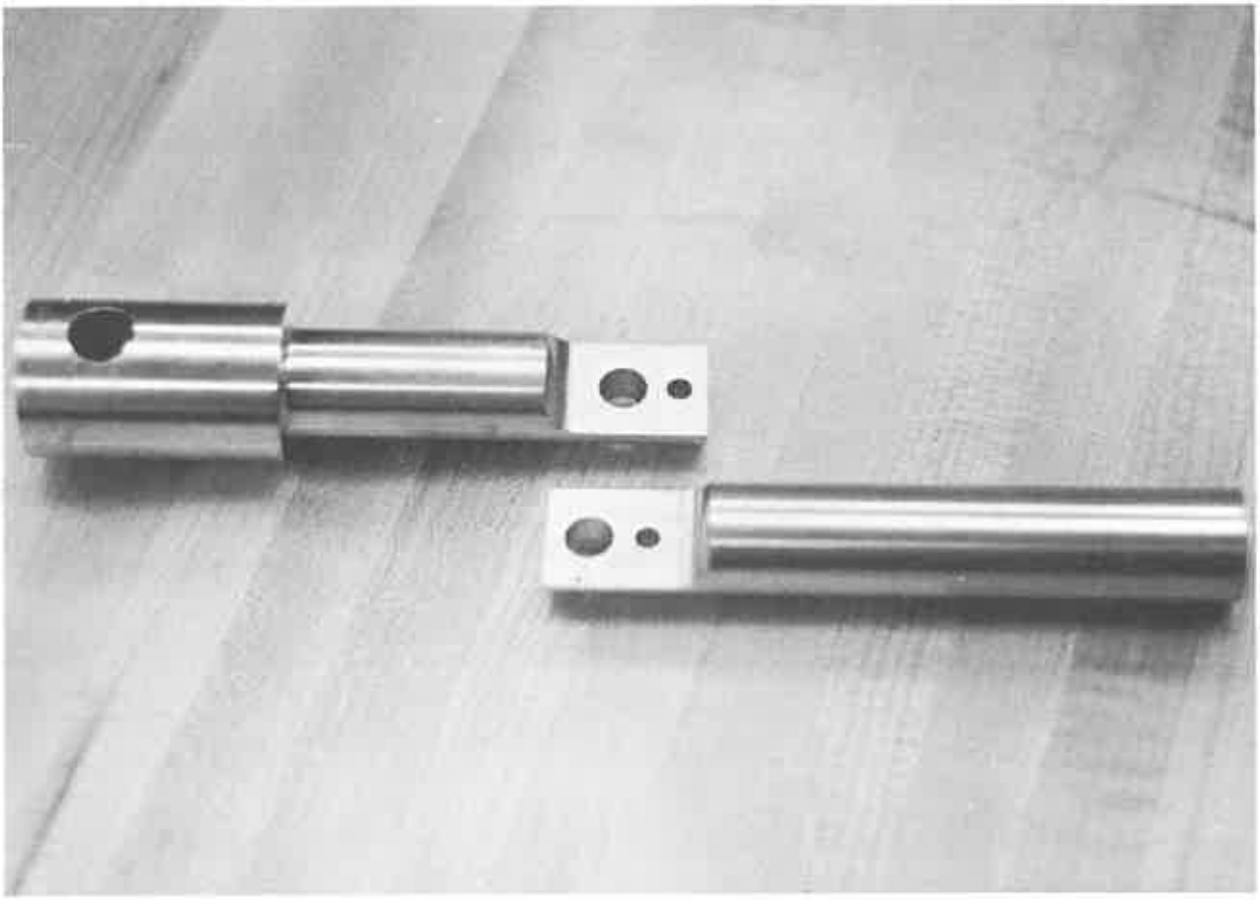

FIGURE 5. SHEAR GRIPS

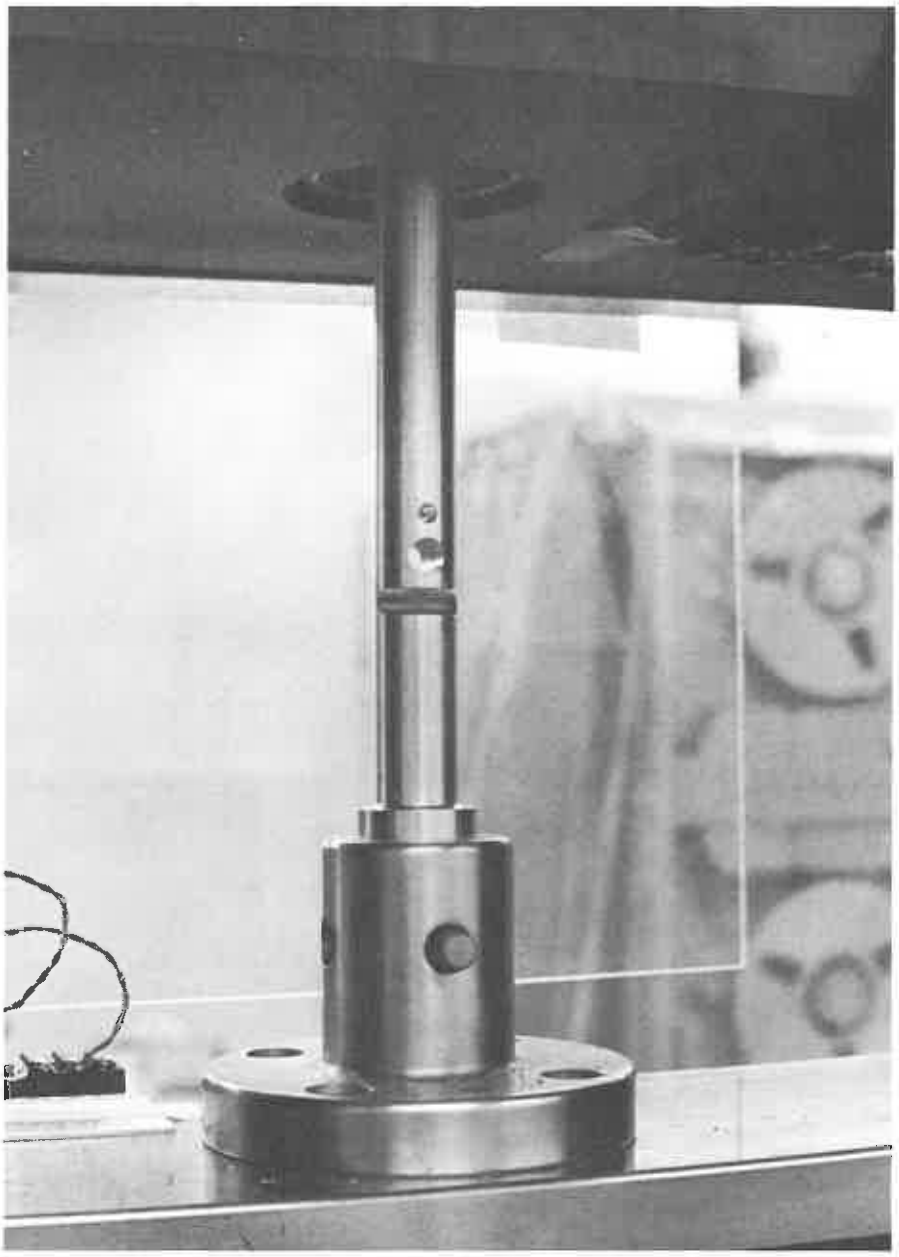

FIGURE 6. SHEAR TEST SETUP

TABLE 1

SPECIMEN TESTED #1

Age: 68

Sex: male

Race: caucasian

Date of death: 1-6-67

Cause of death: myocardial infarction

SPECIMEN TESTED #2

Age: 66

Sex: male

Race: caucasian

Date of death: 4-23-67

Cause of death: Congestive heart failure

SPECIMEN TESTED #3

Age: 73

Sex: male

Race: caucasian

Date of death: 12-30-66

Cause of death: Systicema due to pyelonephoitis

TABLE 2

SHEAR DATA FROM CADAVER MATERIAL

	ST-1	ST-2	ST-3
A-1	N.T.	S = 2255 psi	S = 3163 psi
A-2	S = 2851	S = 1806 psi	N.G.
A-3	S - 2736 psi	S = 2108 psi	N.G.
A-4	S = 2007 psi	S = 2507 psi	S = 1714 psi
A-5	S = 2647 psi	S = 2358 psi	S = 2306 psi
A-6	N.T.	S = 2162 psi	S = 1786 psi
A-7	S = 2539 psi	S = 2124 psi	S = 1908 psi
A-8	S = 2821 psi	S = 1892 psi	S = 1617 psi
A-9	S = 2127 psi	S = 2343 psi	S = 2181 psi
A-10	N.T.	N.T.	N.T.
AA-1	N.T.	S = 1454 psi	S = 2661 psi
AA-2	N.T.	S = 2184 psi	N.G.
AA-3	S = 1595 psi	S = 2705 psi	S = 2901 psi
AA-4	S = 1686 psi	S = 2447 psi	S = 1823 psi
AA-5	S = 1884 psi	S = 1908 psi	S = 2294 psi
AA-6	S = 1830 psi	S - 2765 psi	S = 1978 psi
AA-7	S = 2043 psi	S = 2995 psi	S = 2571 psi
AA-8	S = 2323 psi	S = 1382 psi	S = 2543 psi
AA-9	N. G.	S = 1853	N.G.
AA-10	N.G.	N.T.	N.T.

TABLE 2 Continued
Page 2

	ST-1	ST-2	ST-3
B-1	S = 2392 psi	S = 2065 psi	S = 2502 psi
B-2	N.G.	S = 1855 psi	N.G.
B-3	N.T	S = 1106 psi	S = 2103 psi
B-4	S - 2352 psi	S = 1778 psi	S = 2589 psi
B-5	S = 1804 psi	S = 2354 psi	S = 2188 psi
B-6	N.T.	S = 2138 psi	S = 1914 psi
B-7	S = 2447 psi	N.G.	S = 2218 psi
B-8	S = 2106 psi	S = 2081 psi	S = 2521 psi
B-9	S = 2374 psi	S = 1094 psi	N. T.
B-10	S = 2841 psi		N.T.
BB-1	N.T.	S = 2019 psi	S = 2694 psi
BB-2	N.T.	S = 1741 psi	N.G.
BB-3	N.T.	S = 1935 psi	S = 2507 psi
BB-4	N.T.	S = 1861 psi	S = 1969 psi
BB-5	N.T.	S = 2282 psi	S = 1752 psi
BB-6	N.G.	N.G.	S = 2172 psi
BB-7	S = 2051 psi	N.G.	S = 1977 psi
BB-8	S = 1803 psi	S = 1817 psi	S = 2106 psi
BB-9	N.G.	S = 1844 psi	S = 1869 psi
BB-10	S = 2474	N.T.	N.T.

TABLE 2 Continued
Page 3

	ST-1	ST-2	ST-3
C-1	S = 2136 psi	S = 1908 psi	S = 2371 psi
C-2	S = 1731 psi	S = 1869 psi	S = 2158 psi
C-3	S = 1907 psi	S = 1831 psi	S = 2507 psi
C-4	S = 1803 psi	S = 2021 psi	S = 2221 psi
C-5	S = 1959 psi	S = 1459 psi	S = 1696 psi
C-6	S = 1784 psi	S = 1844 psi	S = 1795 psi
C-7	N.G.	S = 2442 psi	S = 2526 psi
C-8	S = 2327 psi	S = 2014 psi	S = 1687 psi
C-9	S = 2421 psi	S = 2371 psi	N.T.
C-10	S = 2814 psi	N.T.	N.T.
CC-1	N.T.	N.G.	S = 2525 psi
CC-2	N.T.	S = 2028 psi	S = 2267 psi
CC-3	S = 2091 psi	S = 1622 psi	S = 1989 psi
CC-4	N.T.	S = 1646 psi	S = 1796 psi
CC-5	S = 2230 psi	S = 2246 psi	S = 1375 psi
CC-6	S = 1609 psi	S = 2387 psi	S = 1103 psi
CC-7	S = 1823 psi	S = 2406 psi	S = 1934 psi
CC-8	S = 2094 psi	N.G.	S = 2218 psi
CC-9	N.G.	N.G.	N.T.
CC-10	N.T.	N.T.	N.T.

TABLE 2 Continued
Page 4

	ST-1	ST-2	ST-3
D-1	N.T.	S = 1558 psi	S = 1569 psi
D-2	N.T.	S = 1723 psi	S = 2151 psi
D-3	S = 1712 psi	S = 1879 psi	S = 2124 psi
D-4	S = 1749 psi	S = 1969 psi	S = 2136 psi
D-5	S = 1951 psi	S = 2047 psi	S = 1085 psi
D-6	S = 1893 psi	S = 1919 psi	S = 1851 psi
D-7	S = 2131 psi	S = 2197 psi	S = 1963 psi
D-8	S = 2365	S = 1604 psi	N.T.
D-9	S = 2598	S = 2306 psi	N.T.
D-10	N.G.		N.T.
DD-1	N.G.	S = 1465 psi	S = 2158 psi
DD-2	S = 1731 psi	S = 1567 psi	S = 2188 psi
DD-3	S - 1619 psi	S = 1983 psi	S = 2267 psi
DD-4	S = 1741 psi	S = 1959 psi	S = 1622 psi
DD-5	S = 1952 psi	S = 1687 psi	S = 1368 psi
DD-6	N.T.	S = 1806 psi	S = 1569 psi
DD-7	N.G.	N.G.	S = 1678 psi
DD-8	S = 2342 psi	N.T.	N.T.
DD-9	S = 2293 psi	N.T.	N.T.
DD-10	N.T.	N.T.	N.T.

TABLE 2 Continued
Page 5

	ST-1	ST-2	ST-3
E-1	N.T.	S = 1297 psi	N.G.
E-2	S = 1425 psi	S = 1506 psi	S = 2304 psi
E-3	S = 1523 psi	S = 1548 psi	S - 2088 psi
E-4	S = 2130 psi	S = 1914 psi	S = 1301 psi
E-5	S = 1959 psi	S = 1769 psi	S = 1085 psi
E-6	S = 1861 psi	S = 1946 psi	N.G.
E-7	S = 1649 psi	S = 1732 psi	S = 1191 psi
E-8	S = 2267 psi	S = 2383 psi	N.T.
E-9	S = 2261 psi	N.T.	N.T.
E-10	N.T.	N.T.	N.T.
EE-1	S = 1523 psi	S = 1456 psi	N.G.
EE-2	N.G.	S = 1914 psi	S = 2194 psi
EE-3	S = 2023 psi	S = 2111 psi	S = 1551 psi
EE-4	S = 1991 psi	S = 1739 psi	S = 1537 psi
EE-5	S = 2030 psi	S = 2074 psi	S = 1151 psi
EE-6	N.T.	S = 2136 psi	S = 1276 psi
EE-7	S = 2344 psi	S = 1833 psi	S = 1468 psi
EE-8	S = 2142 psi	N.T.	N.T.
EE-9	S = 2096 psi	N.T.	N.T.
EE-10	N.T.	N.T.	N.T.

TABLE 2 Continued
Page 6

	ST-1	ST-2	ST-3
F-1	N.T.	S = 1082 psi	N.G.
F-2	N.G.	N.G.	S = 2304 psi
F-3	S = 2026 psi	S = 2148 psi	N.G.
F-4	S = 1916 psi	S = 1595 psi	S = 1823 psi
F-5	N.T.	S = 2026 psi	S = 1887 psi
F-6	N.T.	S = 2227 psi	S = 2008 psi
F-7	S = 7004 psi	S = 2374 psi	N.T.
F-8	N.G.	N.T.	N.T.
F-9	N.G.	N.T.	N.T.
F-10		N.T	N.T.
FF-1	N.T.	S = 1168 psi	N.G.
FF-2	N.T.	S = 1833 psi	S = 2579 psi
FF-3	S = 2096 psi	S = 2026 psi	S = 1968 psi
FF-4	N.G.	N.G.	S = 1813 psi
FF-5	S = 1732 psi	S = 2206 psi	S = 1549 psi
FF-6	N.T.	S = 1952 psi	S = 1382 psi
FF-7	S = 1952 psi	S = 2062 psi	N.T.
FF-8	N.G.	N.T.	N.T.
FF-9	S = 2442 psi	N.T.	N.T.
FF-10	S = 2276 psi	N.T.	N.T.

TABLE 2 Continued
Page 7

	ST-1	ST-2	St-3
G-4	N.T.	N.T.	S = 2203 psi
G-5	N.T.	S = 1805 psi	S = 1884 psi
G-6	N.T.	S = 2148 psi	N.T.
G-7	S = 2172 psi	N.T.	N.T.
G-8	S = 2276 psi	N.T.	N.T.
GG-2	S = 2304 psi		
GG-3	S = 1705 psi		
GG-4	S = 1732 psi		

TABLE 2 Continued
Page 8

	ST-2	ST-3
A-21	S = 2230 psi	S = 2267 psi
A-22	S = 1418 psi	S = 2164 psi
A-23	N.G.	S = 2056 psi
A-24	S = 1413 psi	S = 2219 psi
A-25	S = 1687 psi	S = 1131 psi
AA-21		S = 1682 psi
AA-27	S = 2039 psi	S = 1978 psi
AA-23	S = 1391 psi	
AA-24	S = 1659 psi	S = 1641 psi
AA-25	S = 1418 psi	S = 1568 psi
B-21	N.T.	S = 1459 psi
B-22		S = 1613 psi
B-23	S = 2363 psi	S = 2324 psi
B-24	S = 2326 psi	S = 1914 psi
B-25	N.T.	N.T.
BB-21		S = 1539 psi
BB-22	S = 1696 psi	S = 1329 psi
BB-23	S = 2184 psi	S = 1881 psi
BB-24	S = 2131 psi	S = 1932 psi
BB-25	S = 1834 psi	S = 1185 psi

TABLE 2 Continued
Page 9

	ST-2	ST-3
C-21	S = 1603 psi	S = 979 psi
C-22	S = 1539 psi	S = 816 psi
C-23	S = 1277 psi	S = 1131 psi
C-24	N.G.	S = 962 psi
C-25	N.T.	N.T.
CC-21	N.T.	S = 2319 psi
CC-22	S = 1539 psi	S = 1226 psi
CC-23	S = 1659 psi	S = 1128 psi
CC-24	S = 1631 psi	S = 939 psi
D-21	S = 1411 psi	S = 1506 psi
D-22	N.T.	S = 936 psi
D-23	S = 1604 psi	S = 1031 psi
DD-21	N.T.	S = 1529 psi
DD-22	S = 1779 psi	S = 894 psi
DD-23	S = 2055 psi	S = 1191 psi

TABLE 2 Continued
Page 10

	ST-2	ST-3
E-21	S = 2275 psi	S = 2383 psi
E-22	S = 1764 psi	S = 939 psi
EE-21	N.T.	S = 2062 psi
EE-22	S = 1696 psi	S = 1382 psi
EE-23	N.G.	S = 834 psi
F-21	S = 1448 psi	S = 1384 psi
F-22	S = 1558 psi	S = 1221 psi
FF-21	N.T.	S = 1531 psi
FF-22	S = 1491 psi	S = 1996 psi

SKIN PUNCTURE TESTS

Appendix F

SKIN PUNCTURE TESTS

The purpose of this aspect of the Head Injury Project is to study the strength of the human scalp by the use of penetrometer. (Fig. 1) The penetrometer is designed to measure skin strength. At times, in collisions, the skin is pinched between bone and a rigid object. Penetrometer readings give an indication of the plyability of skin, and to a certain degree it also indicates the tensile strength of skin. The skin puncture research was started in the past six weeks and will be continued for an additional 10-12 months.

This study is carried out on unembalmed human cadavers. Measurements are taken in the autopsy room at the University Hospital and the Veterans Administration Hospital in Ann Arbor, Michigan. The cause and time of death, length of hospitalization, age, sex and race are also recorded.

At autopsy the pathologist makes an incision in the scalp across the top of the head from behind one ear to the opposite ear. The scalp is reflected forward for the removal of the skull cap and the subsequent removal of the brain. The penetrometer readings are taken 1/2" from the cut edge of the scalp. Three areas were chosen as the test sites: the left and right sides just behind and above the ear and at the midline. Also, three separate measurements are taken at each site.

In addition to recording the penetration strength of the scalp for each of the three locations, the orientation of the penetrometer is also recorded, i.e., whether it is parallel or perpendicular to the cut edge of the scalp.

Thus far in the study, penetration readings have been conducted on twenty-one subjects giving 63 data points. Preliminary data indicates that scalp penetration resistance is in the 15-16 lb. range. There may be some age differences in that a greater spread of the data points were noted above 45 years. This is especially true for the readings at the midline. However, it will be some months before any definite conclusion can be drawn from these data. A technique and method for testing has been established with the first twenty-one cases. In another 6-12 months there should be an adequate number of cases, approximately 250, to determine the puncture resistance of the human scalp.

It is planned that this procedure will be carried out on embalmed human cadavers in the near future. The results obtained from the cadavers will be then compared with the autopsy specimens. Also, data will be obtained from fresh cadavers prior to embalming and at the same location after embalming.

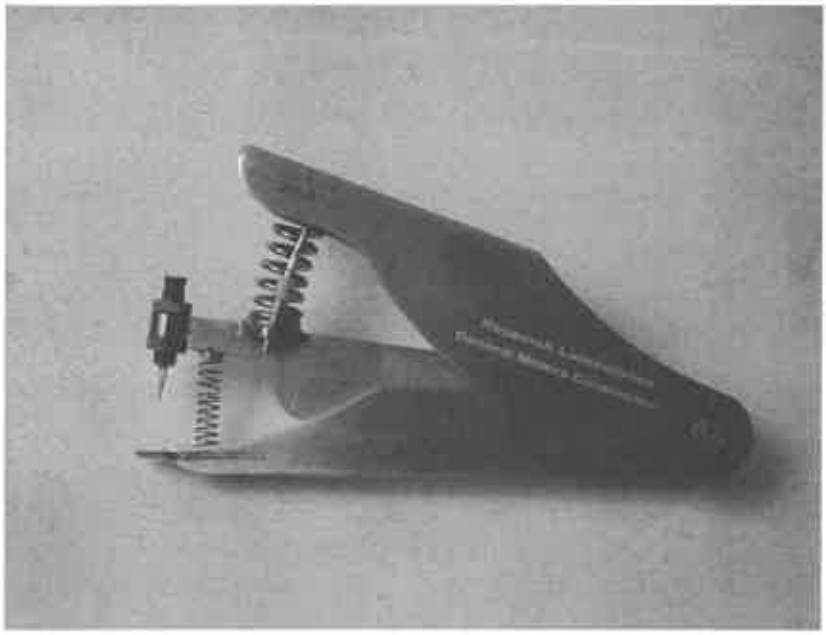

FIGURE 1. PENETROMETER

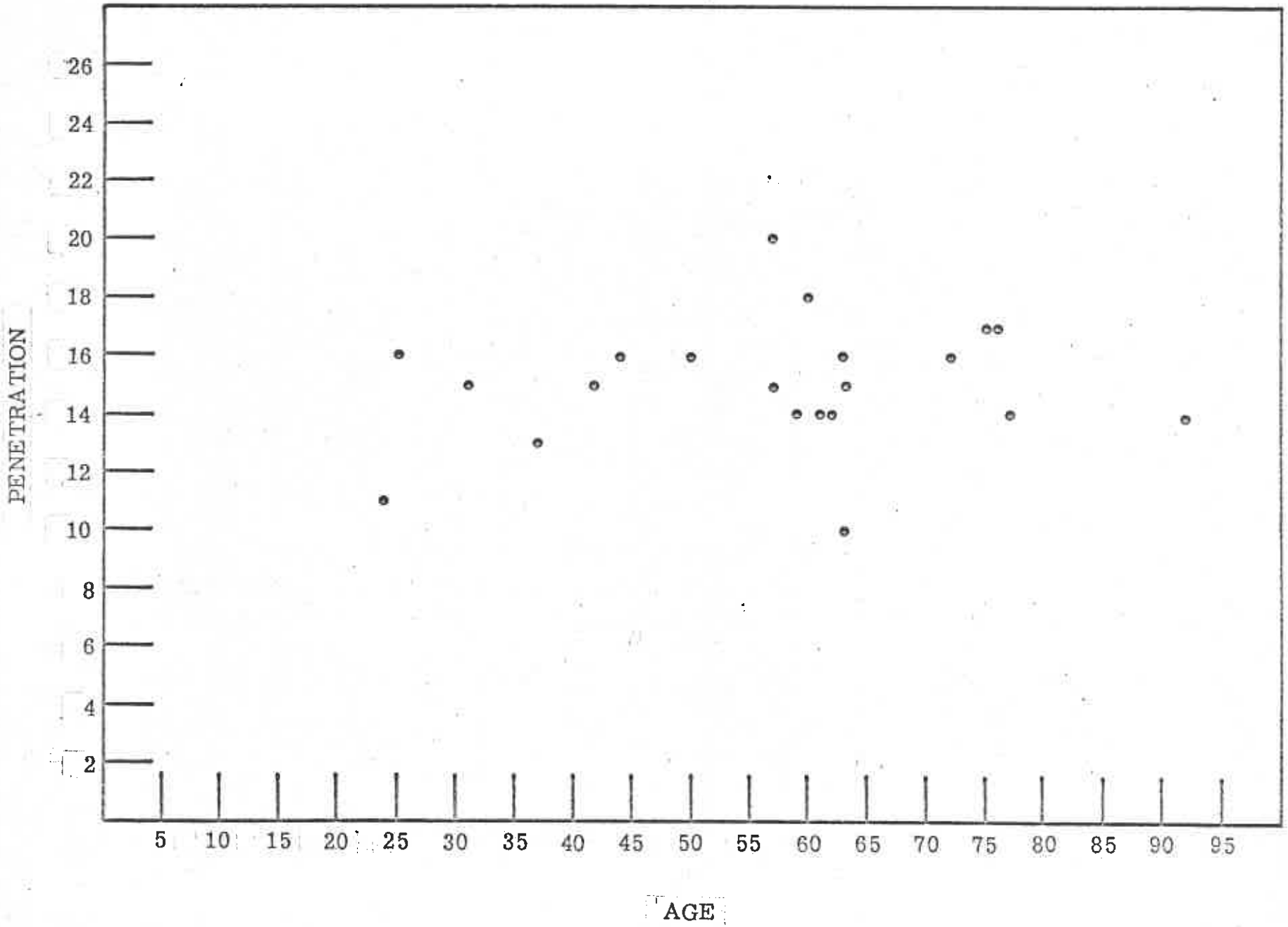

FIGURE 2 MIDLINE SCALP PENETRATION VERSUS AGE

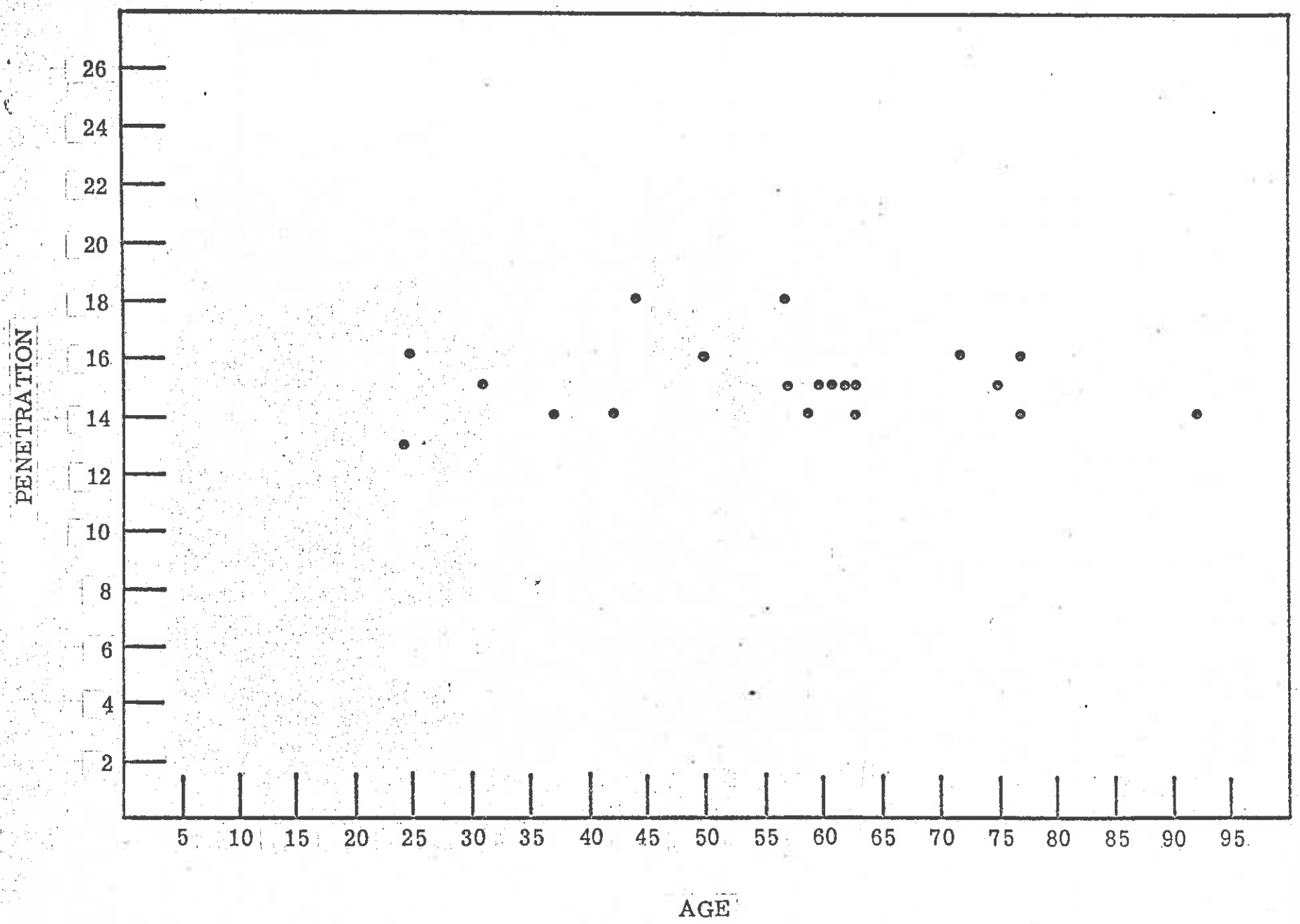

FIGURE 3. SIDE SCALP PENETRATION VERSUS AGE

DYNAMIC SHEAR and BULK MODULI OF BRAIN TISSUE

Appendix G

Table of Contents

	Page Number
Complex Dynamic Shear Modulus	1
Test Description and Objectives	1
Equipment and Instrumentation	2
Test Specimens and Procedure	3
Data Reduction	5
Data and Discussion	7
Secant Bulk Modulus	13
Test Description and Objectives	13
Equipment and Instrumentation	13
Test Specimens and Procedure	14
Data Reduction	15
Data and Discussion	16
Future Work	18

List of Illustrations

Figure 1 - Photograph of Dynamic Mechanical Apparatus

Figure 2 - Schematic of Dynamic Mechanical Apparatus

Figure 3 - Variables in Measurement of Dynamic Elastic Modulus. I. HBM-2-10. Time on Test, Displacement, Vibration History

Figure 4 - Variables in Measurement of Dynamic Elastic Modulus. II. HBM-3-51. Time on Test, Displacement, Vibration History

Figure 5 - Variables in Measurement of Dynamic Elastic Modulus. III. HBM-3-30. Time on Test, Uninterrupted Vibration

Figure 6 - Variables in Measurement of Dynamic Loss Modulus. IV. HBM-2-10. Time on Test, Displacement, Vibration History

Figure 7 - Variables in Measurement of Dynamic Loss Modulus. V. HBM-3-51. Time on Test, Displacement, Vibration History

Figure 8 - Elastic Modulus of Human Brain Tissue. I. Initial Tests, Four Individuals

Figure 9 - Elastic Modulus of Human Brain Tissue. II. Second Scan, Specimens Conditioned by Vibration

Figure 10 - Elastic Modulus of Human Brain Tissue. III. Effect of Refrigerated Aging

Figure 11 - Loss Modulus of Human Brain Tissue. I. Initial Tests, Four Individuals

Figure 12 - Loss Modulus of Human Brain Tissue. II. Second Scan, Specimens Conditioned by Vibration

List of Illustrations (cont.)

Figure 13 - Loss Modulus of Human Brain Tissue. III. Effect of Refrigerated Aging

Figure 14 - Loss Tangent of HBM-1

Figure 15 - Loss Tangent of HBM-2

Figure 16 - Loss Tangent of HBM-3

Figure 17 - Loss Tangent of HBM-4

Figure 18 - Photograph of Compression Cell for Measurement of Bulk Modulus

Figure 19 - Secant Bulk Modulus of Human Tissue. I. Mean Values, Each Test

Figure 20 - Secant Bulk Modulus of Human Tissue. II. Mean Values, Each Individual

List of Tables

Table I - Dynamic Shear Modulus - Rhesus Monkey Brain

Table II - Dynamic Shear Modulus - Human Brain No. 1

Table III - Dynamic Shear Modulus - Human Brain No. 2

Table IV - Dynamic Shear Modulus - Human Brain No. 3

Table V - Dynamic Shear Modulus - Human Brain No. 4

Table VI - Secant Bulk Modulus - Pig Brain

Table VII - Secant Bulk Modulus - Rhesus Monkey Brain

Table VIII - Secant Bulk Modulus - Rhesus Monkey Brain - Suspended in Glycerine

Table IX - Secant Bulk Modulus - Human Brain No. 1

Table X - Secant Bulk Modulus - Human Brain No. 2

Table XI - Secant Bulk Modulus - Human Brain No. 3

Table XII - Secant Bulk Modulus - Human Brain No. 4

Complex Dynamic Shear Modulus

Test Description and Objectives

The complex dynamic shear modulus (G^*) of a viscoelastic material is defined as the vector sum of G' and G'', with G'' 90° out of phase with G'. G' is the dynamic elastic modulus and is a measure of the spring stiffness of the test material under shear stress. In contrast, G'', the dynamic loss modulus, is a measure of the damping ability of the material and represents viscous losses in the material. Most of the energy from G'' is dissipated as heat. The relative damping ability of the material, $\tan \delta$, is defined as G''/G'. Note that a material is said to be resilient if $\tan \delta$ is less than 0.20 and highly damped if $\tan \delta$ is greater than 0.40. The strain amplitude, or shear displacement angle (θs) is defined as the maximum angular displacement of a plane initially normal to the direction of stress.

G^* is determined by applying a dynamic shear stress to the viscoelastic test material and measuring the resulting strain. The Dynamic Mechanical Apparatus (DMA) applies a sinusoidal shear stress to a rectangular solid test piece. The frequency of this stress is adjusted so as to put the vibrating system in resonance, i.e. there will be a zero phase angle between stress and strain. The input force, resonant frequency, and output amplitude are recorded. This procedure is usually repeated for a number of different strain levels in order to determine the dependence of the modulus on amplitude. Since the DMA itself possesses a modulus, it is necessary to repeat the test series without a sample and subtract these values from the sample test values of corresponding amplitude to determine the modulus of the test specimen. From the test data, one is then able to calculate G', G'', G^*, $\tan \delta$, and θs.

Equipment and Instrumentation

The Dynamic Mechanical Apparatus consists of a stress input, a mechanism to impart the shear stress to the sample specimen, and instrumentation to record input force and both frequency and amplitude of the output. An oscilloscope displays Lissajou figures of stress and strain and thus allows one to place the system in resonance by tuning the input frequency. An auxiliary temperature control system provides non-ambient specimen temperatures when required.

Figures 1 and 2 show the apparatus. A 7/16-inch aluminum rod is suspended between twin electro-mechanical transducers. A horizontal drive plate is positioned on the rod equidistant from the two transducers. A fixed horizontal sample cover plate, of clear plastic, is attached to the system frame and is positioned above and parallel to the drive plate. It is adjustable to allow testing of samples of various thicknesses.

A sinusoidal signal from a Hewlett-Packard Model 202A Low Frequency Function Generator is channeled into the transducer at the left to provide the stress. (Though not needed in these tests, a Heath Model AA-40 stereo amplifier is provided for increased input signal strength.) The resulting strain is recorded as an induced output voltage from the second transducer. Both input amperage to the drive coil and induced output voltage are registered on a Hewlett-Packard Model 400D Vacuum Tube Voltmeter. The input amperage is recorded as the voltage drop across a 50-ohm shunt resistor on the input transducer. The phase relationship between input amperage (stress) and output voltage (strain) is plotted as a Lissajou figure on a Tektronix Type 502 Dual Beam Oscilloscope.

The sample holder assembly is encased in a chamber heated by a small electrical air circulating system. Temperature is controlled by means of a Leeds and Northrup No. 8693 Temperature Potentiometer. An iron-constantan thermocouple placed adjacent to the sample monitors the chamber temperature in the control loop. Low temperatures are possible with the included liquid nitrogen provisions.

Test Specimens and Procedure

The brain tissues tested were acquired from a variety of sources. Pig brains were obtained from a local slaughter house near Midland. Rhesus monkey heads and human brain sections were obtained, respectively, from Park Davis and Company (Ann Arbor) and from the VA and University Hospitals in Ann Arbor.

The history of tissue from each individual of a given species was similar prior to initial testing. Pig brain was stored at 3°C within one-half hour after removal from the skull. Whole Rhesus monkey heads were transferred from Ann Arbor to Midland within 2-1/2 hours post-sacrifice. The heads were packed in polyethylene bags and transported on either ice (unfrozen) or dry ice (frozen). Any subsequent storage at Dow Corning was at either 3°C or -6°C, respectively. Human brain sections were packed in polyethylene bags and placed on ice and water within 10 minutes after removal from the skull. They were then transferred to Dow Corning (Midland) within 2-1/2 hours. Initial tests were run immediately upon receipt. Subsequent storage was at 3°C.

Rectangular solid test specimens were cut from the tissues with disposable scalpels and razor blades. The approximate dimensions were generally 2 cm x 3 cm and 0.4-0.7 cm in height. Both of the sample-holder plates contacting the specimen were scored with a cross-hatch pattern to reduce slippage. An aerosol adhesive, Dow Corning Medical Adhesive 'B', was sprayed on both

plates to further reduce slippage. The test specimen was placed on the drive plate and the cover plate was allowed to rest in light contact with the upper specimen surface before being rigidly secured to the DMA frame. A plastic cover was placed over the sample section to form the test chamber and the temperature was adjusted to test specifications. All tests were conducted at either ambient temperature or 37°C. When tested at 37°C, the test specimen was allowed to remain in the environment for 15 minutes before testing began.

The test procedure includes the following operations:

(1) The sinusoidal input amplitude and frequency are grossly adjusted to yield resonant conditions at the desired output amplitude.

(2) The system is fine-tuned for resonance at the desired output amplitude.

(3) The resonant frequency, input amperage, and output voltage are recorded.

(4) Steps 1-3 are repeated for a number of output voltages (strain amplitudes).

(5) A photograph of the sample under the clear plastic cover plate is made from vertically overhead with a no. 583 Close-up Attachment on a Polaroid 100 Color-Pack Camera.

(6) The sample height is measured by a vernier micrometer (0.001 inch/division).

(7) Steps 1-3 are repeated with no sample, i.e. with the machine unloaded, for the range of output voltages previously used.

Data Reduction

All the necessary variables having been measured, the following calculations are made.

(1) The deformation for each output test voltage E is determined from the relation

$$\text{Def. (in mils)} = E/0.00415\ f$$

where f is the frequency and 0.00415 is a machine constant which was determined experimentally for the DMA.

(2) Curves of the resonant frequency (f_o) and corresponding input amperage (I_o) are plotted versus deformation for the unloaded machine.

(3) f_o and I_o are read from the above curves for each sample deformation and recorded.

(4) The sample area is scaled from the photograph of the sample using a planimeter, with the aid of a calibrated grid scored on the cover plate and visible in the photograph.

(5) The moduli and supporting parameters are calculated from the following formuli, which are applicable to operation at resonant conditions.

$$\theta_s = \tan^{-1} (\text{Def}/h) \qquad \text{(a)}$$

$$G' = h_o/A\ (\omega^2 M - K_o) \qquad \text{(b)}$$
$$= (4\pi^2 M h_o/A)\ (f^2 - f_o^2)$$
$$= K_1 (f^2 - f_o^2)$$

$$G'' = \omega h_o/A\ \left(\frac{C_1 I}{E} - Rm_o\right) \qquad \text{(c)}$$
$$= (2\pi C_1 h_o/A)\ (f/E)\ (I - I_o)$$
$$= K_2\ (f/E)\ (I - I_o)$$

$$G^* = [(G')^2 + (G'')^2]^{1/2} \qquad (d)$$

$$\tan \delta = G''/G' \qquad (e)$$

where: h = Sample height, mils

h_o = Sample height, cm

A = Sample area, cm^2

K_o = Volume spring constant of machine, $gm\text{-}sec^{-2}$

M = Vibrating mass, 243 grams

f = Resonant frequency with sample in place, Hertz

f_o = Resonant frequency without sample and at same amplitude as f, Hertz

$\omega = 2\pi f$

C_1 = Force constant of machine, 1.53×10^6 $gram\text{-}ohm\text{-}sec^{-1}$

E = Output voltage, volts

Rm = Mechanical resistivity of machine, $(C_1 I_o/E)$

I = Driving amperage with sample in place, amperes

I = Driving amperage without sample and at same amplitude as I, amperes

These equations were derived by Dow Corning and have been used routinely for dynamic tests of elastomeric samples. A good reference for the basic theory of viscoelasticity from which the apparatus and data reduction were derived is "Dynamic Properties of Elastomers" by S. D. Gehman, which appeared in Vol. 30 (1957) of Rubber Chemistry and Technology.

Data and Discussion

Complete test results are included in tabular form (Tables I through V) for all materials tested and also in graphic form (Figures 3 through 17) for tests of human brain tissue. All tests of human tissue were conducted using white matter from the frontal lobes. The code numbers for the human brain tests identify the test as to - (1) type of brain and sex (as - HBM - Human Brain, Male); (2) the specific brain (1 through 4); (3) hours post-mortem at the beginning of testing; and (4) the individual test, denoted by a letter, where a series of tests was conducted with the same specimen in a short time period.

Figures 3 to 5 show elastic moduli, G', from extensive sets of experiments designed to evaluate the experimental procedure and to identify the dominant variables affecting G'. Two brain sections were used, HBM-2 (Figure 3), and HBM-3 (Figures 4 and 5). Figure 3 shows measurements scanning a range of shear displacements as described above. The initial scan, performed in about 8 minutes, was followed immediately by three more scans. The specimen was at rest for no more than 1-2 minutes between scans. Two more scans were run after long breaks as shown. There appears to be in Figure 3 a strong relationship between G' and shear amplitude (or velocity), and an increase in G' with time for a given amplitude. Time in this case also represents accumulating shear history, with potential shear damage; but the upward trend in G' does not appear to have been interrupted by the long periods at rest.

Figure 4 shows a similar experiment with several modifications. Loss of water at the edges of the sample appeared to be a probable hazard that could account for stiffening with time in Figure 3. In the series of Figure 4, a water soaked paper towel in the air stream to the chamber increased relative humidity somewhat; the repeated scans were conducted somewhat faster and without pause; and the ratio of edge exposure to

specimen volume was only about 70% of that for HBM-2 in Figure 3. Finally, after the first four scans, the specimen was removed from the holder and the edges were trimmed before returning the sample for two more scans.

As in HBM-2, a strong dependence of G' on shear displacement appeared, but only in the first scan and the scan following the long rest period. In the other scans, G' was not clearly affected by shear angle, except for three consecutive low values at $\theta_s = 3°C$. After the exposed edges of the specimen were removed, the initial pattern was repeated, but at lower magnitude. In contrast to Figure 3, no overall rise in G' was evident during about 35 minutes of testing and exposure to air at 37°C. Irreversible change probably was not occurring rapidly, through either drying or shear damage.

Figure 3 provides the key to reconcile the first two figures described. Here, one test scan was completed as usual, from low to high shear displacements. The sample was then sheared at low amplitude ($\theta_s = 3°$) for approximately 110 minutes. G' doubled in 6 minutes and continued to rise at a decreasing rate, presumably because of water loss throughout the period. The maximum reached, about 45 dynes-cm^{-2}, equaled that reached in the experiment of Figure 3 after a one-hour idle period. The early rapid rise with time easily accounts for scatter in the data of Figure 3. Its rate, either at rest or at low amplitude, suggests that the rise is due to edge drying more than bulk change.

With edge drying as a dominant condition, and very little relation evident between G' and θ_s in those scans least subject to drying (Figure 4, the second, third, fourth, and sixth scans), the effect of θ_s on G' evident elsewhere in the figures probably must also be related to drying. Our best present interpretation is that at high shear amplitude, diffusion of water from the bulk of the specimen to the sample edge is facilitated, thus

overcoming the stiffening due to edge drying. G' values are, therefore, a strong function of immediate prior vibration history. The first test in each figure followed a 15-minute exposure to the 37°C environment. High modulus resulted until shearing at moderate to high amplitudes reconditioned the sample (Figures 4 and 5). In Figure 3, the test was begun at high amplitude, perhaps giving one of the most valid results, free of both edge drying and bulk drying. Low G' values at $\theta_s = 3°$ in Figure 4 are also most nearly free of drying effects, following high amplitude conditioning closely. In the tests of Figure 3 there was sufficient time between sequential tests for edge drying to take place. With the effect of drying excluded, it appears likely that G' will either be unaffected by θ_s, or will rise slightly with increasing amplitude.

Other possible variables that might be involved in these tests include thixotropy, a reversible property which would be expected to show decreased stiffness with shear amplitude; and irreversible shear degradation. Neither of these effects, if present, can be thoroughly evaluated until drying is well controlled, although there are indications that irreversible degradation other than bulk drying is not involved.

Figures 6 and 7 show loss moduli for the same test series discussed above (Figures 3 and 4). As in G', G" was affected, at least temporarily, by edge drying on the test apparatus, but returned nearly to its early value with high amplitude shear. G" rose slowly with time compared to G', or not at all, and was consistent from scan to scan after the conditioning provided by the first scan of each series. These characteristics suggest that G" is less subject to the effects of edge drying than G'. Values for vibration-conditioned scans ranged from 6.5×10^3 to 8×10^3 dynes-cm^{-2} for HBM-2-10 (Figure 6) and from 4×10^3 to 6.5×10^3 dynes-cm^{-2} for HBM-3-51 (Figure 7). High values occurred consistently at low shear amplitude, and low values at high amplitude.

The experiments discussed above have resolved one question that had been of concern. The shear moduli for brain are so low as to approach the minimum measureable on the DMA. Precision of the measurements in such a situation may be inadequate. The data plotted in Figures 3-7, with a few exceptions, show machine or operator variations much smaller than the material variations of interest. Machine precision is judged adequate for the measurements required.

Figures 8 through 13 display values of elastic and loss moduli for human brain tissue, selected to demonstrate variations between individuals in initial tests and vibration-conditioned tests, and to demonstrate the effect of refrigerated aging of the material on these properties. The strong mixed influence of edge drying and vibration history is present in these results. Conclusions drawn are, therefore, tentative until further experiments are performed with drying eliminated.

Figure 8 shows G' obtained in the first test scan of each brain section. The decline in G' with displacement ascribed to edge drying and vibration conditioning is evident for all specimens. Change in G' with displacement above $\theta_s = 8°$ is small. Values at higher displacements, tentatively judged more valid, ranged from 3×10^3 dynes-cm^{-2} to 14 dynes-cm^{-2}. Inspection shows no correlation between these G' values and either age of the individual or hours post mortem. The scan on HBM-2 differed from the others, in that it was begun at high shear angle and moved stepwise to low angles, instead of from low to high. This gave the lowest G' values measured for human brain. Even the second scan on this specimen, following within 1 or 2 minutes, gave a substantially higher elastic modulus. The G' values for higher displacements in this scan may be least affected by edge drying of any obtained.

Figure 9 shows values of G' obtained in second scans for HBM-2 and HBM-3 -- that is, after vibration conditioning and a total of 20-25 minutes on the test mount. (Fifteen minutes for temperature equilibration and 5-10 minutes consumed in the first test scan.) Values are similar for both individuals and are less affected by shear angle. Most readings fall between 8×10^3 and 12×10^3 dynes-cm^{-2}.

Figure 10 shows the effect of storing brain tissue from two different individuals for 24 hours at 3°C following initial tests. (Separate specimens were used for the two tests.) The curves for all four tests are typical of initial scans. Values were slightly lower after storing HBM-1, higher after storing HBM-3. No consistent change in 24 hours is shown. Neither does a trend with total storage time post mortem appear. If such trends exist, they appear to be small compared to variations in the edge drying effect, which is strong in these scans.

Figures 11, 12, and 13 show values of loss moduli obtained in the same runs plotted in Figures 8, 9, and 10. Variation between individuals in Figure 11 and Figure 13 was smaller than for G'. Generally values fell within ±20% of the mean. It was concluded above that G" is less sensitive than G' to edge drying, although not free of such effects. Accordingly, the dependence of G" on displacement shown in Figure 12 probably is real. Similar decline in G" with shear angle is normally observed in testing of elastomers. As in G', no correlation is evident between G" and hours of refrigeration post-mortem from 10 through 50 hours (Figure 13).

Loss tangents have been plotted for all tests on human brain tissue in Figures 14 through 17, HBM-1 through 4. Results for the repeated tests of HBM-2 (Figure 15) are widely scattered, reflecting the variations discussed above in the component moduli. Values of tan δ are of limited value until drying effects are eliminated. Long term aging on the test instrument led to low

tan δ (HBM-2-10E and 10F), as G' rose more than G". Evidence that G', measured without drying, will be relatively low, and that G" has been less affected by drying, leads to the conclusion that the true loss tangent for these materials is at the high side of the range observed to date. Most values lay between 0.35 and 0.7. The highest value, 2.1, was obtained at the beginning of the first scan of HBM-2-10, where G' was the lowest seen. This and other high values of tan δ occurred in the situations where drying was considered least influential.

Measurements of shear moduli were made on pig and Rhesus monkey brain tissue before any work with human brain primarily to demonstrate applicability of the test. These tests were not detailed enough to resolve drying effects as was done later, so that for the most part, data are not considered significant. In spite of this, one set of tests of Rhesus monkey brain, recorded in Table I, are believed to show the effect of freezing on dynamic properties. Spring modulus, G', was approximately an order of magnitude lower for frozen material; loss modulus also was low. These differences are supported by visual and tactile observation, the frozen material being softer, with less physical integrity.

Secant Bulk Modulus

Test Description and Objectives

The secant bulk modulus (β) of a compressible material is defined as the ratio of stress to strain for the case of hydrostatic compression and is, therefore, the inverse of compressibility. To measure bulk modulus, the test material was placed in a cylindrical compression cell and compressed by a hydraulic ram. A stress-strain plot was recorded electronically and provided the necessary values for the calculation of β from the equation -

$$\beta = \frac{V_o \Delta p}{\Delta V} \quad (1)$$

where: V_o = volume of test material

Δp = applied hydrostatic pressure

ΔV = change in volume, V_o, produced by Δp

Equipment and Instrumentation

The compression cell utilized for all tests was a modification of a design by P. W. Bridgeman of Harvard University. The effective compressible volume was 32.2 cc (see Figure 18). A nylon sleeve and rubber o-ring at the end of the piston sealed the system. The diameter of the piston is slightly less than that of the cylindrical chamber. Therefore, only the nylon sleeve and rubber o-ring were in contact with the cylinder walls during testing. The removable base was sealed by a rubber o-ring. The compressive load was applied by a Baldwin-Tate-Emory Universal Tester, 60,000 pound maximum load. A stress-strain plot was obtained with a recorder integral to the tester. Stress was read from ram load, and strain from a calibrated mechanical position transducer.

Test Specimens and Procedure

Specimens for secant bulk modulus tests were obtained from the same human brain sections and the same or similarly-conditioned Rhesus monkey and pig brains as were used for dynamic shear measurements. Therefore, the pre-test history for a given test specimen was almost identical to that of dynamic shear modulus specimens. The only noticeable variation would have been time of storage prior to testing.

The test tissue was cut into small cubes of approximately 0.2-0.4 cc volume. For one-phase testing, these cubes were blended with a metal spatula and loaded into the cell. For two-phase testing, the cubes were placed in a carrier fluid in a graduated cylinder for volume determination by displacement. They were then transferred to the cell along with the necessary carrier fluid to fill the cell to test level. After an initial test of Rhesus monkey brain using glycerine as the carrier fluid, subsequent two-phase tests utilized a 1000 centistoke polydimethylsiloxane (silicone) fluid as the carrier. It is important in the two-phase test that the test material and the carrier fluid chosen be incompatible. Partial volumes of phases having some mutual solubility would not usually be additive.

The test procedure follows:

(1) The loaded cell is brought to test temperature.

(2) The piston (ram) is carefully placed in the bore of the cell in contact with the test volume of material or carrier fluid.

(3) The cell is positioned on the Universal Tester. The hydraulic ram is brought into contact with the cell piston. The calibrated position transducer is placed in contact with the piston.

(4) The material is now compressed at a constant rate (approximately 0.14% per second) until the preselected maximum pressure is obtained.

(5) The material is now decompressed at the same rate.

(6) The compression/decompression cycle is repeated twice more without removing the piston, to check repeatability and possible irreversible strains.

The carrier fluids were tested similarly for calculation purposes when a two-phase system was used. A continuous stress-strain curve was recorded during both compression and decompression in the units of psi (stress) and percentage compression (strain).

Data Reduction

The compression and decompression values of the stress-strain cycle curves do not normally coincide, because of friction between the nylon sleeve on the piston and the chamber walls. Friction increases the indicated stress in compression, decreases it during decompression. The true stress for any given strain is taken as the average of the two recorded stresses at that point. The sleeve friction produces deviation from the mean stresses of less than ±5 percent.

With the true stress-strain (compressibility) curve now completed, the secant bulk moduli from a one-phase test are calculated from equation (1).

For the two-phase system, it is first necessary to determine the compression of brain tissue independent of the carrier fluid. This is accomplished by multiplying the compression of the carrier fluid (from the carrier fluid compressibility test curve) by its volume relative to the total test volume, and subtracting this product from the total test compression. β is then calculated from -

$$\beta = \frac{V_{oB}\ \Delta p}{\Delta V_B} \quad (2)$$

where: V_{oB} = original volume of brain tissue only

ΔV_B = calculated compression of brain tissue alone at test pressure, Δp

Data and Discussion

In both types of tests the secant bulk modulus was calculated at 5000 psi intervals. Complete results are presented in Tables VI - XII. Graphic results for all tests of human brain tissue are presented in Figures 19 and 20. The identification code is similar to that employed for the dynamic data but includes the individual human brain number before the brain type identification (HBM) in order to assure distinction between the two types of tests.

Figure 19 shows the average modulus from the repeated compression/decompression cycles in each test of human brain. Figure 20 shows one curve for each of the four individual human brains. Values plotted are average moduli from all tests of a given brain section. Test 1-HBM-29 (Table IX) has been excluded from the graphs as invalid, because carrier fluid leaked past the piston seal during compression. There appears to be a correlation of β with the age of the individual. The values obtained for human brain tissue are close to handbook values for water. Those values obtained from Rhesus brain are considerably larger.

There appears to be good correlation between results obtained with one- and two-phase systems. Note tests 1-HBM-10 and 1-HBM-11. The one-phase system appears less satisfactory for human tests because of the relative firmness of the human brain. It is most difficult to load the compression cell with human tissue without the inclusion of a considerable quantity of entrapped air.

The human brains exhibited a lower modulus than did pig or Rhesus monkey brain. Time post-mortem does not appear to be a significant variable. The variations from test-to-test most probably represent reasonable experimental error.

The tests as completed do not allow an accurate determination of the secant bulk modulus at relatively low pressures, below 1000 psi. Preliminary tests, utilizing an Instron test machine with more sensitive loading mechanism in a limited (0-1000 psi) pressure range, indicate very low modulus through the first 200 psi applied pressure. Possible causes are entrapped air in the vascular structures of the test tissue or a real property of the material. These effects are currently being evaluated more fully in low-pressure tests.

The recorded data from the compression tests described may be processed to yield tangent bulk modulus, as well as secant bulk modulus. Tangent bulk modulus, the slope of the stress strain curve at any point, is potentially more useful for analytical modeling.

Future Work

Dynamic mechanical properties of brain tissue have been measured, and variables in the measurement partially evaluated. The rate of change in properties caused by drying of the test specimen has been determined and found to be excessive for reproducible work. Drying will be controlled in future experiments by one of two methods: 1) sealing the edges of the test specimen with a vapor barrier of negligible stiffness; or 2) enclosing the specimen in a small cell in which humidity will readily equilibrate with the specimen. Testing will be continued to evaluate other variables including shear displacement, frequency of the applied sinusoidal stress, orientation of the specimen with respect to the direction of shear, age of the individual, regional differences within the brain, and sample history post mortem.

A new apparatus for measuring dynamic mechanical properties is proposed. This equipment will duplicate the present DMA in principle, but will be light weight and portable. Loading of the test specimen will be either in shear or normal to the specimen surface, thus providing two types of moduli to improve characterization. Higher resonant frequencies and greater sensitivity will result from the lower mass of the vibrating probe.

No important changes have been observed in storing brain tissue under refrigeration for the periods between 10 and 60 hours post mortem. Changes at death and immediately following death will be examined with Rhesus monkey. The lightweight probe tester will be used with anesthetized monkey for obtaining in vivo data.

Measurement of dynamic properties will be extended to scalp and dura mater.

Bulk modulus measurements or human brain will be continued, with emphasis on shape of the stress-strain curve at low stress.

Shear flow characteristics of cerebrospinal fluid and blood will be investigated through literature and experiment.

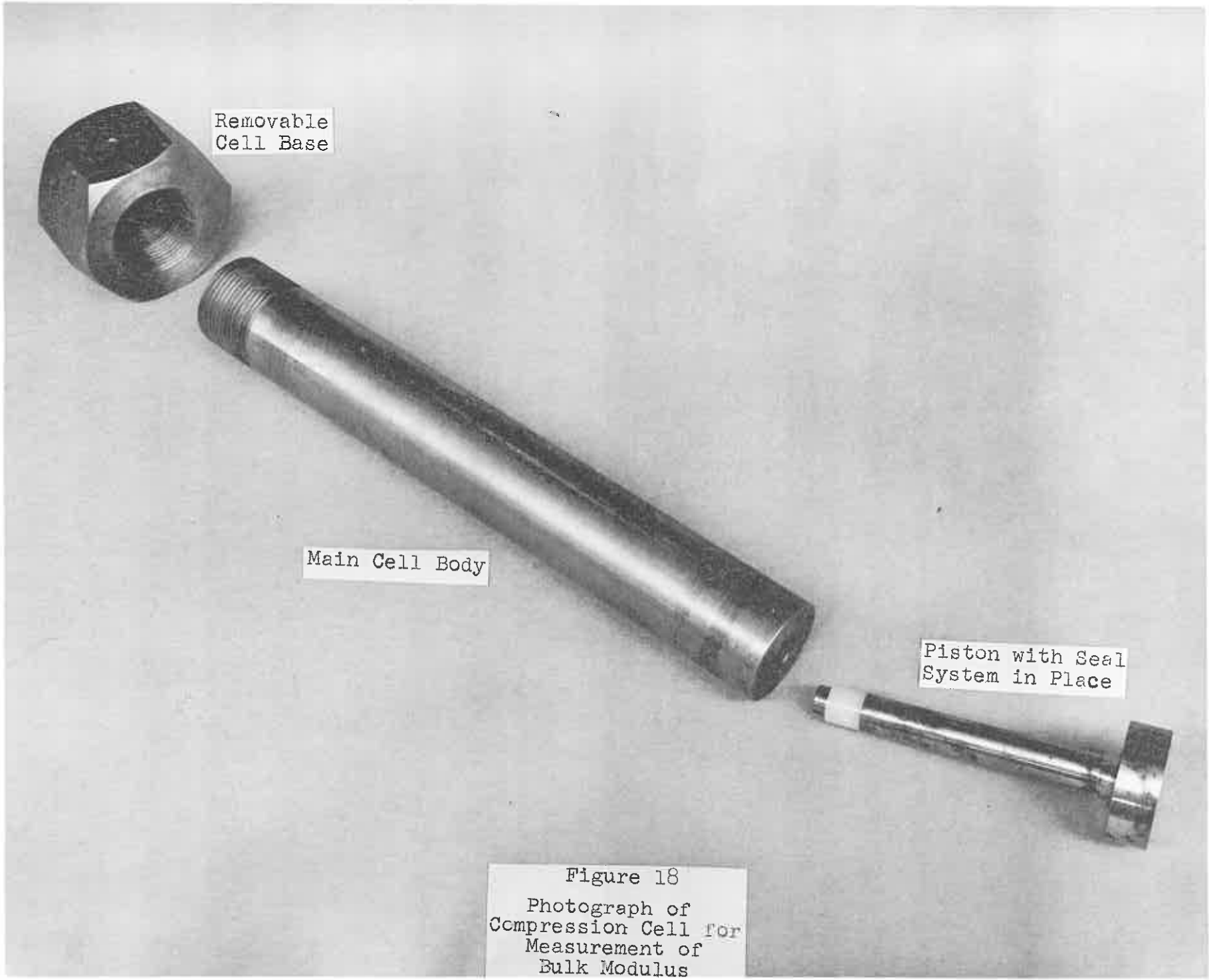

Figure 18

Photograph of
Compression Cell for
Measurement of
Bulk Modulus

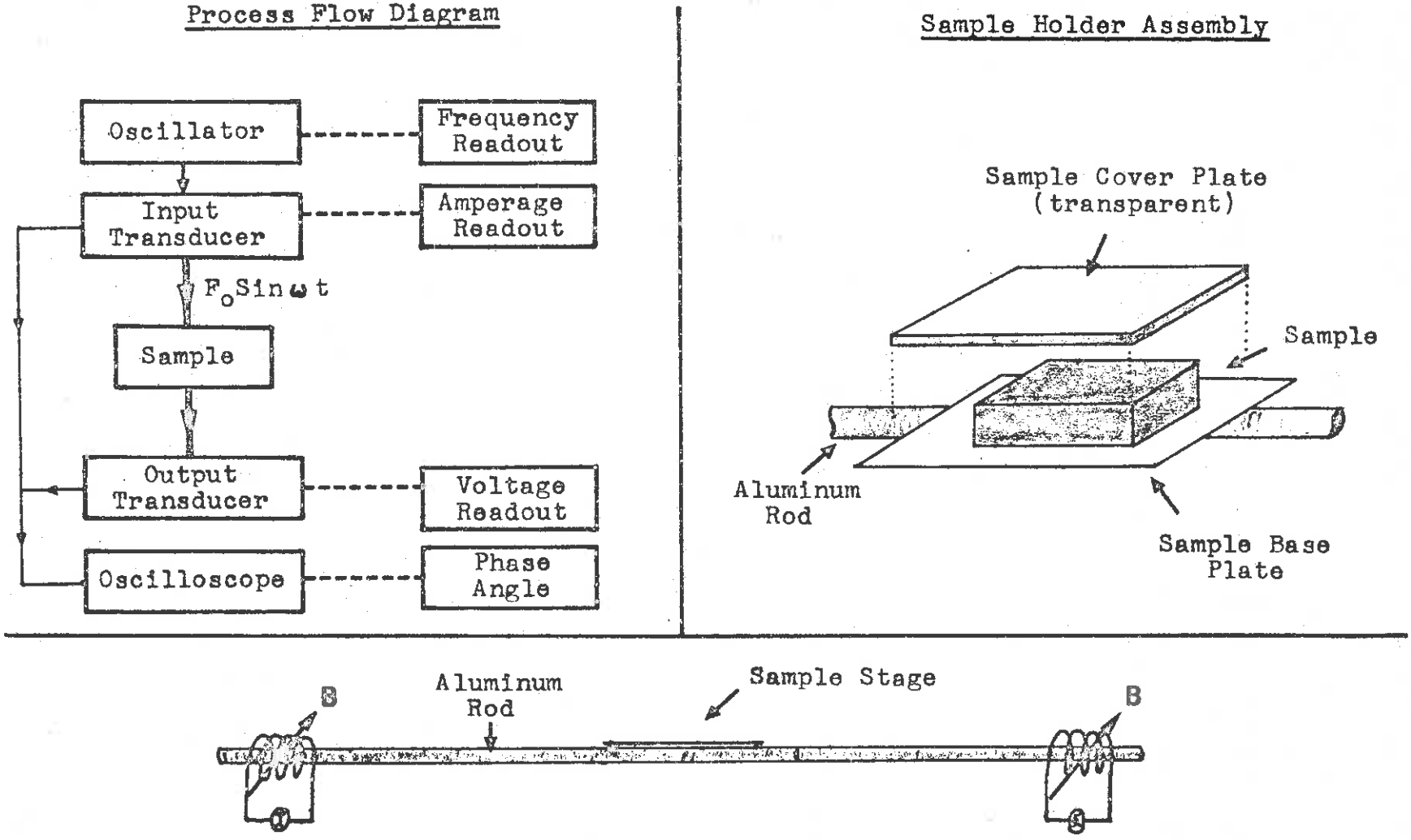

Transducers and Vibrating Mass Assembly

Figure 2

Schematic of Dynamic Mechanical Apparatus

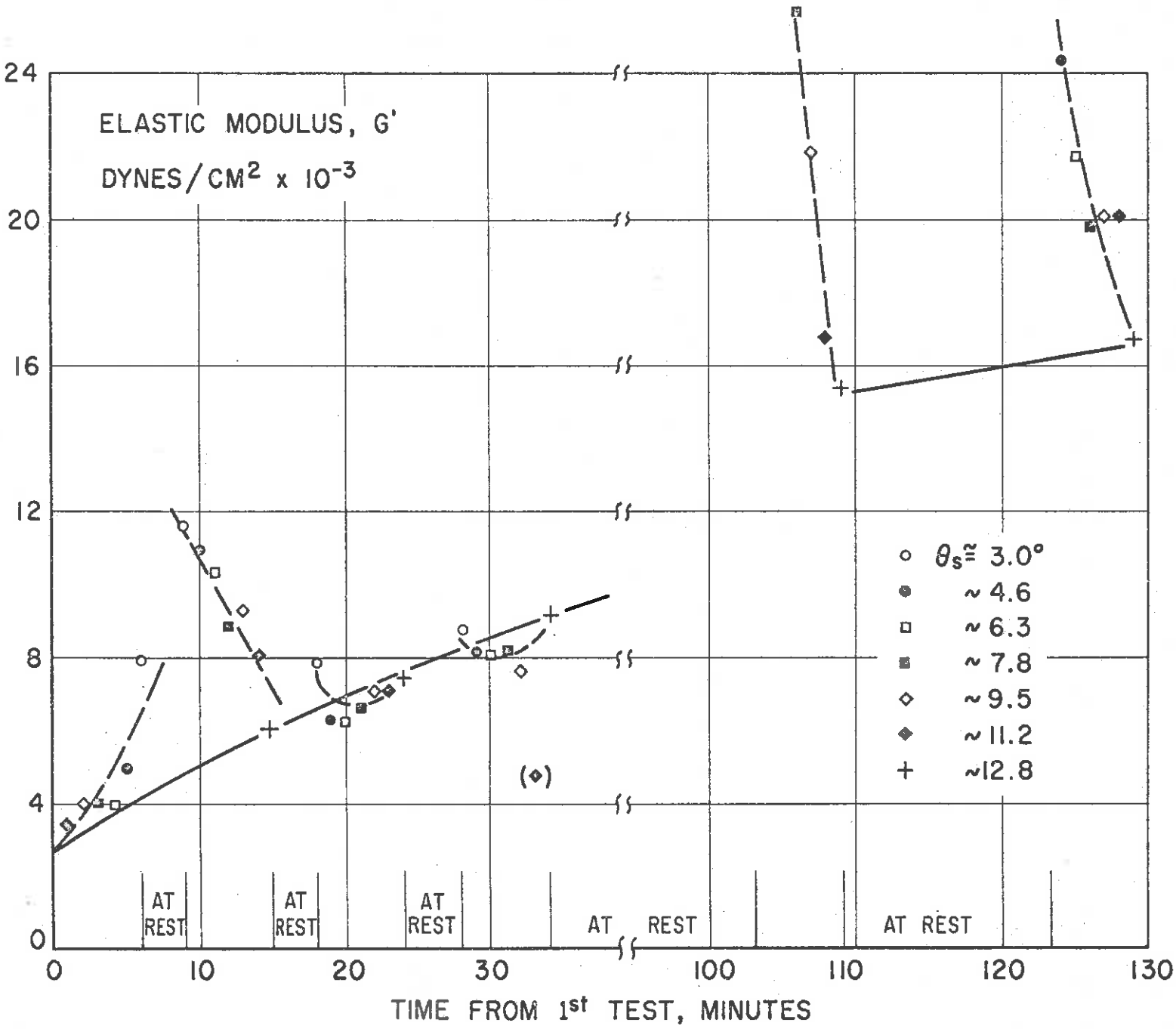

Figure 3

Variables in Measurement of Dynamic Elastic Modulus. I. HBM-2-10. Time on Test, Displacem[illegible], Vibration History

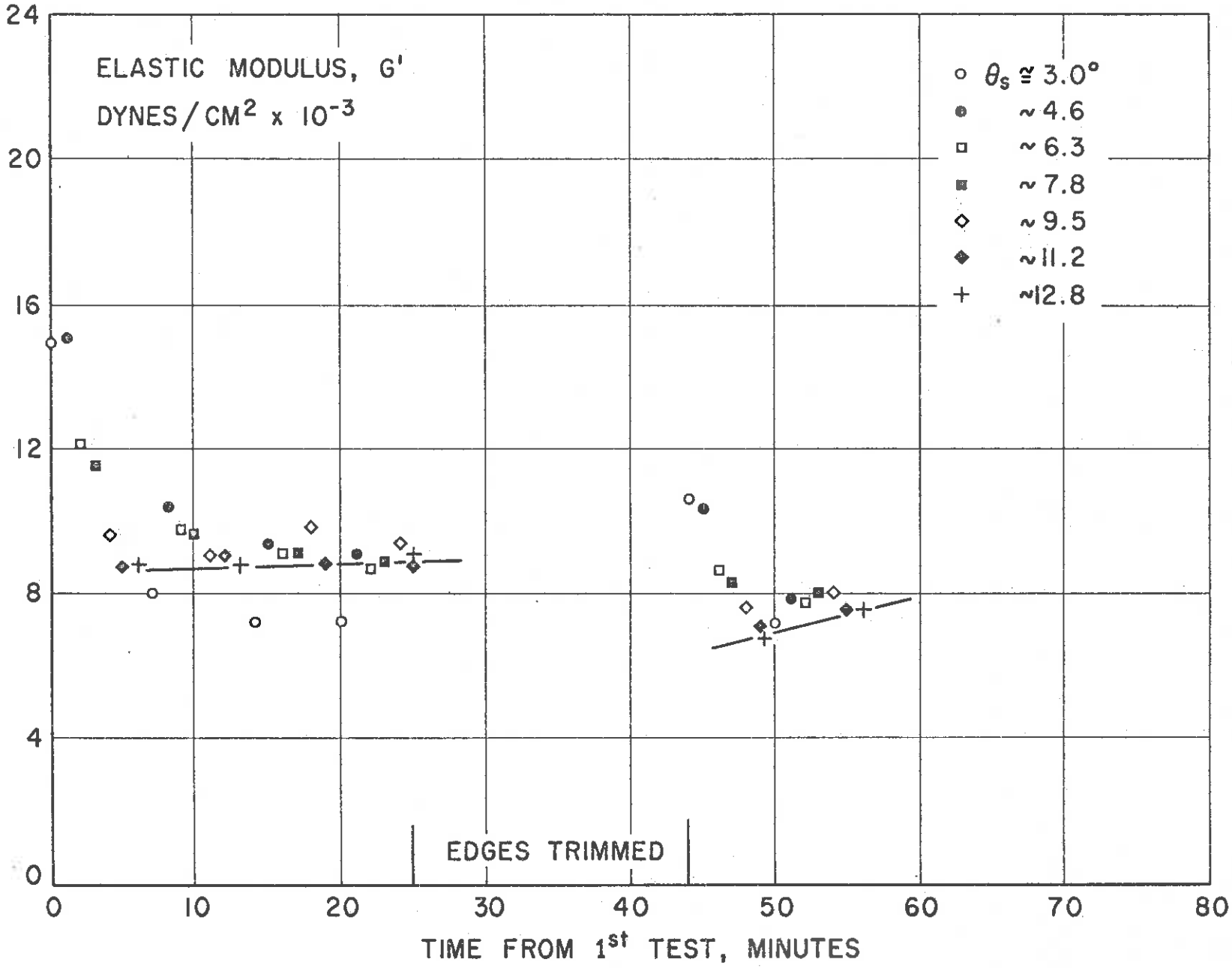

Figure 4

Variables in Measurement of Dynamic Elastic Modulus. II. HBM-3-51.
Time on Test, Displacement, Vibration History

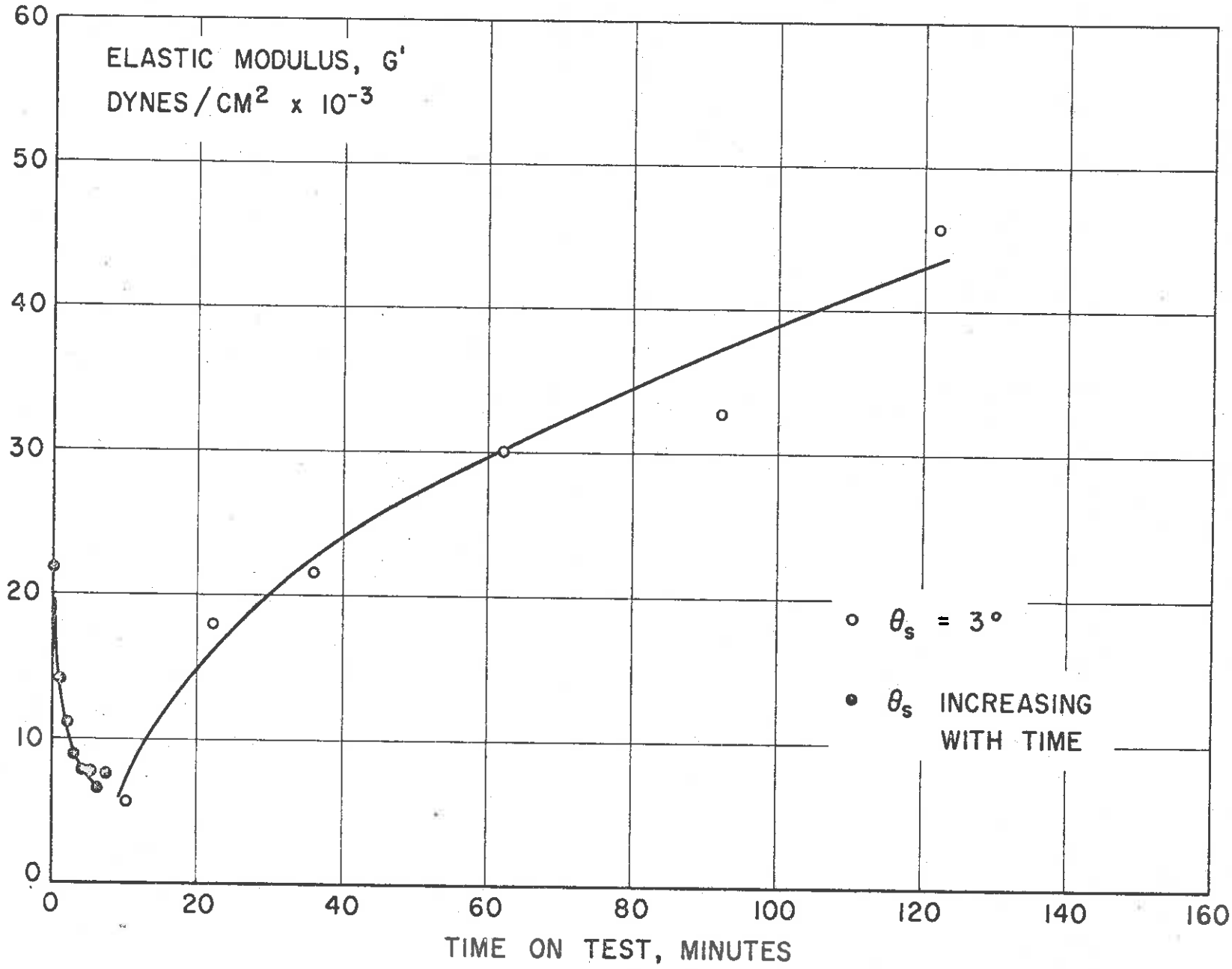

Figure 5

Variables in Measurement of Dynamic Elastic Modulus. III. HBM-3-30. Time on Test, Uninterrupted Vibration

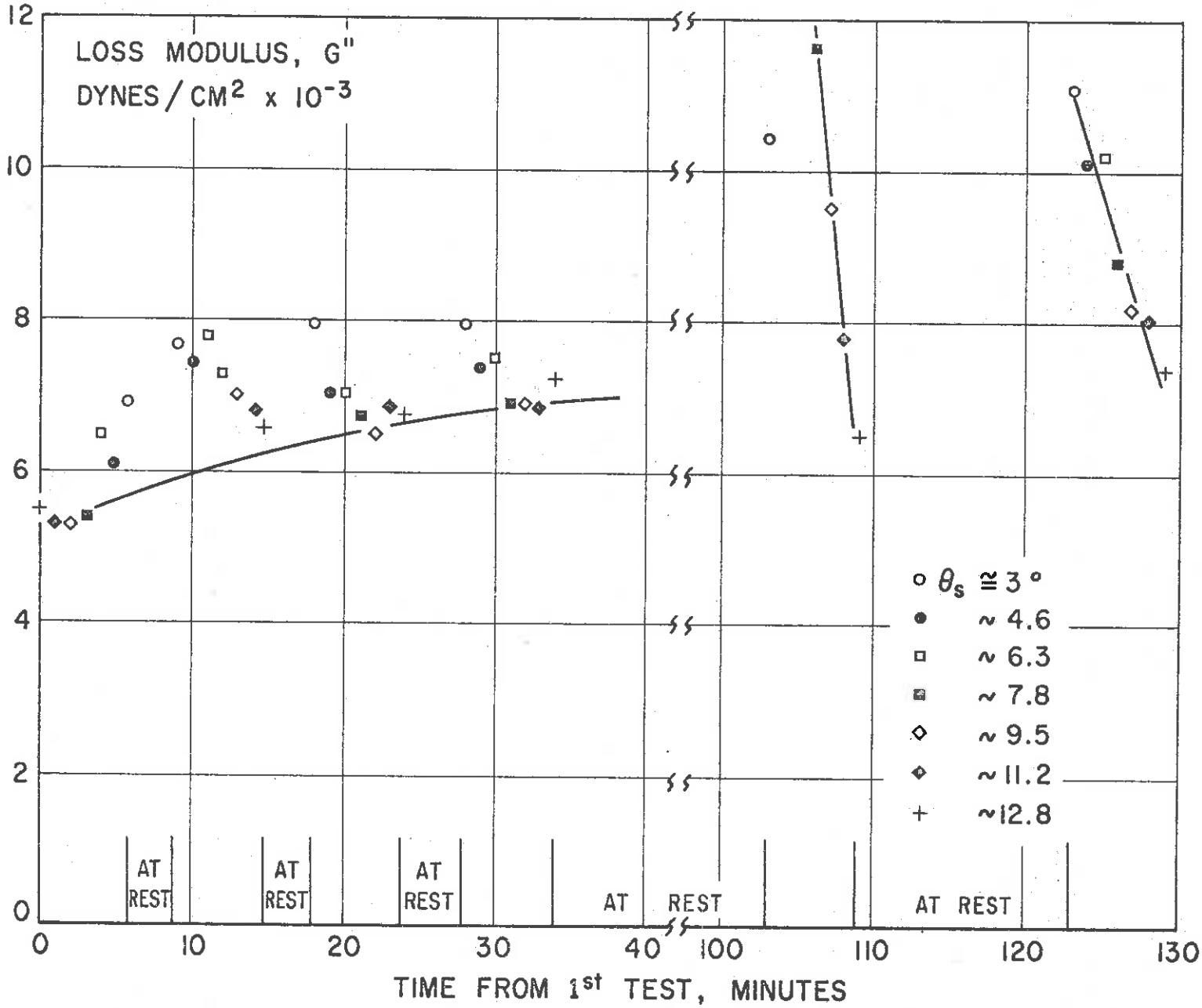

Figure 6

Variables in Measurement of Dynamic Loss Modulus. IV. HBM-2-10. Time on Test, Displacement, Vibration History

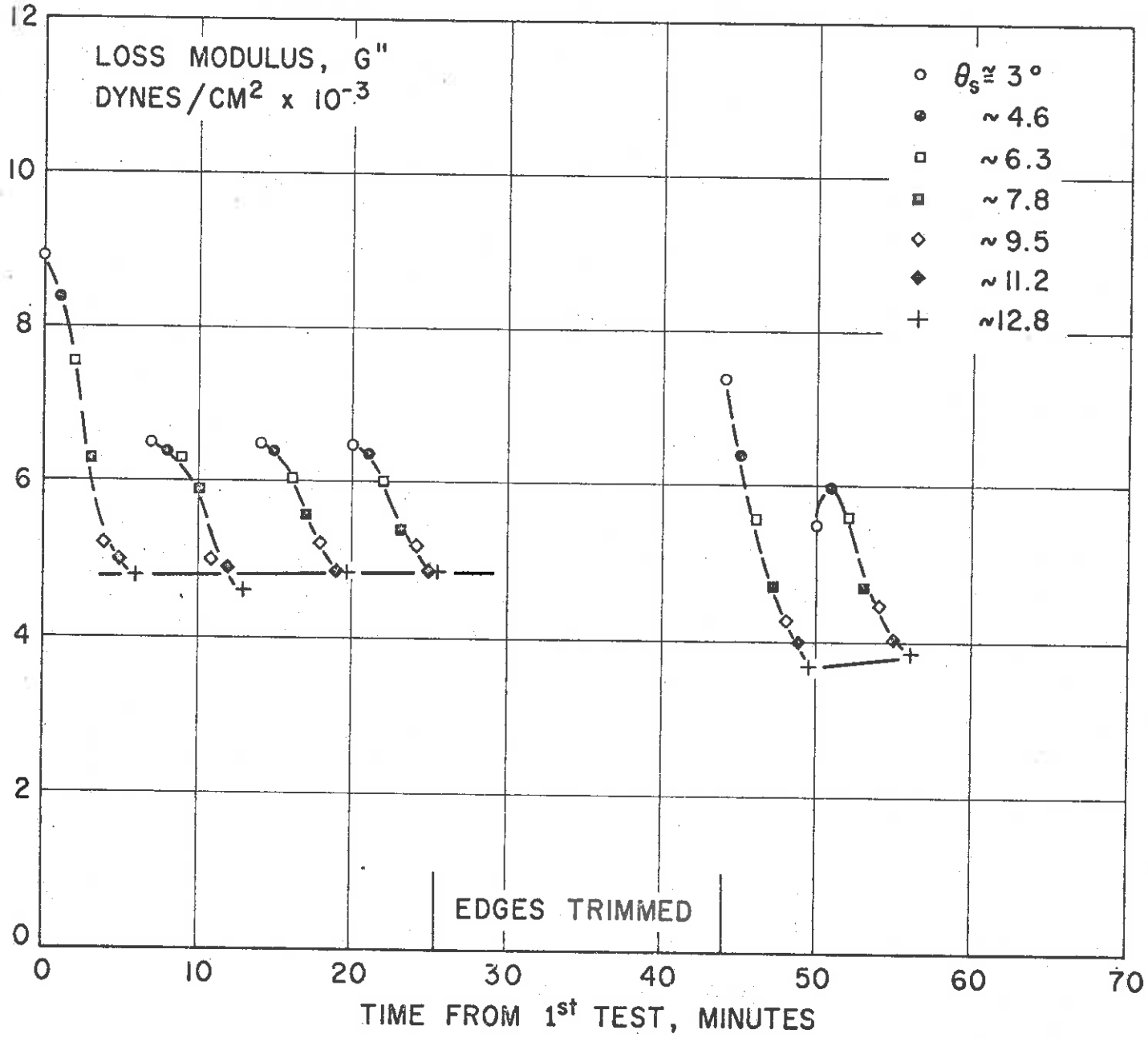

Figure 7

Variables in Measurement of Dynamic Loss Modulus. V. HBM-3-51.
Time on Test, Displacem[illegible], Vibration History

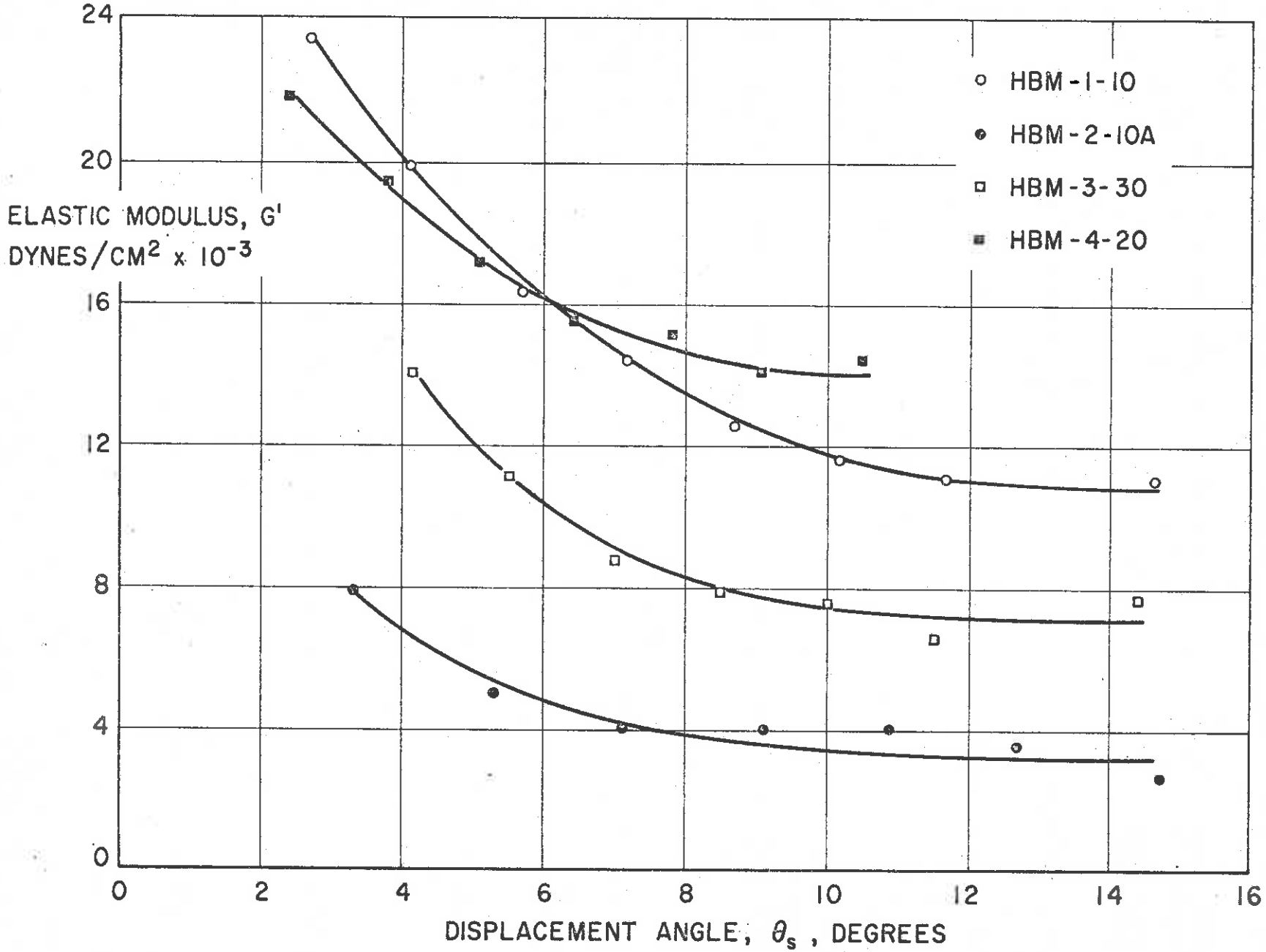

Figure 8

Elastic Modulus of Human Brain Tissue. I. Initial Tests, Four Individuals

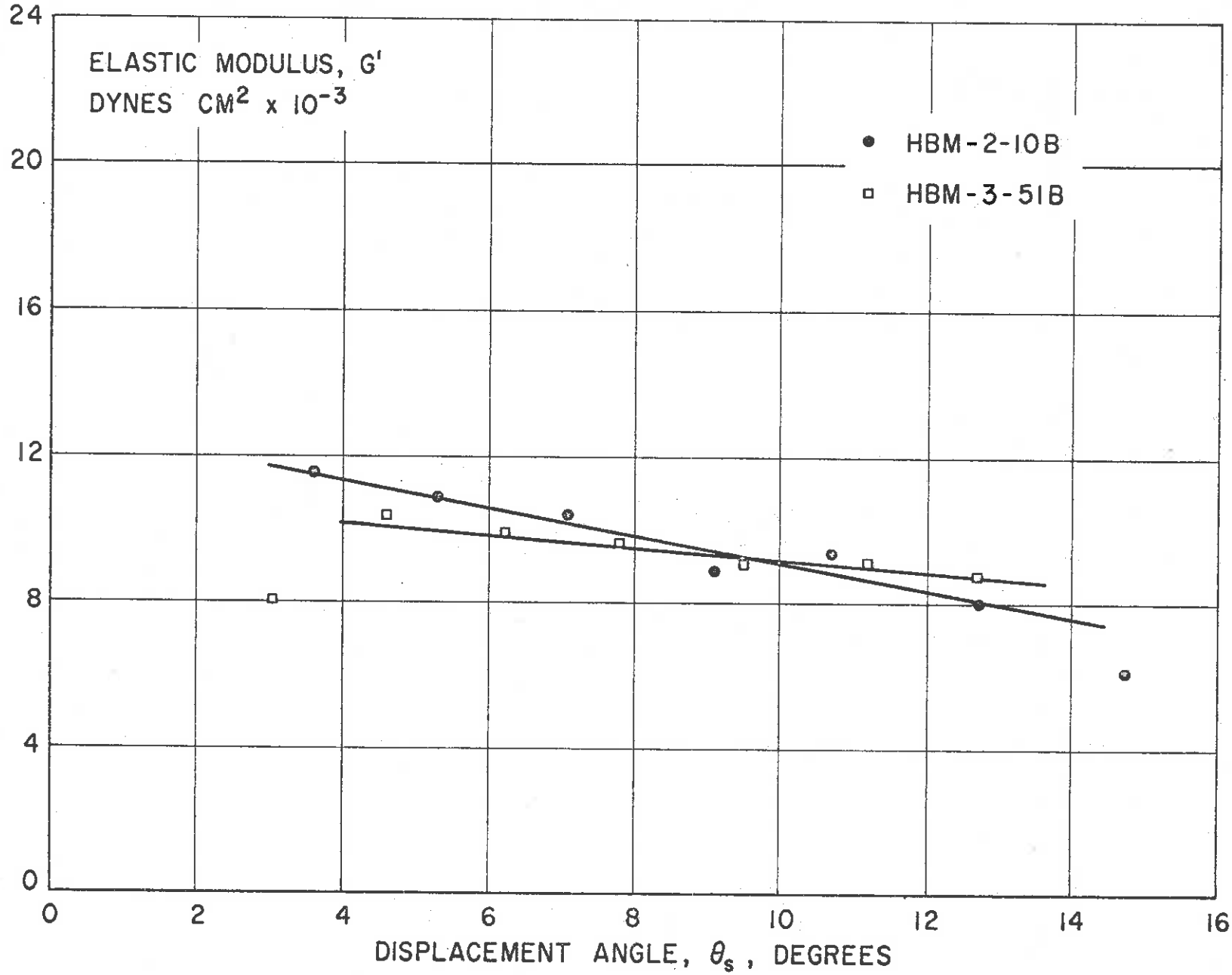

Figure 9

Elastic Modulus of Human Brain Tissue. II. Second Scan, Specimens Conditioned by Vibration

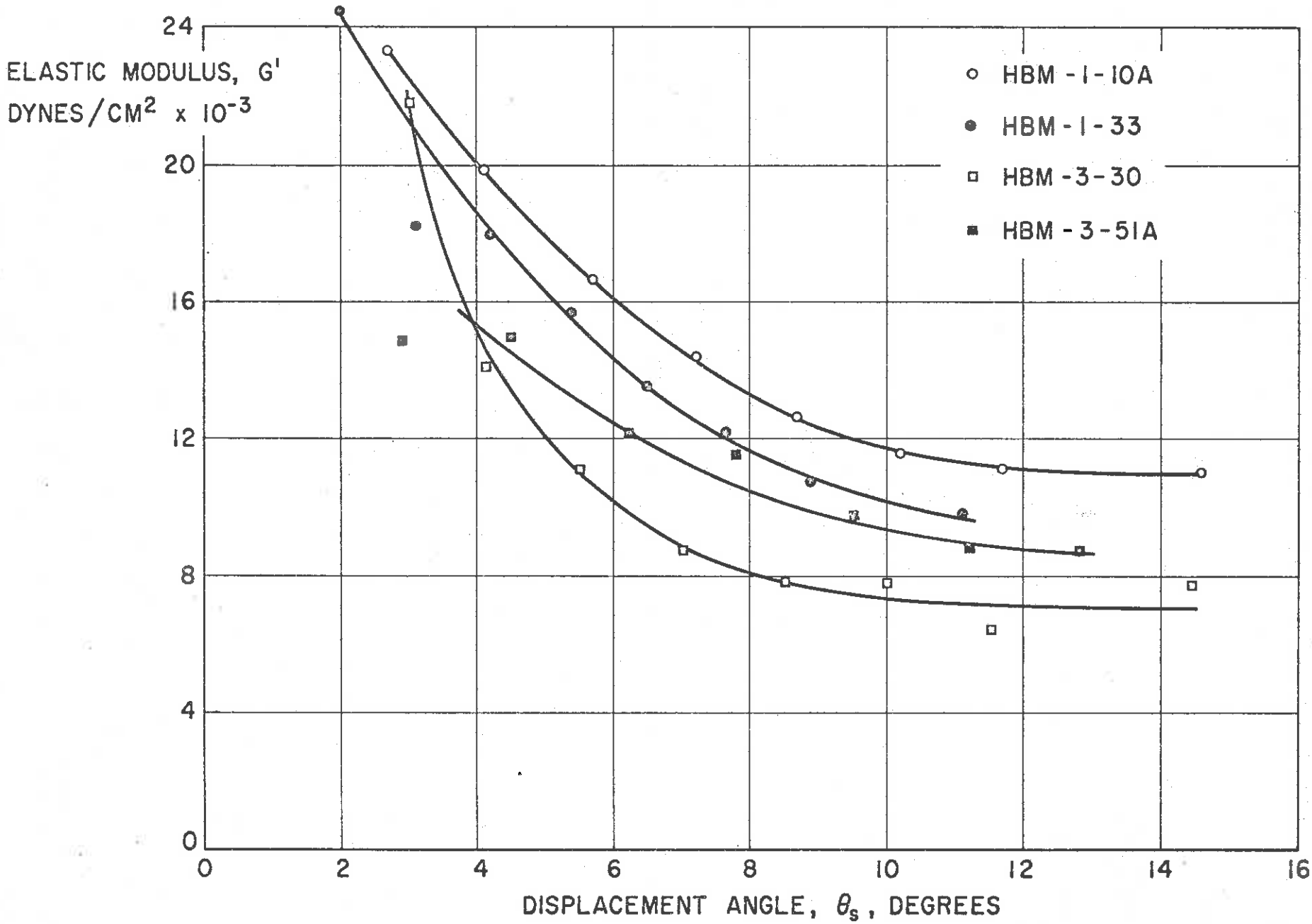

Figure 10

Elastic Modulus of Human Brain Tissue. III. Effect of Refrigerated Aging

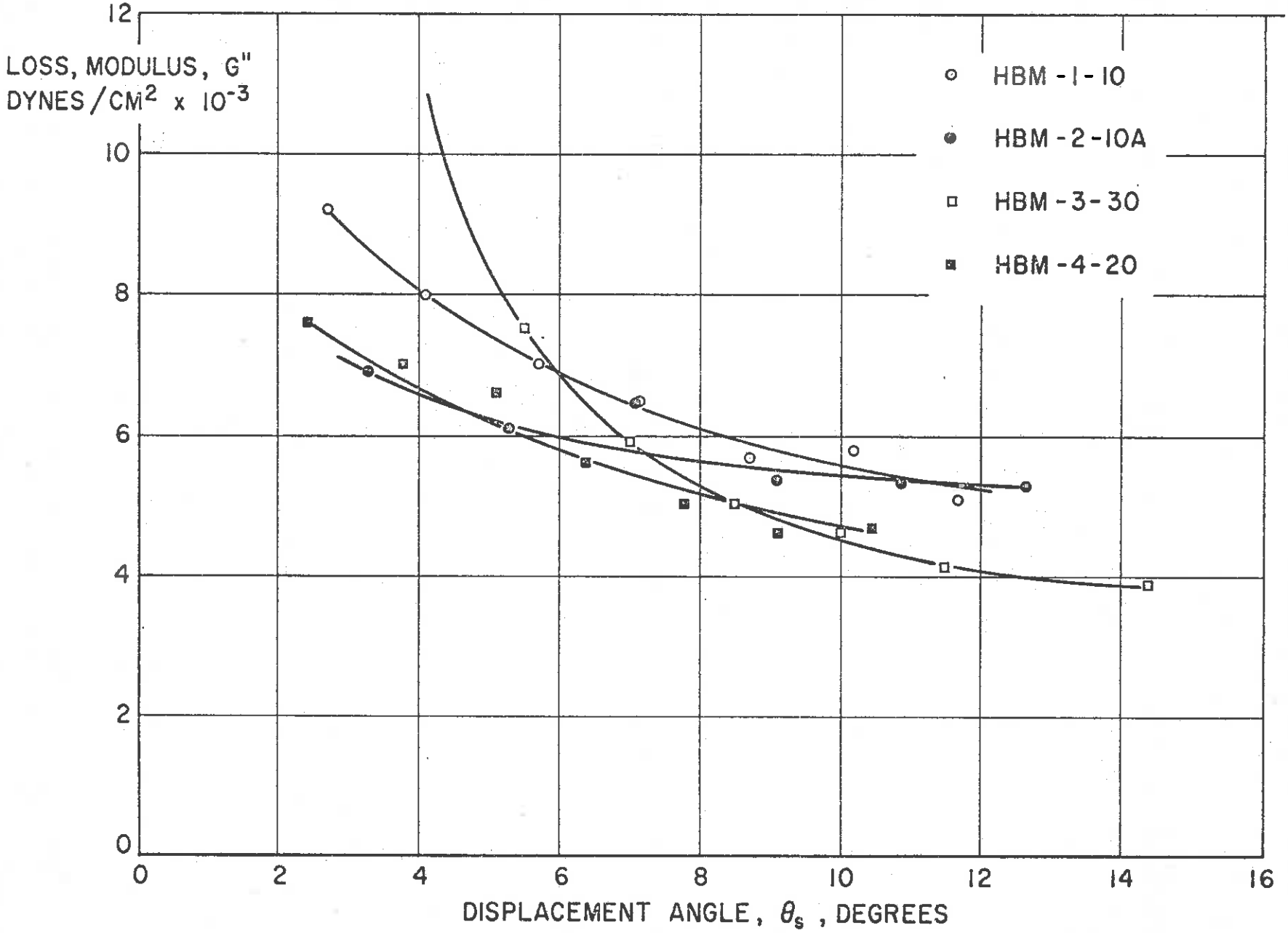

Figure 11

Loss Modulus of Human Brain Tissue. I. Initial Tests, Four Individuals

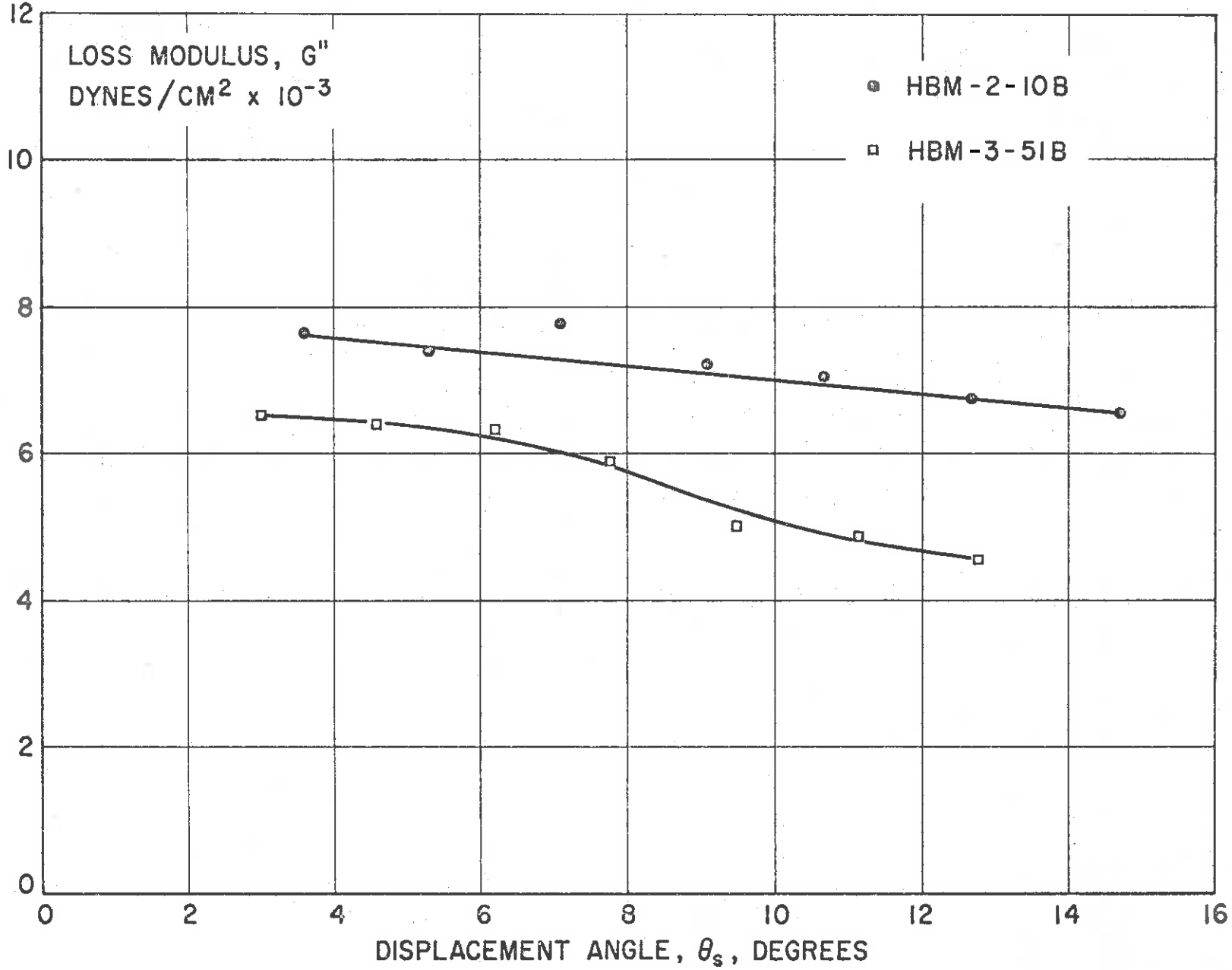

Figure 12

Loss Modulus of Human Brain Tissue. II. Second Scan, Specimens Conditioned by Vibration

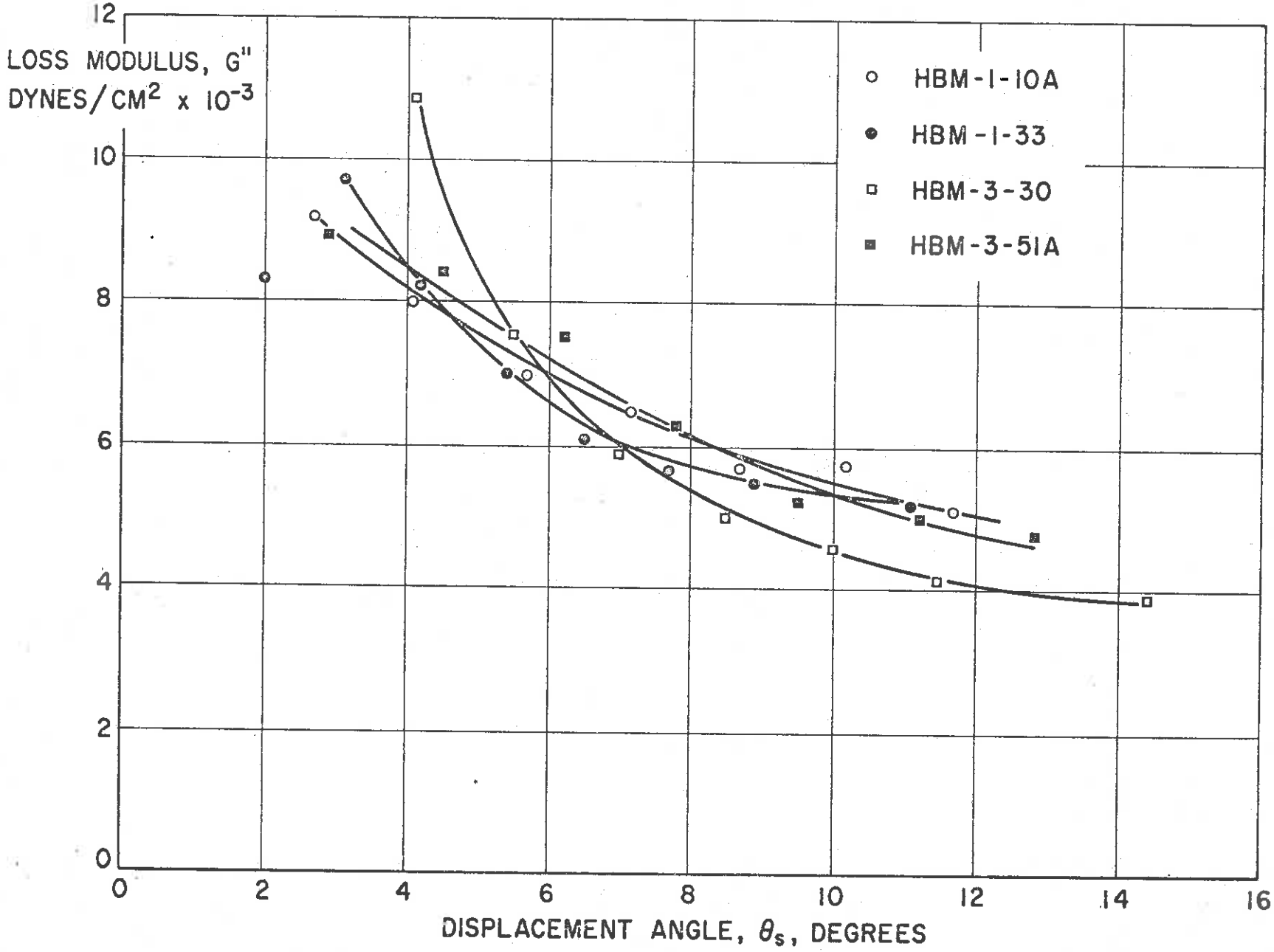

Figure 13

Loss Modulus of Human Brain Tissue. III. Effect of Refrigerat[illegible] Aging

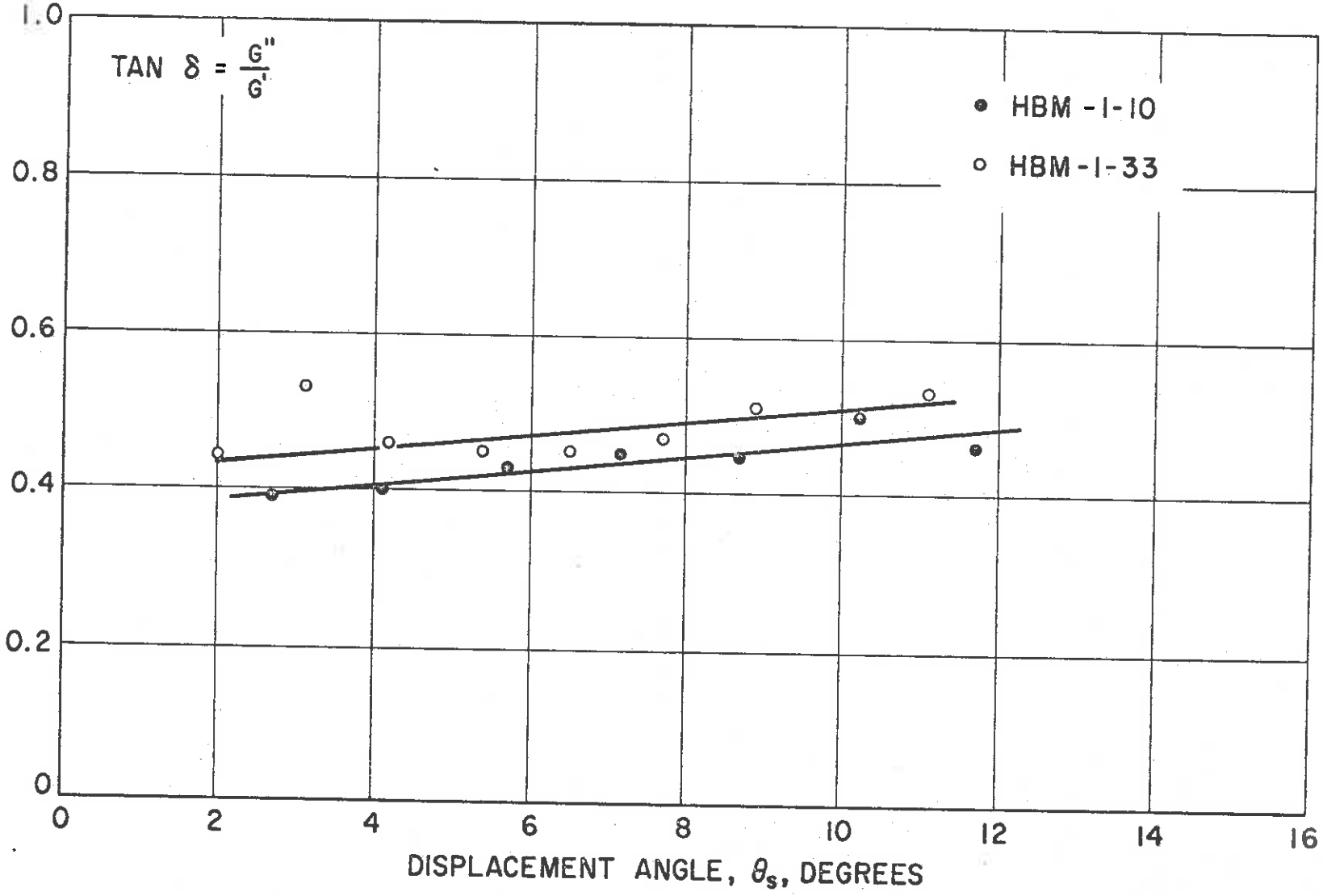

Figure 14

Loss Tangent of HBM-1

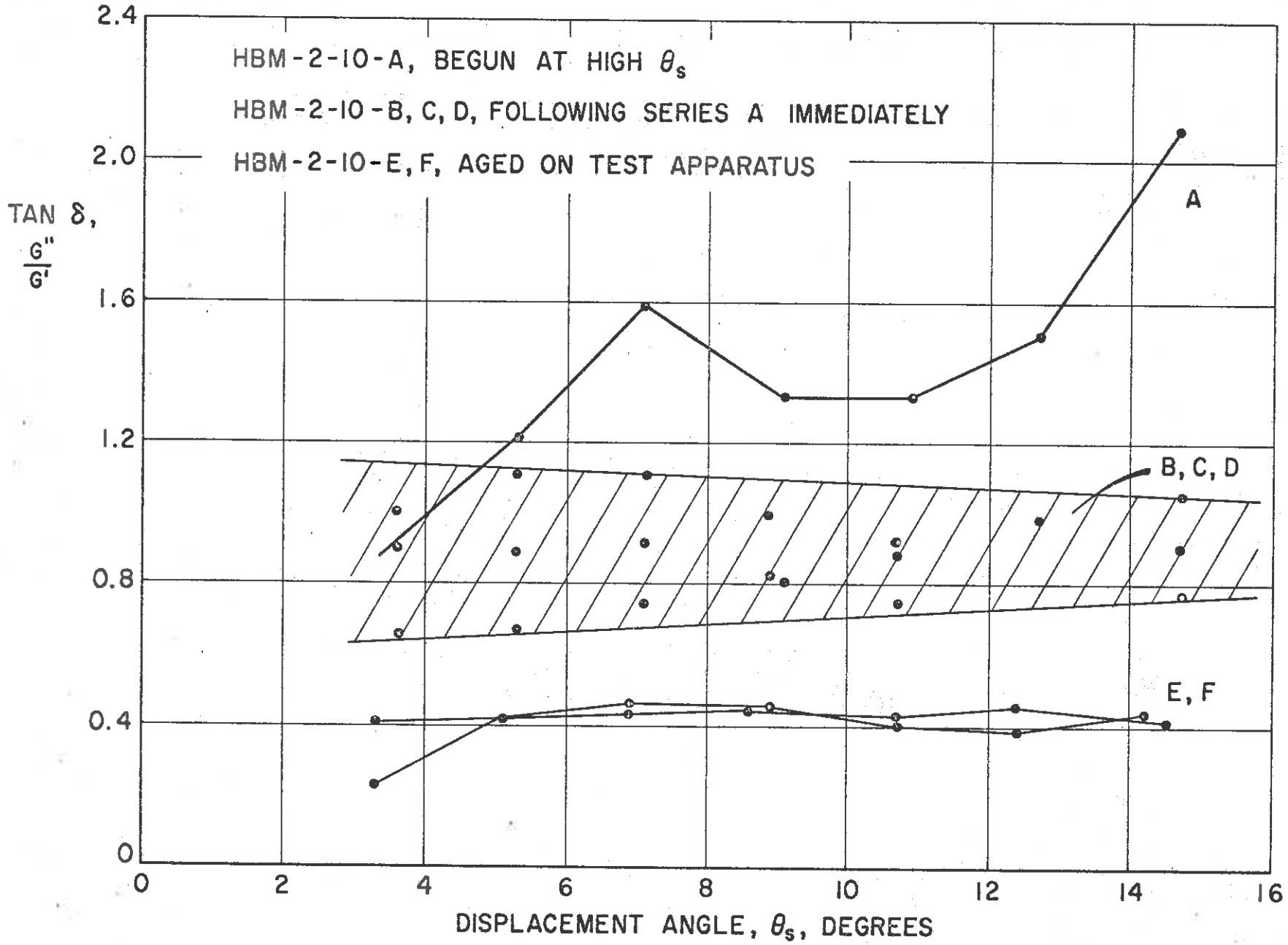

Figure 15

Loss Tange[illegible] of HBM-2

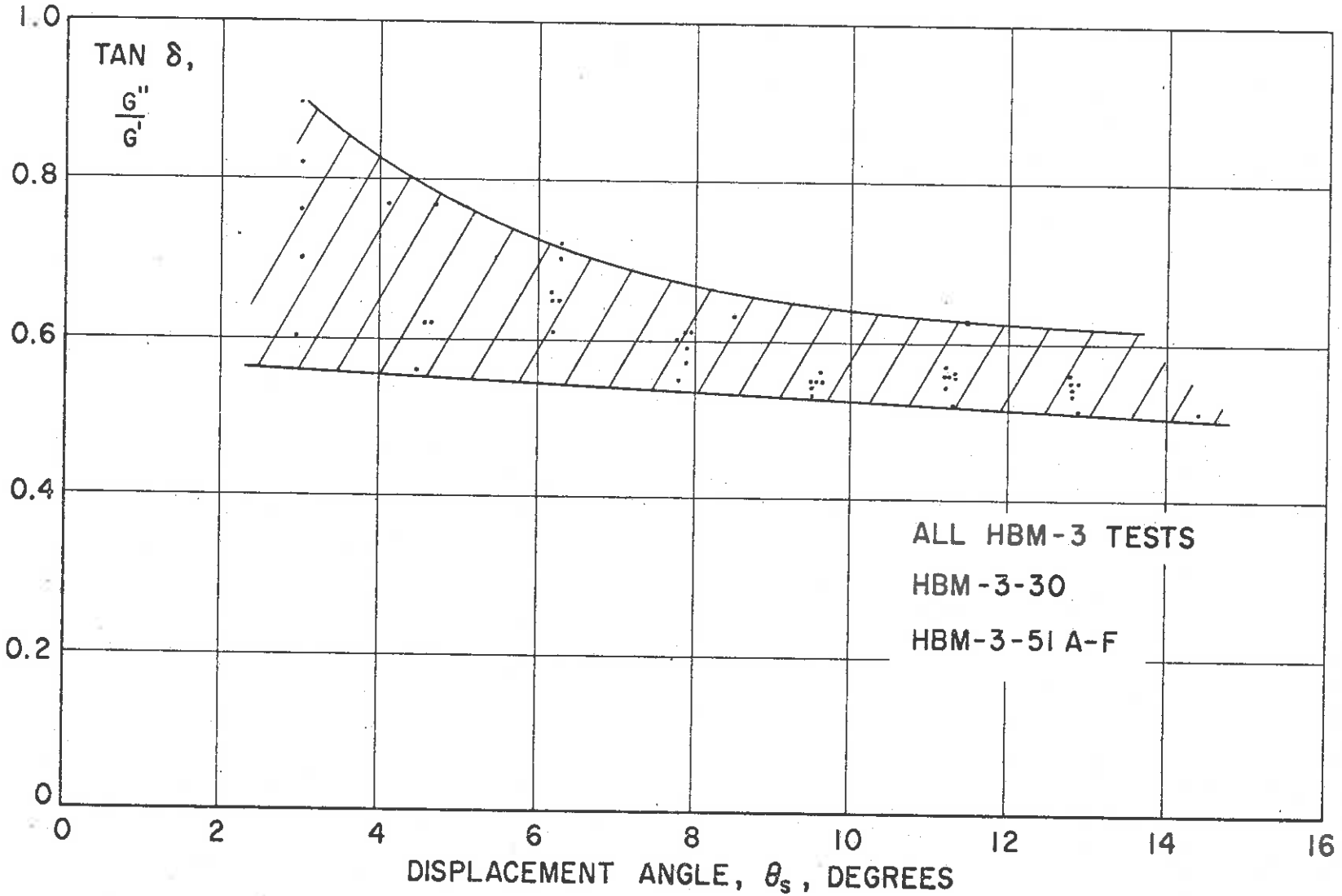

Figure 16

Loss Tangent of HBM-3

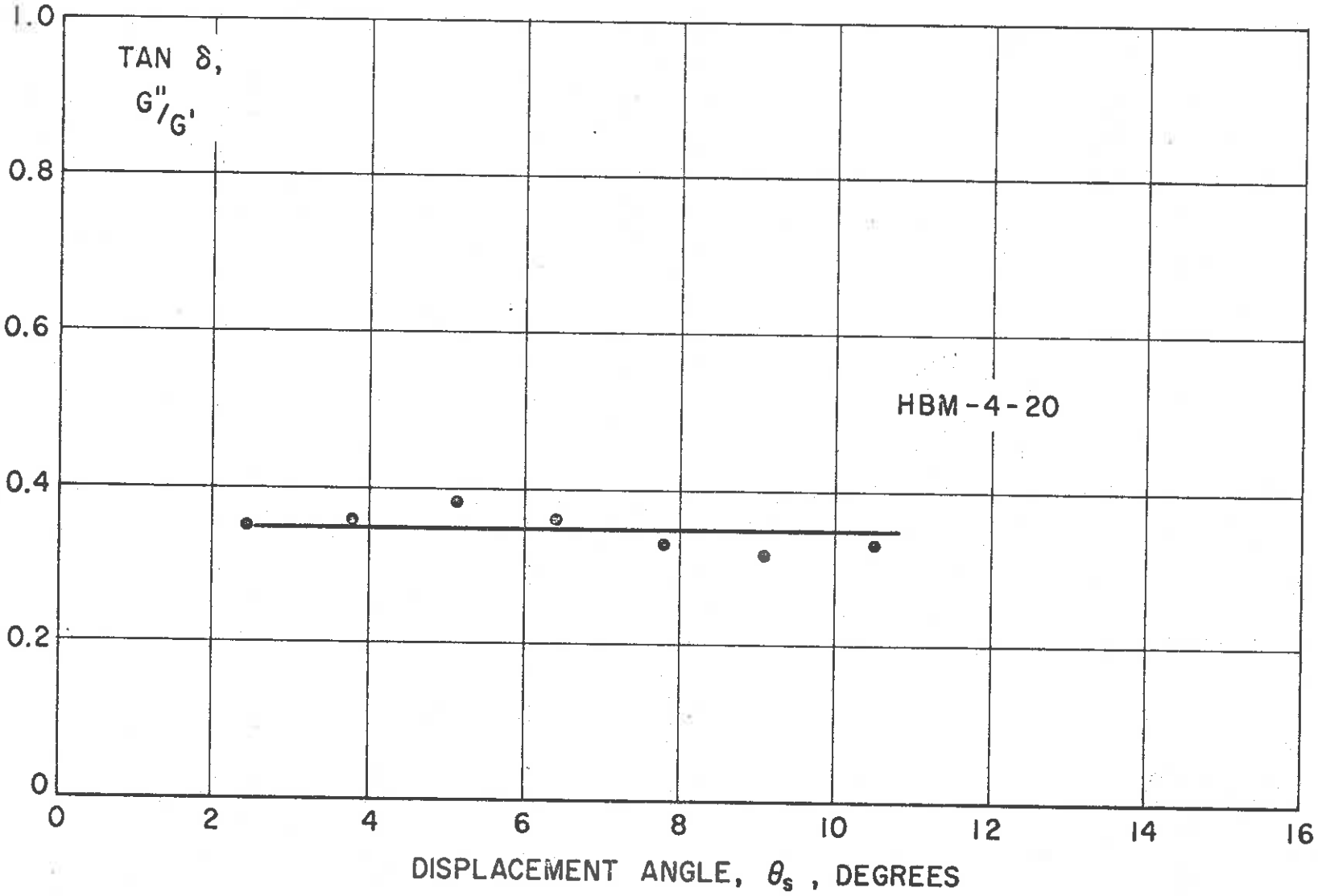

Figure 17
Loss Tangent of HBM-4

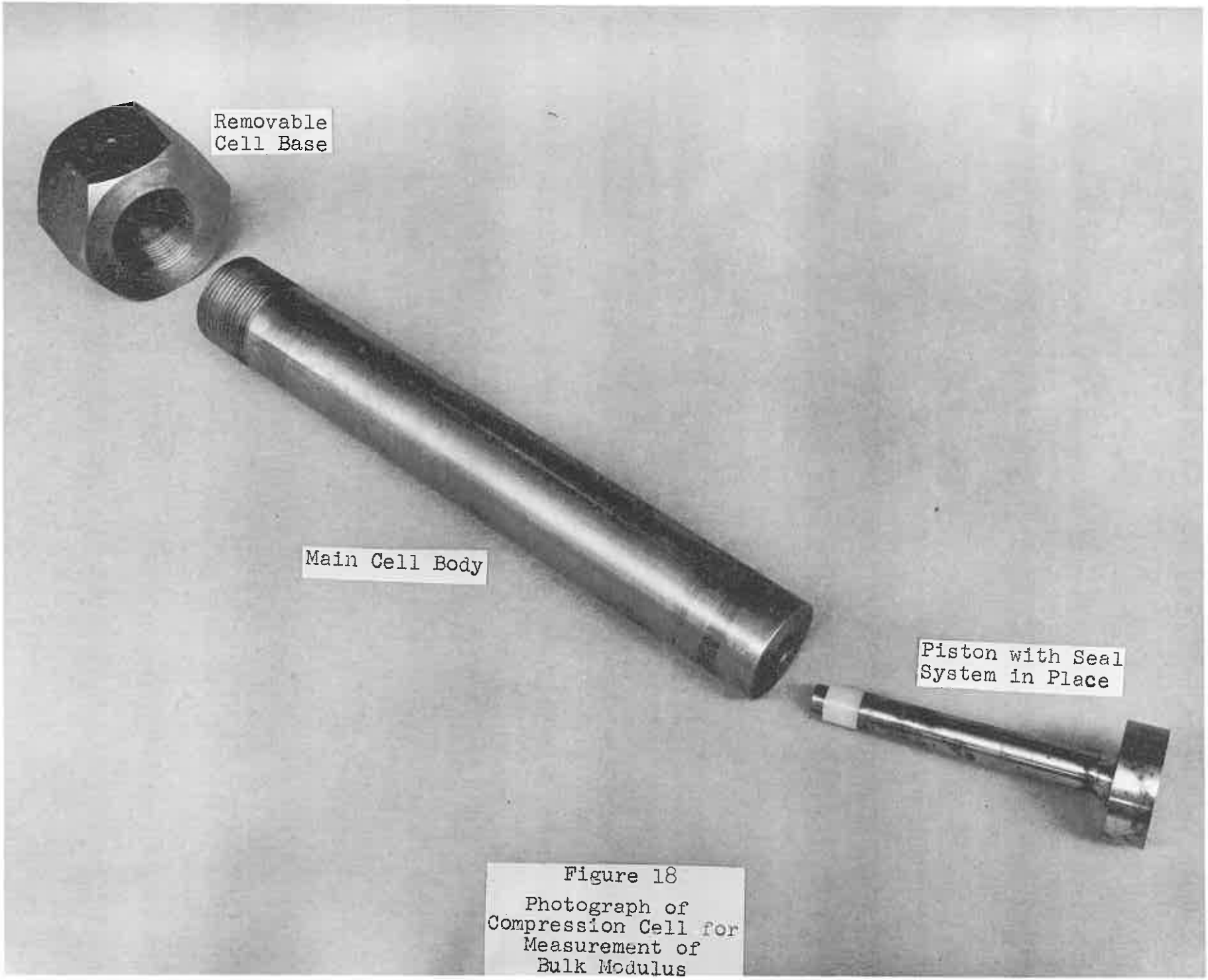

Figure 18

Photograph of
Compression Cell for
Measurement of
Bulk Modulus

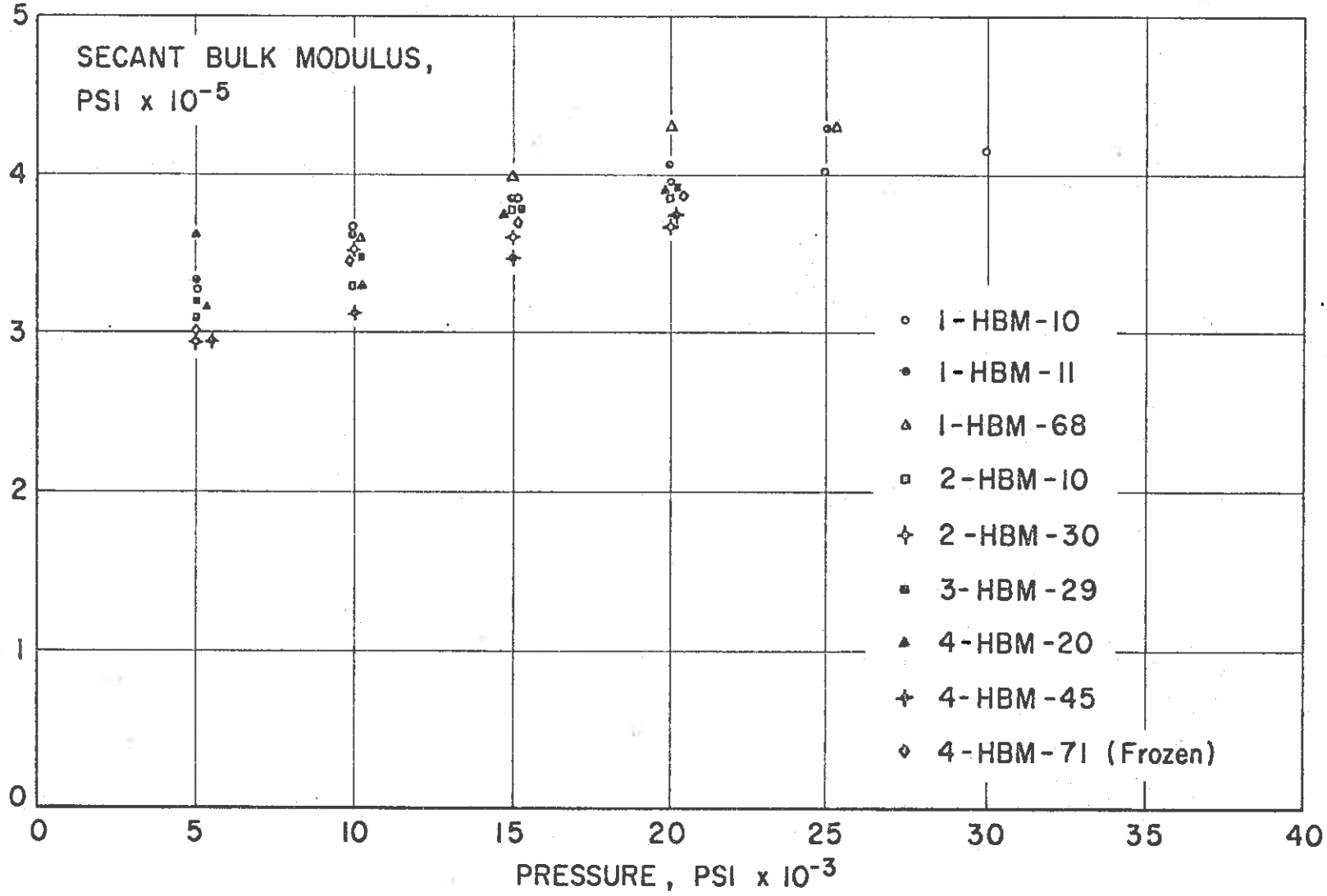

Figure 19

Secant Bulk Modulus of Human Tissue. I. Mean Values, Each Test

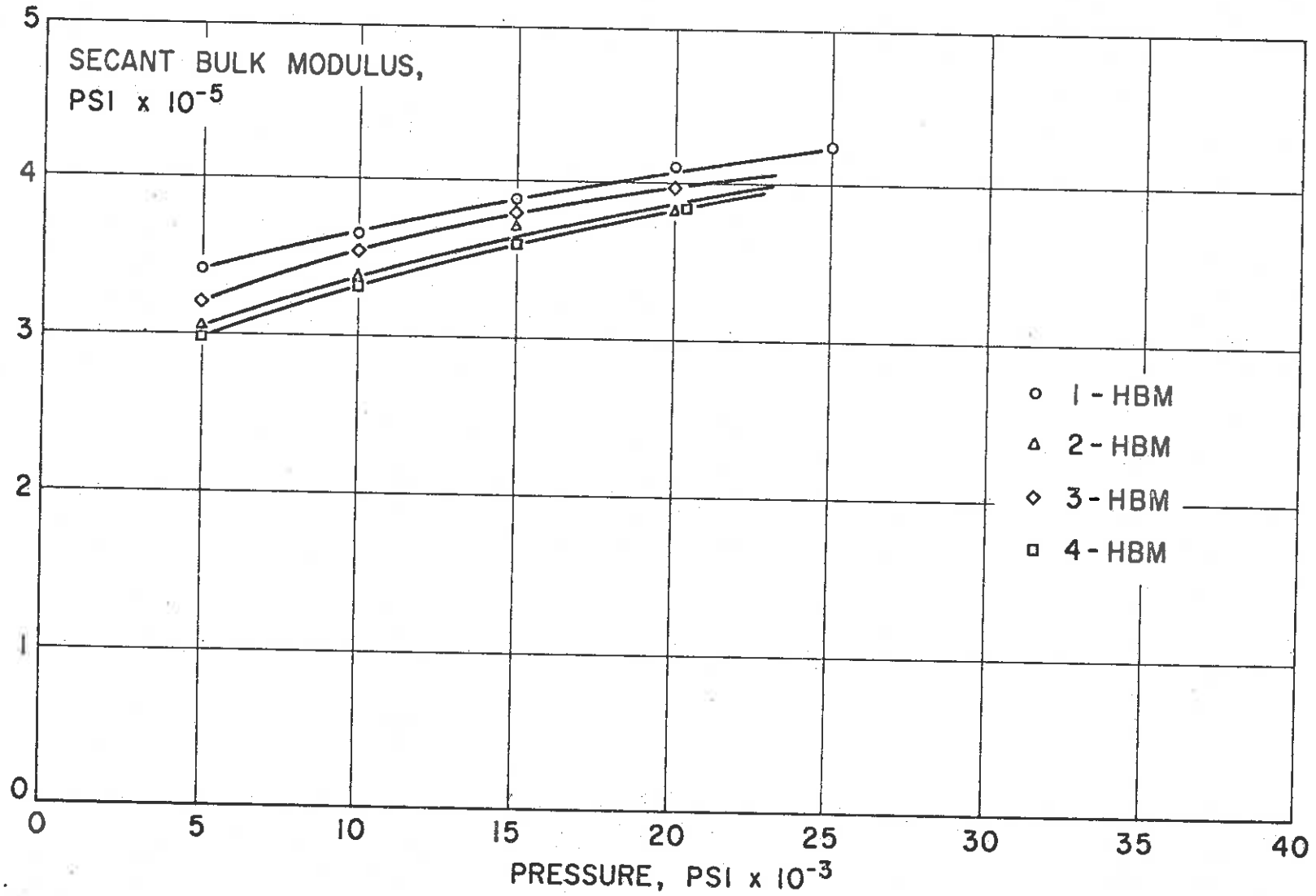

Figure 20

Secant Bulk Modulus of Human Tissue. II. Mean Values, Each Individual

Table I

Dynamic Shear Modulus

Rhesus Monkey Brain

Sample History - Time of sacrifice: 11:00 A.M., 27 Sept. 67

Transfer conditions: Whole heads packed in polyethylene bags and shipped in

1) ice (unfrozen), or

2) dry ice (frozen)

Test No. 1	Freq (Hz)	θs	G' dynes/cm^2	G" dynes/cm^2	G* dynes/cm^2	tan δ
5 Oct. 67	10.29	1.2°	8.9 x 10^3	2.4 x 10^3	9.2 x 10^3	0.27
Room temp.	10.01	3.1	8.0	2.6	8.4	0.32
h_o = 0.82 cm	9.67	6.2	6.3	2.4	6.8	0.38
A = 5.69 cm^2	9.48	9.8	5.2	2.0	5.7	0.39
h_o/A = 0.144 cm^{-1}	9.34	12.7	4.1	1.8	4.5	0.44

The whole head had been stored during the interim period at 3°C.

Test No. 2	Freq (Hz)	θs	G' dynes/cm^2	G" dynes/cm^2	G* dynes/cm^2	tan δ
3 Nov. 67	9.65	4.5°	0.6 x 10^3	0.8 x 10^3	-	1.37
Room temp.	9.48	6.9	0.7	0.6	-	0.77
h_o = 0.419 cm	9.34	9.3	0.3	0.6	-	2.99
A = 5.11 cm^2	9.28	11.7	0.7	-	-	-
h_o/A = 0.08 cm^{-1}						

The whole head had been stored during the interim period at -6°C.

Table II

Dynamic Shear Modulus
Human Brain No. 1

Sample History - Time of death: 5:45 A.M., 14 Nov. 67
Age: 48
Sex: M
Race: C
Cause of death: Cancer of bladder
Time specimen removed at autopsy: 11:30 A.M., 14 Nov. 67
Location of test specimen: Frontal lobe
Transfer conditions: Packed in polyethylene bags and shipped in ice and water

Test No.	Freq (Hz)	θs	G' dynes/cm²	G" dynes/cm²	G* dynes/cm²	tan δ
HBM-1-10	10.39	2.7°	23.4 x 10^3	9.2 x 10^3	25.1 x 10^3	0.39
3:30 - 3:50 P.M.	10.09	4.1	19.9	8.0	21.4	0.40
14 Nov. 67	9.83	5.7	16.3	7.0	17.7	0.43
Temp. - 37°C	9.68	7.2	14.4	6.5	15.8	0.45
White matter	9.56	8.7	12.6	5.7	13.8	0.45
h_o = 0.629 cm	9.46	10.2	11.6	5.8	13.0	0.50
A = 4.8 cm^2	9.40	11.7	11.1	5.1	12.2	0.46
h_o/A = 0.131 cm^{-1}						

HBM-1-33	10.41	2.0°	24.5 x 10^3	10.9 x 10^3	26.8 x 10^3	0.44
3:00 - 3:15 P.M.	10.02	3.1	18.2	9.7	20.6	0.53
15 Nov. 67	9.92	4.2	18.0	8.2	19.8	0.46
Temp. - 37°C	9.76	5.4	15.7	7.0	17.2	0.45
White matter	9.61	6.5	13.5	6.1	14.8	0.45
h_o = 0.83 cm	9.52	7.7	12.2	5.7	13.5	0.47
A = 6.39 cm^2	9.44	8.9	10.8	5.5	12.1	0.51
h_o/A = 0.13 cm^{-1}	9.38	11.1	9.8	5.2	11.1	0.53

Table III

Dynamic Shear Modulus
Human Brain No. 2

Sample History - Time of death: 4:30 A.M., 28 Nov. 67
Age: 77
Sex: M
Race: C
Cause of death: Pulmonary edema - myocardial infarction
Time specimen removed at autopsy: 10:50 A.M., 28 Nov. 67
Location of test specimen: Frontal lobe
Transfer conditions: Packed in polyethylene bags and shipped in ice and water

Test No.	Freq (Hz)	θs	G' dynes/cm²	G" dynes/cm²	G* dynes/cm²	tan δ
HBM-2-10A	9.63	3.3°	7.9 x 10^3	6.9 x 10^3	10.5 x 10^3	0.88
2:08 - 2:16 P.M.	9.40	5.3	5.0	6.1	7.9	1.22
28 Nov. 67	9.27	7.1	4.0	6.4	7.6	1.60
Temp. - 37°C	9.19	9.1	4.0	5.4	7.7	1.34
White matter	9.13	10.9	4.0	5.3	6.6	1.34
h_o = 0.528 cm	9.08	12.7	3.5	5.3	6.4	1.51
A = 2.09 cm^2	9.04	14.7	2.6	5.5	6.1	2.10
h_o/A = 0.253 cm^{-1}						
HBM-2-10B	9.69	3.6°	11.6 x 10^3	7.6 x 10^3	13.9 x 10^3	0.66
2:17 - 2:25 P.M.	9.53	5.3	10.9	7.4	13.1	0.68
28 Nov. 67	9.41	7.1	10.4	7.8	13.0	0.75
	9.30	9.1	8.9	7.2	11.4	0.81
	9.26	10.7	9.3	7.1	11.7	0.76
	9.19	12.7	8.0	6.8	10.4	0.98
	9.12	14.7	6.1	6.5	8.9	1.06

Table III (cont.)

Test No.	Freq (Hz)	θs	G' dynes/cm²	G" dynes/cm²	G* dynes/cm²	tan δ
HBM-2-10C	9.61	3.6°	7.9 x 10^3	7.9 x 10^3	11.2 x 10^3	1.00
2:26 - 2:33 P.M.	9.43	5.3	6.4	7.0	9.5	1.11
28 Nov. 67	9.32	7.1	6.3	7.0	9.4	1.12
	9.25	8.9	6.7	6.7	9.4	1.00
	9.21	10.7	7.1	6.5	9.6	0.92
	9.17	12.7	7.1	6.9	9.9	0.98
	9.15	14.7	6.5	6.8	10.1	0.91
HBM-2-10D	9.63	3.6°	8.8 x 10^3	8.0 x 10^3	11.9 x 10^3	0.90
2:36 - 2:45 P.M.	9.47	5.3	8.2	7.4	11.0	0.90
28 Nov. 67	9.36	7.1	8.1	7.5	15.0	0.92
	9.29	8.9	8.2	6.9	10.7	0.84
	9.23	10.7	7.7	6.9	10.4	0.89
	9.12	12.7	4.8	6.8	8.4	1.42
	9.19	14.7	9.3	7.3	11.8	0.78

Sample remained in static condition at 37°C between tests A-D and E and F.

HBM-2-10E	10.32	3.3°	45.8 x 10^3	10.4 x 10^3	47.0 x 10^3	0.23
3:51 - 4:00 P.M.	10.01	5.1	37.7	15.9	40.9	0.42
28 Nov. 67	9.79	6.9	32.0	14.0	34.9	0.44
	9.59	8.6	25.7	11.6	28.2	0.45
	9.46	10.7	21.9	9.5	23.9	0.43
	9.32	12.4	16.8	7.8	18.5	0.46
	9.26	14.5	15.4	6.5	16.7	0.42

Table III (cont.)

Test No.	Freq (Hz)	θs	G' dynes/cm²	G" dynes/cm²	G* dynes/cm²	tan δ
HBM-2-10F	9.92	3.3°	27.1 x 10^3	11.1 x 10^3	29.3 x 10^3	0.41
4:14 - 4:21 P.M.	9.72	5.1	24.3	10.1	26.3	0.42
28 Nov. 67	9.57	6.9	21.7	10.2	24.0	0.47
	9.46	8.9	19.7	8.8	21.6	0.45
	9.42	10.7	20.1	8.2	21.7	0.41
	9.40	12.4	20.5	8.1	22.0	0.39
	9.29	14.2	16.8	7.4	18.4	0.44

Table IV

Dynamic Shear Modulus
Human Brain No. 3

Sample History - Time of death: 10:00 A.M., 29 Nov. 67
Age: 44
Sex: M
Race: C
Cause of death: Carcinoma of lung
Time specimen removed at autopsy: 11:05 A.M.; 30 Nov. 67
Location of test specimen: Frontal lobe
Transfer conditions: Packed in polyethylene bags and carried in ice and water

Test No.	Freq (Hz)	θs	G' dynes/cm²	G'' dynes/cm²	G* dynes/cm²	tan δ
HBM-3-30	9.59	4.1°	14.1 x 10^3	10.9 x 10^3	17.8 x 10^3	0.77
3:55 - 4:05 P.M.	9.38	5.5	11.1	7.5	13.4	0.68
30 Nov. 67	9.22	7.0	8.8	5.9	10.6	0.58
Temp. - 37°C	9.13	8.5	7.9	5.0	9.3	0.63
White matter	9.08	10.0	7.6	4.6	8.9	0.60
h_o = 0.665 cm	9.02	11.5	6.5	4.1	7.7	0.63
A = 4.19 cm^2	8.96	14.4	7.7	3.9	8.6	0.51
h_o/A = 0.159 cm^{-1}						

HBM-3-51A	9.93	2.9°	14.9 x 10^3	8.9 x 10^3	17.4 x 10^3	0.60
1:18 - 1:25 P.M.	9.70	4.5	15.0	8.4	17.2	0.56
1 Dec. 67	9.48	6.2	12.2	7.5	14.3	0.61
Temp. - 37°C	9.38	7.8	11.5	6.3	13.1	0.55
White matter	9.26	9.5	9.7	5.2	11.0	0.54
h_o = 0.589 cm	9.20	11.2	8.8	5.0	10.1	0.57
A = 4.02 cm^2	9.17	12.8	8.8	4.8	10.0	0.55
h_o/A = 0.146 cm^{-1}						

Table IV (cont.)

Test No.	Freq (Hz)	θs	G' dynes/cm²	G" dynes/cm²	G* dynes/cm²	tan δ
HBM-3-51B	9.67	3.0°	8.0 x 10^3	6.5 x 10^3	10.3 x 10^3	0.82
1:26 - 1:31 P.M.	9.52	4.6	10.4	6.4	12.2	0.62
1 Dec. 67	9.38	6.2	9.8	6.3	11.6	0.65
	9.31	7.8	9.7	5.9	11.4	0.60
	9.24	9.5	9.1	5.0	10.4	0.55
	9.21	11.2	9.1	4.9	10.3	0.54
	9.17	12.2	8.8	4.6	9.9	0.53
HBM-3-51C	9.63	3.0°	7.2 x 10^3	6.5 x 10^3	9.7 x 10^3	0.90
1:32 - 1:37 P.M.	9.48	4.6	9.4	6.4	11.4	0.68
1 Dec. 67	9.36	6.2	9.2	6.1	11.0	0.66
	9.29	7.9	9.2	5.6	10.8	0.61
	9.27	9.5	9.9	5.2	11.2	0.53
	9.20	11.2	8.8	4.9	10.1	0.56
	9.17	12.8	8.8	4.9	10.1	0.56
HBM-3-51D	9.63	3.0°	7.2 x 10^3	6.5 x 10^3	9.7 x 10^3	0.90
1:38 - 1:43 P.M.	9.47	4.6	9.1	6.4	11.1	0.70
1 Dec. 67	9.34	6.3	8.7	6.0	10.6	0.70
	9.28	7.9	8.9	5.4	10.4	0.61
	9.25	9.5	9.4	5.2	10.7	0.55
	9.20	11.2	8.8	4.9	10.1	0.56
	9.18	12.8	9.1	4.9	10.3	0.54

Table IV (cont.)

Test No.	Freq (Hz)	θs	G' dynes/cm²	G'' dynes/cm²	G* dynes/cm²	tan δ
HBM-3-51E	9.72	3.0°	10.6 x 10^3	7.4 x 10^3	12.9 x 10^3	0.70
2:02 - 2:07 P.M.	9.47	4.6	10.3	6.4	12.1	0.62
1 Dec. 67	9.30	6.3	8.7	5.6	10.3	0.65
Temp. - 37°C	9.22	7.9	8.3	4.7	9.5	0.57
White matter	9.15	9.6	7.7	4.3	8.8	0.55
h_o = 0.556 cm	9.09	11.3	7.1	4.0	8.1	0.56
A = 3.36 cm^2	9.06	12.9	6.8	3.7	7.7	0.55
h_o/A = 0.165 cm^{-1}						

HBM-3-51F	9.60	3.0°	7.2 x 10^3	5.5 x 10^3	9.1 x 10^3	0.76
2:08 - 2:13 P.M.	9.38	4.6	7.9	6.0	9.9	0.76
1 Dec. 67	9.27	6.3	7.8	5.6	9.6	0.72
	9.21	7.9	8.0	4.7	9.3	0.59
	9.16	9.6	8.0	4.5	9.2	0.56
	9.11	11.3	7.6	4.0	8.6	0.52
	9.09	12.9	7.6	3.9	8.5	0.51

Tests nos. 51E and 51F were conducted with the same test specimen as used in the series 51A-51D. The exposed edges were removed to explore the effects of drying and shear degradation.

Table V

Dynamic Shear Modulus
Human Brain No. 4

Sample History - Time of death: 6:00 P.M., 4 Dec. 67
Age: 92
Sex: M
Race: C
Cause of death: Heart failure
Time specimen removed at autopsy: 10:30 A.M., 5 Dec. 67
Location of test specimen: Frontal lobe
Transfer conditions: Packed in polyethylene bags and shipped in ice and water

Test No.	Freq (Hz)	θs	G' dynes/cm²	G'' dynes/cm²	G* dynes/cm²	tan δ
HBM-4-20	9.89	2.4°	21.8 x 10^3	7.6 x 10^3	23.1 x 10^3	0.35
2:17 - 2:25 P.M.	9.67	3.8	19.4	7.0	20.6	0.36
5 Dec. 67	9.49	5.1	17.1	6.6	18.3	0.38
Temp. - 37°C	9.38	6.4	15.5	5.6	16.5	0.36
White matter	9.31	7.8	15.1	5.0	15.9	0.33
h_o = 0.719 cm	9.24	9.1	14.1	4.6	14.8	0.32
A = 3.80 cm^2	9.22	10.5	14.4	4.7	15.1	0.33
h_o/A = 0.189 cm^{-1}						

Table VI

Secant Bulk Modulus

Pig Brain

Sample History - The pig brain was obtained freshly slaughtered from a local slaughter house. It was refrigerated at 3°C until testing time.

Sample Preparation - An entire brain was cut into small cubes and slowly blended with a spatula. This blend was then transferred to the compression cell for testing.

Test Conditions - Three tests were conducted using one sample filling at room temperature approximately 30 hours post-slaughter.

Test No.	Pressure	% Compression	Secant Bulk Modulus
1	5×10^3 psi	1.43	3.49×10^5 psi
	10	2.46	3.79
	15	3.75	4.00
	20	4.79	4.18
	25	5.73	4.36
2	5×10^3 psi	1.35	3.70×10^5 psi
	10	2.55	3.92
	15	3.65	4.11
	20	4.71	4.25
	25	5.65	4.42
3	5×10^3 psi	1.38	3.62×10^5 psi
	10	2.57	3.89
	15	3.68	4.08
	20	4.74	4.22
	25	5.65	4.42

Table VII

Secant Bulk Modulus

Rhesus Monkey Brain

Sample History - Whole Rhesus monkey heads were received from HSRI in polyethylene bags placed on ice. The heads were so-kept until the time of sample preparation.

Sample Preparation - A whole brain was cut into small cubes and hand blended with a spatula. The blend was loaded into the compression cell for testing.

Test Conditions - Two series of tests were conducted at room temperature. Each series includes tests of one sample filling. Series A was conducted 10 hours post-sacrifice; Series B - 34 hours post-sacrifice.

Test No.	Pressure	% Compression	Secant Bulk Modulus
A-1	5×10^3 psi	1.40	3.57×10^5 psi
	10	2.72	3.67
	15	3.70	4.05
	20	4.75	4.21
	25	5.75	4.35
	30	6.68	4.49
	35	7.53	4.65
A-2	5×10^3 psi	1.40	3.57×10^5 psi
	10	2.64	3.79
	15	3.78	3.97
	20	4.80	4.17
	25	5.73	4.36
	30	6.64	4.52
	35	7.50	4.67
	40	8.30	4.82

Table VII (cont.)

Test No.	Pressure	% Compression	Secant Bulk Modulus
B-1	5×10^3 psi	1.50	3.33×10^5 psi
	10	2.65	3.77
	15	3.75	4.00
	20	4.78	4.18
	25	5.75	4.35
	30	6.67	4.50
B-2	5×10^3 psi	1.27	3.94×10^5 psi
	10	2.50	4.00
	15	3.63	4.13
	20	4.70	4.26
	25	5.70	4.38
	30	6.63	4.52
	35	7.53	4.65
	40	8.39	4.77
B-3	5×10^3 psi	1.28	3.91×10^5 psi
	10	2.45	4.08
	15	3.60	4.17
	20	4.65	4.30
	25	5.65	4.42
	30	6.56	4.57
	35	7.45	4.70
	40	8.26	4.84

Table VIII

Secant Bulk Modulus
Rhesus Monkey Brain
Suspended in Glycerine

Sample History - Whole Rhesus monkey heads were received 27 September 67 from the HSRI. The heads had been frozen (on dry ice) within 2 hours post sacrifice. The heads had been stored for 22 days at -6°C. Thawing was accomplished by immersing a head, in its polyethylene bag, in water at room temperature for 16 hours.

Sample Preparation - The test brain was cut into roughly-cubical pieces of volume approximating 0.1-0.2 cc each. The pieces were placed in the compression cell which was then filled with glycerine.

Test Volumes - Brain - 15.0 cc - 46.6%
Glycerine - 17.2 cc - 53.4%

	Percentage Compression			
Pressure	Total	Glycerine	Brain	Secant Bulk Modulus
5 x 10^3 psi	1.00%	0.46%	1.12%	4.46 x 10^5 psi
10	1.87	0.85	2.19	4.56
15	2.70	1.19	3.22	4.66
20	3.45	1.53	4.10	4.88
25	4.17	1.86	4.96	5.04
30	4.83	2.17	5.69	5.27
35	5.46	2.47	6.42	5.45
40	6.00	2.74	7.00	5.71

Table IX

Secant Bulk Modulus
Human Brain No. 1

Sample History - Time of death: 5:45 A.M., 14 Nov. 67
Age: 48
Sex: M
Race: C
Cause of death: Cancer of bladder
Time specimen removed at autopsy: 11:30 A.M., 14 Nov. 67
Location of test specimen: Frontal lobe
Transfer conditions: Packed in polyethylene bags and shipped in ice and water

Test No.	Pressure	Compression	Secant Bulk Modulus
1-HBM-11	5×10^3 psi	1.50%	3.33×10^5 psi
Mixed grey and	10	2.76	3.62
white matter	15	3.91	3.84
4:30 P.M.,	20	4.93	4.06
14 Nov. 67	25	5.84	4.28
Room temperature			
100% brain solids			

Test No.	Pressure	Total Compression	Brain Compression	Secant Bulk Modulus
1-HBM-10	5×10^3 psi	2.08%	0.94%	3.30×10^5 psi
Mixed grey and	10	3.67	1.69	3.67
white matter	15	5.08	2.42	3.85
3:30 P.M.,	20	6.40	3.15	3.94
14 Nov. 67	25	7.59	3.85	4.03
Temp. - 37°C	30	8.68	4.48	4.16
62.1% brain				
37.9% carrier fluid				

Table IX (cont.)

Test No.	Pressure	Total Compression	Brain Compression	Secant Bulk Modulus
1-HBM-29A	5 x 10^3 psi	1.79%	0.75%	5.01 x 10^5 psi
Mixed grey and	10	3.21	1.39	5.30
white matter	15	4.76	2.31	4.66
10:30 A.M.,	20	6.03	3.05	4.69
15 Nov. 67				
Temp. - 37°C				
65.2% brain				
34.8% carrier fluid				
	---	---	---	---
1-HBM-29B	5 x 10^3 psi	1.95%	0.91%	4.02 x 10^5 psi
	10	3.60	1.78	4.02
	15	4.95	2.50	4.27
	20	6.18	3.20	4.45
	---	---	---	---
1-HBM-29C	5 x 10^3 psi	1.83%	0.79%	4.72 x 10^5 psi
	10	3.47	1.65	4.38
	15	4.80	2.35	4.57
	20	5.96	2.98	4.81
	---	---	---	---
1-HBM-68A	5 x 10^3 psi	2.06%	0.92%	3.37 x 10^5 psi
Mixed grey and	10	3.74	1.76	3.53
white matter	15	5.08	2.42	3.85
3:30 P.M.,				
16 Nov. 67				
Temp. - 37°C				
62.1% brain				
37.9% carrier fluid				
	---	---	---	---

Table IX (cont.)

Test No.	Pressure	Total Compression	Brain Compression	Secant Bulk Modulus
1-HBM-68B	5 x 10^3 psi	1.97%	0.83%	3.74 x 10^5 psi
	10	3.66	1.68	3.70
	15	4.97	2.31	4.03
1-HBM-68C	5 x 10^3 psi	1.97%	0.83%	3.74 x 10^5 psi
	10	3.66	1.68	3.70
	15	4.97	2.31	4.03
	20	6.14	2.89	4.30
	25	7.26	3.52	4.41

Table X

Secant Bulk Modulus
Human Brain No. 2

Sample History - Time of death: 4:30 A.M., 28, Nov. 67
Age: 77
Sex: M
Race: C
Cause of death: Pulmonary edema - myocardial infarction
Time specimen removed at autopsy: 10:50 A.M., 28 Nov. 67
Location of test specimen: Frontal lobe
Transfer conditions: Packed in polyethylene bags and shipped in ice and water

Test No.	Pressure	Total Compression	Brain Compression	Secant Bulk Modulus
2-HBM-10A	5×10^3 psi	2.26%	0.98%	2.93×10^5 psi
Mixed grey and	10	3.91	1.78	3.22
white matter	15	5.33	2.34	3.68
2:30 P.M.,	20	6.66	3.01	3.81
28 Nov. 67				
Temp. - 37°C				
57.4% brain				
42.6% carrier fluid				
	---	---	---	---
2-HBM-10B	5×10^3 psi	2.25%	0.97%	2.96×10^5 psi
	10	3.92	1.79	3.21
	15	5.28	2.29	3.76
	20	6.71	3.06	3.75
	---	---	---	---

Table X (cont.)

Test No.	Pressure	Total Compression	Brain Compression	Secant Bulk Modulus
2-HBM-10C	5 x 10^3 psi	2.14%	0.86%	3.34 x 10^5 psi
	10	3.79	1.66	3.46
	15	5.22	2.23	3.86
	20	6.53	2.88	3.99

2-HBM-30	5 x 10^3 psi	2.44%	0.74%	2.94 x 10^5 psi
Mixed grey and	10	4.19	1.23	3.54
white matter	15	5.78	1.81	3.60
10:45 A.M.,	20	7.21	2.37	3.67
29 Nov. 67				
Temp. - 37°C				
43.5% brain				
56.5% carrier fluid				

Table XI

Secant Bulk Modulus
Human Brain No. 3

Sample History - Time of death: 10:00 A.M., 29 Nov. 67
Age: 44
Sex: M
Race: C
Cause of death: Carcinoma of lung
Time specimen removed at autopsy: 11:05 A.M., 30 Nov. 67
Location of test specimen: Frontal lobe
Transfer conditions: Packed in polyethylene bags and carried in ice and water

Test No.	Pressure	Total Compression	Brain Compression	Secant Bulk Modulus
3-HBM-29A	5×10^3 psi	2.07%	1.03%	3.16×10^5 psi
Mixed grey and	10	3.67	1.85	3.52
white matter	15	5.03	2.58	3.79
3:00 P.M.,	20	6.28	3.30	3.95
30 Nov. 67				
Temp. - 37°C				
65.2% brain				
34.8% carrier fluid				
	---	---	---	---
3-HBM-29B	5×10^3 psi	2.06%	1.02%	3.20×10^5 psi
	10	3.67	1.85	3.52
	15	5.03	2.58	3.79
	20	6.31	3.33	3.92

Table XII

Secant Bulk Modulus
Human Brain No. 4

Sample History - Time of death: 6:00 P.M., 4 Dec. 67
Age: 92
Sex: M
Race: C
Cause of death: Heart Failure
Time specimen removed at autopsy: 10:30 A.M., 5 Dec. 67

Location of test specimen: Frontal lobe
Transfer conditions: Packed in polyethylene bags and shipped in ice and water

Test No.	Pressure	Total Compression	Brain Compression	Secant Bulk Modulus
4-HBM-20A	5×10^3 psi	1.93%	1.14%	3.20×10^5 psi
Mixed grey and	10	3.47	2.06	3.54
white matter	15	4.83	2.93	3.74
2:00 P.M.,	20	6.06	3.75	3.89
5 Dec. 67				
Temp. - 37°C				
73.0% brain				
27.0% carrier fluid				

4-HBM-20B	5×10^3 psi	1.95%	1.16%	3.15×10^5 psi
	10	3.46	2.05	3.56
	15	4.81	2.91	3.76
	20	6.03	3.72	3.92

Table XII (cont.)

Test No.	Pressure	Total Compression	Brain Compression	Secant Bulk Modulus
4-HBM-20C	5 x 10^3 psi	1.94%	1.15%	3.17 x 10^5 psi
	10	3.48	2.07	3.53
	15	4.81	2.91	3.76
	20	5.99	3.68	3.97
4-HBM-20D	5 x 10^3 psi	1.98%	1.19%	3.07 x 10^5 psi
	10	3.49	2.08	3.51
	15	4.83	2.93	3.74
	20	6.04	3.73	3.91
4-HBM-45	5 x 10^3 psi	2.26%	0.98%	2.93 x 10^5 psi
Mixed grey and	10	3.97	1.84	3.12
white matter	15	5.47	2.48	3.47
2:30 P.M.,	20	6.72	3.07	3.74
6 Dec. 67				
Temp. - 37°C				
57.4% brain				
42.6% carrier fluid				
4-HBM-71A	5 x 10^3 psi	2.04%	1.18%	3.02 x 10^5 psi
Mixed grey and	10	3.59	2.09	3.42
white matter	15	4.92	2.91	3.68
5:00 P.M.,	20	6.16	3.71	3.85
7 Dec. 67				
Temp. - 37°C				
71.4% brain				
28.6% carrier fluid				

Table XII (cont.)

Test No.	Pressure	Total Compression	Brain Compression	Secant Bulk Modulus
4-HBM-71B	5 x 10^3 psi	2.06%	1.20%	2.97 x 10^5 psi
	10	3.59	2.09	3.42
	15	4.98	2.97	3.61
	20	6.18	3.73	3.83
4-HBM-71C	5 x 10^3 psi	2.03%	1.17%	3.05 x 10^5 psi
	10	3.52	2.02	3.54
	15	4.86	2.85	3.76
	20	6.10	3.65	3.91

Note: Series 4-HBM-71A-C was conducted using brain tissue which had been frozen (-6°C) for 20 hours and then thawed at room temperature for 7 hours.

THE AXISYMMETRIC RESPONSE OF A CLOSED SPHERICAL SHELL TO A LOCAL RADIAL IMPULSE

Appendix H

List of Symbols

A_o, A_{nm}, A_{nc}	Arbitrary constants (Constants of Integration)
E	Young's Modulus
M_z	Moment along polar axis
$P_n(\cos \xi)$	Legnedre polynomials of the first kind.
$P'_n(\cos \xi)$	Associated Legendre polynomials of the first kind and first order
a	Radius of spherical shell
a_o, a_n	Coeeficients of Legendre polynomial expansion of ζ
b_n	Coefficients of associated Legendre polynomial expansion of Ψ
c	Wave velocity, $[E/(1-\nu^2)]^{1/2}$
h	Shell thickness
r, θ, ϕ	Spherical coordinates of the deformed midsurface
t	Time
$\bar{u}$	Meridional displacement with respect to center of mass of the shell
w	Radial displacement, a-r
$\bar{w}$	Radial displacement with respect to center of mass of the shell
z	Distance from the midsurface
α^2	Thickness parameter, $h^2/12^2$
α_o, α_{nc}, α_{nm}	Phase angles (Constants of Integration)
β	Angle between midsurface normal and radial ray
γ_o	Midsurface shear strain
δ_{nc}, δ_{nm}	Amplitude ratios
$\varepsilon_{o\xi}$, $\varepsilon_{o\eta}$	Midsurface normal strains
ε_ξ, ε_η	z-surface normal strains

ζ	Non-dimensional radial displacement, $\frac{a-r}{a}$
Ψ	Non-dimensional angular meridional displacement
α, η, ξ	Spherical coordianates of the undeformed midsurface
k_o , k_o	Midsurface curvature
ν	Poisson's ratio
ρ	Mass density
σ_ξ, σ_η	Normal stresses
τ	Dimensionaless time, ct/a
ω_o, ω_{nc}, ω_{nm}	Angular frequencies of breathing, composite, and membrane modes respectively.

Introduction

The first mathematical model for head injury which is being studied is a closed spherical shell subjected to a local radial impulse. The shell is not filled with a fluid. The problem of a deformable, fluid-filled shell subjected to this loading has not been solved in the published literature. The problem discussed in this Appendix is shown schematically in Figure 1. The next step is inclusion of a fluid.

General formulation of problem.

The equations of motion for free vibration of a closed spherical shell may be derived by an energy formulation as it was done in [1]. In this reference, Lagrangian representation of spherical shell deformation is considered. If the undeformed and deformed configurations of the midsurface are represented by spherical coordinates a, η, ξ and r, θ, ϕ respectively, in the Lagrangian sense the deformed state coordinates are taken as functions of initial configuration and time, i.e. $r=r(\xi,\eta,\tau)$, $\theta=\theta(\xi,\eta,\tau)$ and $\phi=\phi(\xi,\eta,\tau)$. Defining the following non-dimensional variables:

$$\psi = \phi-\xi \quad \text{(Angular meridional displacement)}$$

$$\zeta = \frac{1}{a}\left[\frac{E}{\rho(1-\nu^2)}\right]^{\frac{1}{2}}\tau. \quad \text{If} \quad c = \left[\frac{E}{\rho(1-\nu^2)}\right]^{\frac{1}{2}}, \text{ then } \quad \tau = \frac{c}{a}t.$$

$$\alpha^2 = \frac{h^2}{12a^2} \quad \text{(a thickness parameter)}$$

where for torsionless axisymmetric motion $\psi = \psi(\xi,\tau)$ and $\zeta = \zeta(\xi,\tau)$ i.e. $\frac{\partial}{\partial\eta} = 0$ and denoting $\frac{\partial}{\partial\xi}$ by dot the two partial differential equations governing the free torsionless axisymmetric motion are:

$$\ddot{\psi} + \dot{\psi}\cot\xi - \psi(\nu-\cot^2\xi) - \dot{\zeta}(1+\nu) + \alpha^2[\ddot{\psi} + \dot{\psi}\cot\xi - \psi(\nu+\cot^2\xi) + \dddot{\zeta} + \ddot{\zeta}\cot\xi + \zeta(\nu+\cot^2\xi)] = \frac{\partial^2\psi}{\partial\tau^2} \qquad (1)$$

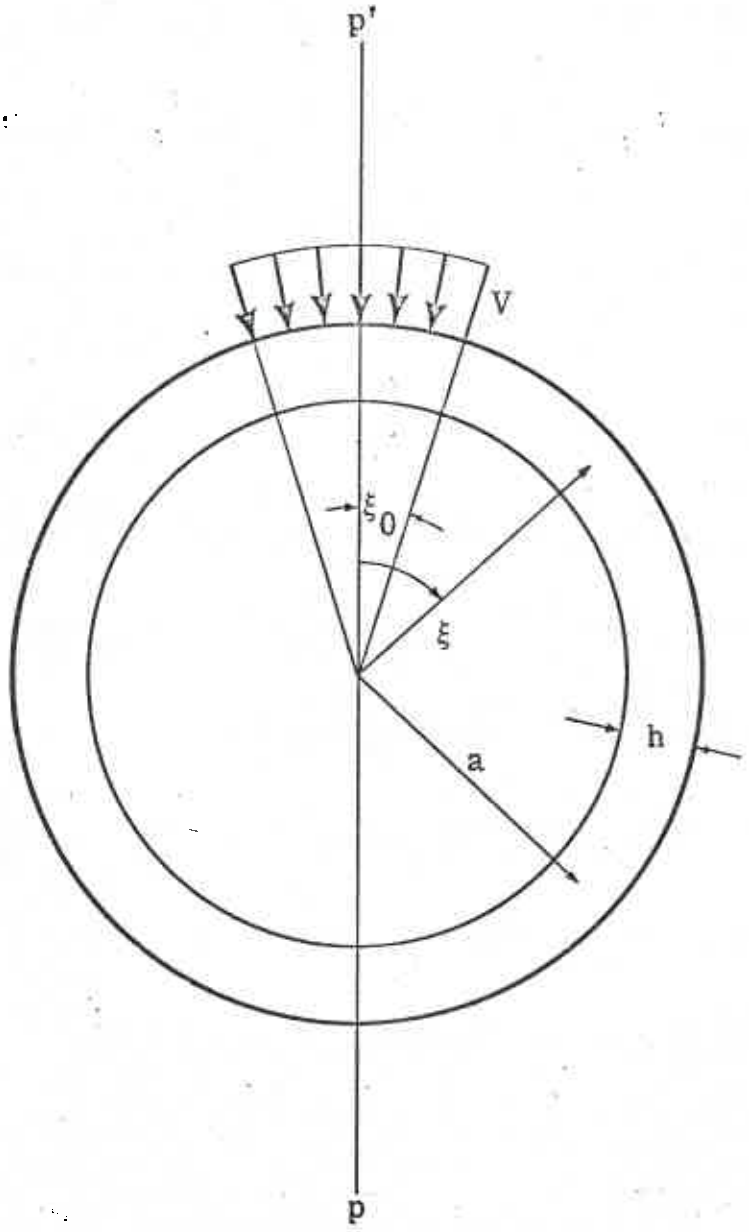

FIGURE 1. CLOSED SPHERICAL SHELL SUBJECTED TO LOCAL IMPULSE

$$(1+\nu)\,(\dot{\Psi}+\cot\xi-2\zeta) - \alpha^2[\dot{\Psi}+2\ddot{\Psi}\cot\xi+\dot{\Psi}(1+\nu+\cot^2\xi) + \Psi\cot\xi\,(2-\nu$$

$$+\cot^2\xi) + \dddot{\zeta} + 2\dot{\zeta}\cot - (1+\cot^2) + \cot(2-\cot^2) = \frac{\partial^2\Psi}{\partial\tau^2} \qquad (2)$$

Equations (1) and (2) are obtained from [1] for sufficiently small deformations by neglecting the second order terms in the two nonlinear partial differential equations. For the solution of the two linear partial differential equations, assume the displacements ζ and Ψ are represented by;

$$\zeta = \sum_{n=0}^{\infty} a_n(t)P_n(\cos\xi) \qquad (3)$$

$$\Psi = \sum_{n=1}^{\infty} b_n(t)P'_n(\cos\xi) \qquad (4)$$

where $P_n(\cos\xi)$ are Legendre polynomials of the first kind, and $P'_n(\cos\xi)$ are associated Legendre polynomials of the first kind and first order.

The quantity $P_n(\cos\xi)$ satisfies the recursion relation

$$\ddot{P}_n(\cos\xi) + \dot{P}_n(\cos\xi)\cot\xi + n(n+1)P_n(\cos\xi) = 0 \qquad (5)$$

and $P'_n(\cos\xi)$ satisfies the similar equation

$$\ddot{P}'_n(\cos\xi) + \dot{P}'_n(\cos\xi)\cot\xi + [n(n+1) - \csc^2]P'_n(\cos\xi) = 0 \qquad (6)$$

Substitution of (3) and (4) into equations (1) and (2) and repeated use of Legendre equations (5) and (6) in proper places yield the following equations satisfied by the coefficients $a_n(t)$ and $b_n(t)$.

$$\frac{d^2a_o}{dt^2} + 2(1+)a_o=0 \qquad \text{for } n=0 \qquad (7a)$$

$$\frac{d^2b_n}{dt^2} + a_n\{1+\nu - \alpha^2[1-\nu-n(n+1)]\}-b_n[1-\nu-n(n+1)](1+\alpha^2)=0 \qquad (7b)$$

$$\text{for } n\geq 1$$

$$\frac{d^2a_n}{dt^2} + b_n(1+\nu)n(n+1)+2a_n(1+\nu) + \alpha^2(a_n+b_n)[n^2(n+1)^2-(1-\nu)n(n+1)=0 \qquad (7c)$$

Since (7a,b,c) are analogous to a linear, two degree of freedom system their solutions are well known.

The solutions of (7a,b,c,) have the following form;

$$a_o=A_o\sin(w_o\tau + \alpha_o) \qquad n=o \qquad (8a)$$

$$a_n=A_{nm}\sin(w_{nm}\tau + \alpha_{nm}) + A_{nc}\sin(w_{nc}\tau + \alpha_{nc}) \qquad (8b)$$

$$b_n=\phi_{nm}A_{nm}\sin(w_{nm}\tau + \alpha_{nm}) + \phi_{nc}A_{nc}\sin(w_{nc}\tau + \alpha_{nc}) \qquad n\geq 1 \qquad (8c)$$

where A_o, A_{nm}, A_{nc}, α_o, α_{nm}, α_{nc}, are arbitrary constants. The amplitude ratios, ϕ_{nm}, ϕ_{nc} and frequencies w_{nm}, w_{nc} are independent of any initial conditions and can be determined from the shell parameters.

Equations (7a,b,c,) can be written more compact form by defining;

$$P_1 = 1+\nu - \alpha^2[1-\nu-n(n+1)] \;, \quad P_2 = 2(1+\nu) + \alpha^2[n^2(n+1)^2-(1-\nu)n(n+1)]$$

$$q_1 = [1-\nu-n(n+1)](1+\alpha^2) \;, \quad q_2 = (1+\nu)n(n+1) + \alpha^2[n^2(n+1)^2-(1-\nu)n(n+1)]$$

$$\frac{d^2b_n}{d\tau^2} + p_1a_n + q_1b_n=0 \;, \quad \frac{d^2a_n}{d\tau^2} + q_2b_n + p_2a_n=0 \qquad (9a,b)$$

Now assume $a_n = A_n \sin(w_n\tau + \alpha_n)$

$$b_n = B_n \sin(w_n\tau + \alpha_n)$$

Substitution of these into (9a,b) gives

$$(q_1 - w_n^2)\, B_n + P_1A_n=0$$

$$(P_2 - w_n^2)\, A_n + q_2B_n=0$$

For the non-trivial solution to exist the frequency equation is

$$w_n^4 - (q_1+P_2)w_n^2 + q_1P_2 - P_1q_2 =0 \qquad (10)$$

Substituting for the values P_1, P_2, q_1, q_2 and after some manipulations the frequency equation (10) becomes;

$$\omega_n^4 - [1+3\nu-\alpha^2(1-\nu) + n(n+1) + \nu\alpha^2 n(n+1) + \alpha^2 n^2(n+1)^2]\omega_n^2 + [-2(1-\nu^2)(1+\alpha^2) + n(n+1)(1-\nu^2) + \alpha^2 n(n+1)(5-\nu^2) - 4\alpha^2 n^2(n+1)^2 + \alpha^2 n^3(n+1)^3] = 0$$

Solving for the square of the frequencies; for $n \geq 1$

$$2\omega_n^2 = [1+3\nu - \alpha^2(1-\nu) + n(n+1) + \nu\alpha^2 n(n+1) + \alpha^2 n^2(n+1)^2]$$

$$\mp\{[1+3\nu-\alpha^2(1-\nu) + n(n+1) + \nu\alpha^2 n^2(n+1)^2]^2 - 4[-2(1-\nu^2)(1+\alpha^2) + n(n\pm1)(1-\nu^2) + \alpha^2 n(n+1)(5-\nu^2) - 4\alpha^2 n^2(n+1)^2 + \alpha^2 n^3(n+1)^3]\}^{\frac{1}{2}}$$

for $n \geq 1$

and $\omega_o = [2(1+\nu)]^{\frac{1}{2}}$ [from (7a)]

Postive and negative signs give frequencies ω_{nm} and ω_{nc} respectively.

The amplitude ratios are:

$$\delta_{nm} = \frac{B_{nm}}{A_{nm}} = -\frac{P_1}{q_1-\omega_{nm}^2} = \frac{1+\nu-\alpha^2[1-\nu-n(n+1)]}{\omega_{nm}^2 + (1+\alpha^2)[1-\nu-n(n+1)]} \tag{11a}$$

$$\delta_{nc} = \frac{B_{nc}}{A_{nc}} = -\frac{P_1}{q_1-\omega_{nc}^2} = \frac{1+\nu - \alpha^2[1-\nu-n(n+1)]}{\omega_{nc}^2 + (1+\alpha^2)[1-\nu-n(n+1)]} \tag{11b}$$

Substituting (8a,b,c,) into (3) and (4) formally gives the solutions for ζ and Ψ

$$\zeta(\xi,\tau) = A_o \sin(\omega_o\tau + \alpha_o) + \sum_{n=1}^{\infty}[A_{nm} \sin(\omega_{nm}\tau + \alpha_{nm}) + A_{nc} \sin(\omega_{nc}\tau + \alpha_{nc})]$$

$$P_n(\cos\xi) \tag{12a}$$

$$\Psi(\xi,\tau) = \sum_{n=1}^{\infty}[\delta_{nm}A_{nm} \sin(\omega_{nm}\tau + \alpha_{nm}) + \delta_{nc}A_{nc} \sin(\omega_{nc}\tau + \alpha_{nc})]\, P'_n(\cos\xi) \tag{12b}$$

Note that, $P_o(\cos\xi) = 1$

$P_1(\cos\xi) = \cos\xi$ and $P'_n(\cos\xi) = \dot{P}_n(\cos\xi)$

$P_2(\cos\xi) = \frac{1}{2}(3\cos^2\xi - 1) = \frac{1}{4}(3\cos 2\xi + 1)$

$P_3(\cos\xi) = \frac{1}{2}(5\cos^3\xi - 3\cos\xi) = \frac{1}{8}(5\cos^3\xi + {}^3\cos\xi)$

Determination of initial conditions

For the dynamic response of a closed spherical shell to a sudden local radial impulse the initial conditions for the free vibration solution are

$$\zeta(\xi,o) = (r=a \text{ for every point a } \tau=o) \tag{13}$$

$$\Psi(\xi,o) = o \ (\phi=\xi \text{ for every point a } \tau=o) \tag{14}$$

There are also two velocity conditions on ζ and Ψ. To determine the first the local velocity imput is expressed a series expansion.

If $w=a-r$ $\quad \frac{\partial w}{\partial \tau} = \sum_{n=o}^{\infty} v_n P_n(\cos\xi) = \begin{cases} V & (-\xi_o<\xi<\xi_o) \\ o & (\xi_o<\xi<-\xi_o) \end{cases}$ (15)

Both sides of (15) may now be multiplied $P_m(\cos\ )\sin$ and integrated. The orthogonality condition is

$$\int_{-1}^{+1} P_m(x)P_n(x)dx = o \qquad (m\neq n)$$

Let $x=\cos\xi \rightarrow dx = \sin\xi d\xi$ or $\int_{\pi}^{o} P_m(\cos\xi)P_n(\sin\xi)\sin\xi d\xi = o \qquad (m\neq n)$

$$\int_{\pi}^{o} \sum_{n=0}^{\infty} v_n P_n(\cos\xi)P_m(\cos\xi)\sin\xi d\xi = \int_{\pi}^{o} \frac{\partial w}{\partial \tau} P_m(\cos\xi)\sin\xi d\xi =$$

$$\int_{\xi_o}^{o} VP_m(\cos\xi)\sin\xi d\xi$$

In view of the orthogonality condition;

$$V_m \int_{\pi}^{o} P_m^2(\cos\xi)\sin\xi d\xi = V \int_{\xi_o}^{o} P_m(\cos\xi)\sin\xi d\xi,$$

$$V_m = \frac{V\int_{\xi_o}^{o} P_m(\cos\xi)\sin\xi d\xi}{\int_{\pi}^{o} P_m^2(\cos\xi)\sin\xi d\xi} \tag{16}$$

The norm of P_n is

$$N(P_n) = \int_{-1}^{+1} P_n^2(x)dx = \frac{2}{2n+1} \qquad n=0,1,2...$$

or

$$N[P_m(\cos\xi)] = \int_{\pi}^{o} -P_m^2(\cos\xi)\sin\xi d\xi = \frac{2}{2m+1} \tag{17}$$

From (16) and (17)

$$V_m = \frac{2m+1}{2} V \int_{o}^{\xi_o} P_m(\cos\xi)\sin\xi d\xi. \tag{18}$$

Now $P_m(\cos\xi)$ may be expanded in trigonometric functions for $0<\xi<\pi$

$$P_m(\cos\xi) = \frac{2^{2m+2}(m!)^2}{\pi(2m+1)!}\left[\sin(m+1)\xi + \frac{m+1}{2m+3}\sin(m+3)\xi\right.$$

$$\left. + \frac{1\cdot 3\cdot (m+1)(m+2)}{2!(2m+3)(2m+5)} \sin(m+5)\xi + \ldots\right]$$

also $\int \sin mx \sin nx\, dx = \frac{\sin(m-n)x}{2(m-n)} - \frac{\sin(m+n)x}{2(m+n)}$. $[m^2 \neq n^2]$

Hence in principle by means of (18), V_m is known for every m.

$$V_o = \frac{V}{2}(1-\cos\xi_o)$$

$$V_1 = \frac{3V}{8}(1-\cos 2\xi_o)$$

$$V_2 = \frac{5V}{4} \left(\cos\xi_o - \cos^3\xi_o\right)$$

$$V_3 = \frac{7V}{16} \left(2 - 5\cos^4\xi_o + \cos 2\xi_o\right)$$

$$V_4 = \frac{9V}{16} \left(-7\cos^5\xi_o + 10\cos^3\xi_o - 3\cos\xi_o\right)$$

etc.

For determination of the second initial condition it should be noted that the linear momentum along the polar axis pp', M_z, is the component of the radial momentum due to initial radial velocity V for $-\xi_o \leq \xi < +\xi_o$.

Let V_z be the component of V along the polar axis pp', then the linear momentum along the polar axis is;

$$M_z = \int V_z \rho d\forall = \int \frac{\partial w}{\partial t} \cos\xi \rho h da \qquad \text{where } dA = 2\pi a^2 \sin\xi d\xi$$

partial shell vol. p.s.v.

$$M_z = \int_o^{\xi_o} \frac{\partial w}{\partial t} 2\pi a^2 \rho h \sin\xi\cos\xi d\xi$$

$$M_z = 2\pi a^2 \rho h \int_o^{\xi_o} \sum_{n=o}^{\infty} V_n P_n(\cos\xi) \sin\xi\cos\xi d\xi \tag{19}$$

The total mass of the sphere $\simeq 4\pi a^2 h\rho$

This approximation is consistent with the one made for thin shell theory. Because the exact mass of the sphere is

$$m_{total} = \rho\forall = \rho\frac{4}{3}\pi\left[\left(a + \frac{h}{2}\right)^3 - \left(a - \frac{h}{2}\right)^3\right] = \frac{4}{3}\pi\rho\left[3ha^2 + \frac{h^3}{4}\right] \simeq 4\pi a^2 h\rho$$

The expansion of the expression (19) for the first two terms is;

$$M_z = 2\pi a^2 \rho h \left[\int_0^{\xi_o} V_o P_o(\cos\xi) \sin\xi\cos\xi d\xi + \int_0^{\xi_o} V_1 P_1(\cos\xi) \sin\xi\cos\xi d\xi \right.$$

$$\left. + \int_0^{\xi_o} \sum_{n=2}^{\infty} V_n P_n(\cos\xi) \sin\xi\cos\xi d\xi \right]$$

Since V_o, V_1, V_2, etc. are constant coefficients

$$M_z = 2\pi a^2 \rho h \left[\frac{V_o}{4} (1-\cos 2\xi_o) + \frac{V_1}{3} (1-\cos^3 \xi_o) + \int_0^{\xi_o} \sum_{n=2}^{\infty} V_n P_n(\cos\xi) \sin\xi\cos\xi d\xi \right] \tag{20}$$

The rigid-body velocity is V_z which is imparted to the center of mass of the spherical shell in the negative polar axis direction.

$$V_z = \frac{1}{2} \left[\frac{V_o}{4} (1-\text{Cos}2\ _o) + \frac{V_1}{3} (1-\cos^3\ _o) + \int_0^{\xi_o} \sum_{n=2}^{\infty} V_n P_n(\cos\xi) \sin\xi\cos\xi d\xi \right] \tag{21}$$

To find the relative distribution of the deformation velocity the closed spherical shell is divided into two portions;

1) $-\xi_o < \xi < +\xi_o$ (Region where the velocity impulse is applied)

2) Outside of region (1) $+\xi < \xi < -\xi_o$

For region (1) the deformation velocity in the radial direction is $\frac{\partial \bar{w}}{\partial t}$ and in the meridional direction $\frac{\partial \bar{u}}{\partial t}$, then.

$$\frac{\partial \bar{w}}{\partial t} = \frac{\partial w}{\partial t} - V_z \cos\xi = \frac{\partial w}{\partial t} - V_z P_1(\cos\ ) \tag{22}$$

$$\frac{\partial \bar{u}}{\partial t} = o - V_z \sin\xi = V_z P'_1(\cos\xi)$$

Writing (22) more explicitly

$$\frac{\partial \bar{w}}{\partial t} = \sum_{n=o}^{\infty} V_n P_n(\cos\ ) - \frac{1}{2} V_z P_1(\cos\xi)$$

$$\frac{\partial \bar{w}}{\partial t} = V_o + \{ V_1 - \frac{1}{2} [\frac{V_o}{4} (1-\cos 2\xi_o) + \frac{V_1}{3} (1-\cos^3\xi_o)$$

$$+ \int_o^{\xi_o} \sum_{n=2}^{\infty} V_n P_n(\cos\xi) \sin\xi\cos\xi d\xi] \} P_1(\cos\xi)$$

$$+ \sum_{n=2}^{\infty} V_n P_n(\cos\xi) \qquad (22a)$$

$$\frac{\partial \bar{u}}{\partial t} = -\frac{1}{2} [\frac{V_o}{4} (1-\cos 2\xi_o) + \frac{V_1}{3} (1-\cos^3\xi_o) + \int_o^{\xi_o} \sum_{n=2}^{\infty} V_n P_n(\cos\xi) \sin\xi\cos\xi d\xi]$$

$$P'_n(\cos\xi) \qquad (22b)$$

Initially for region (2) the shell only suffers the velocity which is imparted to the center of mass of the shell in the negative polar axis direction. This velocity is V_z. Hence the last two initial conditions in terms of the variables of the problem are:

$$\frac{\partial \zeta(\xi,o)}{\partial \tau} = \frac{1}{c} \frac{\partial \bar{w}}{\partial t} \quad \text{for} \quad -\xi_o < \xi < +\xi_o$$

$$\frac{\partial \Psi(\xi,o)}{\partial \tau} = \frac{1}{c} \frac{\partial \bar{u}}{\partial t} \quad \text{for} \quad -\xi_o < \xi < +\xi_o$$

This completes the determination of the initial conditions.

Application of the initial conditions (13) and (14) into solution (12a,b) lead to $\alpha_o = \alpha_{nm} = \alpha_{nc} = o$. Hence from (12a,b),

$$\frac{\partial \zeta(\xi,o)}{\partial \tau} = A_o w_o + \sum_{n=1}^{\infty} [A_{nm}\omega_o + A_{nc}\omega_{nc}] P_n(\cos\xi) = \frac{1}{c}\frac{\partial \bar{w}}{\partial t} \tag{23a}$$

$$\frac{\partial \Psi(\xi,o)}{\partial \tau} = \sum_{n=1}^{\infty} [\delta_{nm}A_{nm}\omega_{nm} + \delta_{nc}A_{nc}\omega_{nc}] P'_n(\cos\xi) = \frac{1}{c}\frac{\partial \bar{u}}{\partial \tau} \tag{23b}$$

From equations (22) and (23) one can conclude that;

$$A_o = \frac{V_o}{c\omega_o} \qquad \text{for } n=o$$

$$A_{1m}\omega_{1m} + A_{1c}\omega_{1c} = \frac{1}{c}(V_1 - V_z) \tag{24a}$$

$$\delta_{1m}A_{1m}\omega_{1m} + \delta_{1c}A_{1c}\omega_{1c} = \frac{1}{c}V_z \qquad \text{for } n=1 \tag{24b}$$

$$A_{nm}\omega_{nm} + A_{nc}\omega_{nc} = \frac{1}{c}V_n \tag{25a}$$

$$\delta_{nm}A_{nm}\omega_{nm} + \delta_{nc}A_{nc}\omega_{nc} = o \qquad \text{for } n \geq 2 \tag{25b}$$

From (24a) and (24b)

$$A_{1c} = \frac{\delta_{1m}V_1 + V_z(1-\delta_{1m})}{c\omega_{1c}(\delta_{1m}-\delta_{1c})} \qquad \text{and } A_{1m} = \frac{\delta_{1c}V_1 + V_z(1-\delta_{1c})}{c\omega_{1m}(\delta_{1c}-\delta_{1m})}$$

From (25a) and (25b) for $n \geq 2$

$$A_{nc} = \frac{\delta_{nm}V_n}{\omega_{nc}\, c(\delta_{nm}-\delta_{nc})} \qquad \text{and} \quad A_{nm} = \frac{\delta_{nc}V_n}{\omega_{nm}\, c(\delta_{nc}-\delta_{nm})}$$

Since all the A_{nc}, A_{nm}, δ_{nc}, δ_{nm}, ω_{nc} and ω_{nm} are known the solutions (12a) and (12b) are complete and determined.

The linear midsurface strain and rotation quantities in terms of $\zeta(\xi,\tau)$ and $\Psi(\xi,\tau)$ are;

$$\varepsilon_{o\xi}(\xi,\tau) = \frac{\partial \Psi}{\partial \xi} + \zeta$$

$$\varepsilon_{o\eta}(\xi,\tau) = -\zeta + \Psi\cot\xi$$

$$k_{o\xi}(\xi,\tau) = \frac{1}{a}\left(1 + \zeta + \frac{\partial^2 \zeta}{\partial \xi^2}\right)$$

$$k_{o\eta}(\xi,\tau) = \frac{1}{a \sin\xi}(1 + \zeta - \Psi\cot\xi)$$

$$\beta(\xi,\tau) = -\frac{\partial \zeta}{\partial \xi}$$

For isotropic and homogeneous continuum, Hooke's Law yields biaxial stress-strain relations:

$$\sigma_\xi(\xi,\tau) = \frac{E}{1-\nu^2}(\varepsilon_\xi + \nu\,\varepsilon_\eta)$$

$$\sigma_\eta(\xi,\tau) = \frac{E}{1-\nu^2}(\varepsilon_\eta + \nu\,\varepsilon_\xi)$$

Where ε_ξ and ε_η are the z-surface strain quantities

The z-surface strain quantities are:

$$\varepsilon_\xi(\xi,\tau) = \varepsilon_{o\xi} + z\left(k_{o\xi} - \frac{1}{a}\right)(1+\varepsilon_{o\xi})\left(1 - \frac{z}{a}\right)$$

$$\varepsilon_\eta(\xi,\tau) = \varepsilon_{o\eta} + z\left[k_o \sin(\phi-\beta) - \frac{1}{a}\right](1 + \varepsilon_{o\eta})\left(1 - \frac{z}{a}\right)$$

Note that $\phi = \Psi + \xi = \Psi(\xi,\tau) + \xi = \phi(\xi,\tau)$

$$\beta = - \frac{\partial \zeta(\xi,\tau)}{\partial \xi}$$

Numerical Results

At the present time numerical values for the solutions prepared in this Appendix are being determined on a digital computer for the following set of parameters, roughly representative of human skull properties.

$h = .015$ inches

$a = 3.0$ inches

$E = 2 \times 10^6$ psi

$P = 1.82$ gm/cm.^{3}

$\nu = 1/4$

$\xi_0 = .262$ radians

$V = 30$ mph.

BIBLIOGRAPHY

Sonstegard, A. David 1965 The Axisymetric Response of a Closed Spherical Shell to a Nearly Uniform Radial Impulse. The University of Michigan Industry Program of the College of Engineering.

Love, A.E.H. 1944 The Mathematical Theory of Elasticity. Dover Publication. New York.

_____ On Free and Forced Vibration of an Elastic Spherical Shell Containing a Given Mass of Liquid. Proceeding of the London Mathematical Society, Vol. XIX: 170-207.

Lamb, H. On the Vibrations of a Spherical Shell. Proceeding of the London Mathematical Society, Vol. XIV: 50.

Baker, W.E. 1961 Axisymetric Modes of Vibration of Thin Spherical Shell. The Journal of the Acoustical Society of America, 33: 1749.

Naght, P.M. and Kalnins, A. 1962 On Vibrations of Elastic Spherical Shells. Journal of Applied Mechanics, 29: 65.

Kalnins, A. 1964 Effect of Bending on Vibrations of Spherical Shells. The Journal of the Acoustical Society of America, 36: 74.

Sternberg, E. and F. Rosenthal 1962 The Elastic Sphere Under Concetrated Locks. ASME Trans. Vol. 74: 413.

Leckie, F.A. 1961 Localized Loads Applied to Spherical Shells. Journal of Mechanical Engineering Sciences, Vol. 3: 111-118.

Humphrey and Winter 1965 A Dynamic Response of a Cylinder to a Side Pressure Puke. AIAA Journal, Vol.3: 27.

Long, C.F. 1966 Vibration of Radially Loaded Shell. ASCE Proceedings, Vol. 92: 235-250.